OSLOMET

GROUP MEMBER
Christian Edward Nordli

Master's degree in:

Phone: 67 23 50 00

Structural Engineering and Building Technology
Department of Civil Engineering and Energy Technology

Master's Thesis

Title Dynamic Analyses of Railway Bridges with Elastic Bearings	**DATE** May 25, 2022
	PAGES: 55 **APPENDICES:** 7
AUTHOR Christian Edward Nordli	**SUPERVISOR** Emrah Erduran

ABSTRACT

With an increasing trend in the development of new railway lines together with a greater focus on optimizing the life expectancy of infrastructure such as railway bridges, the importance of effectively monitoring and maintaining such structures becomes ever more crucial. Analysing models that accurately present the interaction between the traversing train and bridge, enables proper delegation of such maintenance.

The current thesis, studies the effect of elastic spring supports on the dynamic behaviour of railway bridges and the traversing trains. By developing a MATLAB code, which implements both elastic spring supports together with a proposed sprung mass model, a parametric study is conducted to gain an insight into this field of study.

As a conclusion, the parametric study indicates that a lower support stiffness and a faster train velocity are not necessarily related to a greater dynamic response of the bridge. Especially at a support stiffness at $1x10^6$ kN/m, does the resonance condition bring a significant response. This is also the only case which contributes to an additional response on the traversing sprung masses. The calculation time for the proposed sprung mass model becomes nonviable at slower train velocities than 80 km/h with the defined CPU.

3 Keywords
Elastic Bearing
Sprung Mass Model
Railway Bridge

Acknowledgement

The following thesis was written as a conclusion for the two-year master's program in Structural Engineering and Building Technology at the faculty of Technology, Art and Design (TKD) in OsloMet.

I want to give special thanks to my supervisor, Associate Professor Emrah Erduran, for his exceptional motivation, guidance and patience through this thesis. Without his presence, I would surely not be as proud of my work as I am today. I also want to give my thanks to Postdoctoral Fellow Semih Gonen, who has also provided crucial feedback on my work through these months.

Finally, I want to give my thanks to both my parents for continuously supporting me through this thesis. Their encouragement has been invaluable and it will forever be appreciated.

25.05.2022

Christian Edward Nordli

Definitions and Abbreviations

AMA: Absolute Maximum Acceleration

DAF: Dynamic Amplification Factor

DOF: Degree of Freedom

FAS: Fourier Amplitude Spectrum

FEM: Finite Element Method

FFT: Fast Fourier Transformation

MDOF: Multi Degree of Freedom

SDLC: Software Development Life Cycle

SDOF: Single Degree of Freedom

SMM: Sprung Mass Model

VBI: Vehicle Bridge Interaction

Abstract

Over the last decade, an increasing trend in development of railway lines and railway bridges has occurred in Norway, as the following mode of transport is deemed both effective and sustainable for passengers and goods. When also considering the increased focus on optimizing the life expectancy of structures such as railway bridges, the importance of effectively monitoring and maintaining such infrastructure becomes ever more crucial. Due to the amount, it is beneficial to model and properly predict when it is necessary to conduct physical measuring and maintenance of such bridges. Analysing models that accurately present the interaction between the traversing train and bridge, enables proper delegation of maintenance in a period of significant deterioration on infrastructure all across Norway.

While a significant body of knowledge has been dedicated to the study of dynamic behaviour of railway bridges using different vehicle bridge interaction models, almost none of these directly consider the effect of elastomeric bearings for such cases. The aim of the current thesis is therefore to analyse the impact of elastic supports on the dynamic response of railway bridges. By conducting a parametric study in which the vertical stiffness of the supports varies, the effect of deterioration is also considered.

Using the MATLAB software previously developed by A.M Al-Kanany [1], the current thesis further implements both elastic supports and the relatively more complex sprung mass model with basis from 2D planar FEM. Different parameters such as the number of bridge spans, train velocity and support stiffness were varied through the parametric study. While the support stiffness usually varied equally in stiffness, some analyses were conducted when implementing a different stiffness on each support. Although most of the parametric study is dedicated to the dynamic behaviour of the bridge, the dynamic response of the sprung masses, which represent the axles of the train, were also analysed.

As a conclusion, the parametric study indicates that a lower support stiffness and a faster train velocity are not necessarily related to a greater dynamic response of the bridge. This response is often affected by the potential resonance condition, which is prevalent when applying elastomeric bearings. Especially for the vertical support stiffness at $1x10^6\ kN/m$, does the resonance condition bring a significant response. This support stiffness is also the only case which contributes to significant bridge induced vibrations on the traversing sprung masses representing the train axles. It is further observed that the locations of local maximum accelerations when $k_s \leq 1x10^7\ kN/m$ correlate with the FAS presenting the relevant dominant mode vibrations of the bridge. Although the proposed sprung mass model brings satisfactory results for the current study, due to it's simplified principles, the model becomes nonviable at slower train velocities than 80 km/h with the defined CPU.

Sammendrag

Over det siste tiåret, har utviklingen av toglinjer og togbruer hatt en økende trend i Norge, ettersom denne type transport er ansett som effektiv og miljøvennlig både for passasjerer og diverse varer. Når man også tar hensyn til den økende priortieringen for optimalisering av levealderen for strukturer som togbruer, blir det enda mer aktuelt å effektivt overvåke og vedlikeholde slik infrastruktur. Grunnet mengden er det gunstig å modellere for å forutsi når det er nødvendig med fysiske målinger og vedlikehold av slike bruer. Analyser av modeller som nøyaktig presenterer interaksjonen mellom det kryssende toget og brua, gjør det mulig å nøyaktig delegere vedlikehold i en periode med betydelig forfallelse av infrastruktur rundt om i Norge.

Selv om mye av den nåværende kunnskapen er dedikert til studier av dynamisk respons av togbruer ved bruk av forskjellige tog-bru interaksjons modeller, så tar nesten ingen av dem direkte hensyn til effekten ved bruk av elastiske støtter for slike tilfeller. Målet med følgende hovedoppgave er derfor å analysere innvirkningen av elastiske støtter på den dynamiske responsen av togbruer. Ved å gjennomføre en parametrisk studie hvor den vertikale stivheten av støttene varierer, blir effekten av forverring også tatt hensyn til.

Ved anvendelse av en MATLAB programvare tidligere utviklet av A.M Al-Kanany [1], blir det videre implementert både elastiske støtter og en relativt mer kompleks fjær-masse modell. Mens stivheten på støttene varierer likeverdig, ble det også gjennomført noen analyser av variasjon i stivhet mellom dem. Selvom mesteparten av det parametriske studiet er dedikert til den dynamiske responsen av selve brua, ble den dynamiske reaksjonen av fjær-massene som representerer akslene på toget også analysert.

Som en konklusjon indikerer det parametriske studiet at en lavere støtte-stivhet og et raskere tog ikke nødvendigivis er relatert til en større dynamisk respons av brua. Denne responsen er ofte påvirket av den potensielle resonans tilstanden som er utbredt når man bruker elastiske støtter. Spesielt for støtte-stivheten $1x10^6\ kN/m$, gir resonans tilstanden en betydelig respons. Denne støtte-stivheten er også det eneste tilfellet som bidrar til betydelige vibrasjoner fra brua på de kryssende fjær-massene som representerer tog akslene. Det er også observert at den relative posisjonen av lokale maksimal akselerasjoner når $k_s \leq 1x10^7\ kN/m$ korrelerer med FAS som presenterer den relevante dominerende modus av vibrasjon til brua.
Selv om den foreslåtte fjær-masse modellen gir tilfredstillende resultater fra følgende studie, grunnet dens forenklede prinsipper, blir modellen ikke gjennomførbar for tregere toghastigheter enn 80 km/t med den definerte prosessoren.

List of Figures

List of Tables

Contents

1 Introduction

It has been announced by the Norwegian Government that further development and construction of new railway lines will become necessary in the future [8]. This is an option of transportation that is promoted as both effective and sustainable to the environment. Hence, the state-owned enterprise Bane NOR has continuously received an increased budget over the years. With an increased amount of infrastructure in a country such as Norway, the importance of effective monitoring and maintenance becomes ever more crucial given the focus of optimizing the life expectancy of varying structures. By achieving a greater life expectancy, the structure becomes more cost efficient while also achieving a lower carbon footprint. This is one of many means a structural engineer can contribute in order to achieve the UN's Sustainable Development Goal for 2030, which also applies to Norway.

As there is an increased focus on development of new railway lines and maintenance, the development of accurate models which predict the behaviour of railway bridges becomes a significant tool when delegating maintenance to the appropriate infrastructures. In most cases, the dynamic behaviour of a bridge is simplified through the use of a dynamic amplification factor (DAF), which is introduced through the European Standard. The dynamic behaviour is considered by multiplying the static response of the bridge with a defined factor. This is not a viable approach when a more detailed dynamic analysis is required. Taking this into consideration, the development of varying interaction models between the traversing train and the bridge has previously been developed to create a more detailed description of the dynamic behaviour for different railway bridges.

The elastomeric bearings of a bridge is prone to deterioration, which is imposed by periodic loading and the environment. This type of support is often applied to bridges in order to prevent increased stresses when exposed to thermal expansion and concrete shrinkage. It is also applied to provide vertical stiffness while remaining flexible enough to handle motion from the ground during a potential earthquake.

Although several studies have been conducted for the dynamic response of railway bridges using different vehicle bridge interaction (VBI) models, only a few directly consider the effect when implementing elastic supports for such cases. These few relevant studies further idealize by only using simple VBI models such as the moving load or moving mass model. It is therefore necessary to gain a better understanding on the impact of elastomeric bearings on the dynamic response from both the bridge and the traversing train, as this may significantly impact the results. Since the train is also of interest to analyse, the relatively more complex sprung mass model is implemented while considering the introduction of elastic supports. Since this VBI model is relatively complex to code, simplified principles are further proposed.
Through the following sub chapters, a literature review is firstly conducted to gain a more detailed overview on the current body of knowledge regarding this field of study. Afterwards, using this overview as a basis, the aim and scope of the current thesis is established.

1.1 Literature Review

The interaction between a traversing train on a bridge has continuously been studied over the years. With varying models predicting this interaction through the use of finite element method (FEM), it has been possible to efficiently determine the dynamic behaviour of a bridge given defined parameters. Although a number of these studies has been conducted with consideration to the dynamic behaviour of railway bridges, it is important to understand how many of these directly regard the effect of using elastomeric bearings on the dynamic behaviour of railway bridges. A preliminary scope review is therefore conducted in order to gain an overview of the current body of knowledge regarding this field of research. In doing so, only relevant studies will efficiently be selected for further investigation, using different databases and criteria.

1.1.1 Preliminary Scope Review

With the framework presented by Arksey and O'Malley [9], the present scope review can be described through the following steps in a chronological order: 1. Identify the research question; 2. Identify relevant studies; 3. Study selection; 4. Chart data; and 5. Collate summarise and report the results. Given the purpose of this preliminary scope review, certain adaptations are made in which only the first three steps become relevant.

Table 1.1: General framework for preliminary scope review.

1. General guidelines	**2. Databases**
• Sources: Databases gathered online, relevant journals • Timespan of 22 years (2000-2022) • Full-text availability • English language only	• Oria (Norwegian university library) • Scopus • Elsevier Engineering Village • Web of Science • Recommended literature from supervisor and colleagues

Through this preliminary scope review, the current research question will consist of ''Dynamic Behaviour of Railway Bridges with Elastic Bearings". This is a general definition that can consist of different terminology if necessary. Terms such as ''Dynamic Response" and ''Elastic Supports" are therefore relevant through the search queries. Initially, through the first search query, a wide selection of samples is selected.

By using a wide selection of operators with the relevant keywords defined through the research question, it is possible to narrow down each successive search query. Initially, the operator ''OR" is used to include one or more of the appropriate keywords. By further using ''AND" in combination with ''OR", an additional criterion of including all the relevant terms is applied. Finally, ''TITLE-ABS-KEY" is used to determine the location of the relevant keywords. Using all these operators in combination narrows down the search in an efficient manner. Through Table 1.2, the appropriate terminology used with the relevant operators is presented in a chronological order.

Table 1.2: Relevant terminology for each chronological search query.

Approach 1	**Approach 2**
• Dynamic Behaviour • Dynamic Response • Railway Bridge	• Elastic Bearings • Elastic Support

The term ''Dynamic Behaviour" is general within the field of study in structural dynamics. Even though this is the case, specific keywords such as ''Resonance" and ''Damping" are not used when filtering the relevant samples, as this makes the search query too narrow. Other keywords are therefore used to compensate for this somewhat general definition.

Table 1.3: Overview of search history.

Search number	**Addition to the search string (Scopus search format)**	**Oria**	**Web of Science**	**Scopus**	**Engineering Village**
1	((Dynamic Behaviour) OR (Dynamic Response)) AND (Railway Bridge)	29 574	1 111	13 513	2 751
2	((Dynamic Behaviour) OR (Dynamic Response)) AND (Railway Bridge) AND ((Elastic Bearings) OR (Elastic Support))	3 605	52	1 331	183
Narrow down to only journal articles					
3	TITLE-ABS-KEY (((Dynamic Behaviour) OR (Dynamic Response)) AND (Railway Bridge) AND ((Elastic Bearings) OR (Elastic Support)))	2	29	14	60
Preliminary review based on abstract of potential journal article					
4	TITLE-ABS-KEY (((Dynamic Behaviour) OR (Dynamic Response)) AND (Railway Bridge) AND ((Elastic Bearings) OR (Elastic Support)))	0	1	1	0
[1]Duplicates of the same journal articles across each database are excluded when reviewing relevance. [2]Additional samples gathered through a separate "hand search" is later included.					

With the preliminary review within the fourth search query, a majority of studies is filtered out when evaluating each of the samples by title, keywords, abstracts and duplicates manually between each database. Although many of these filtered out studies from the third search query regard the use and effect of elastomeric bearings for railway bridges, almost none of these directly study the effect of such bearings on the dynamic response of railway bridges with a span. The excluded studies generally look only at the elastomeric bearing itself or the effect of such a bearing either when considering seismic activity on a railway bridge or foundation-soil interaction. Since the search string may miss relevant studies, by further performing a manual search according to Arksey and O'Malley [9] and following recommendations from colleagues and supervisor, an additional 7 studies were included. This brings a total of 9 unique samples directly concerning the effect of elastomeric bearings on the dynamic response of railway bridges, which is presented more in detail through Appendix A.

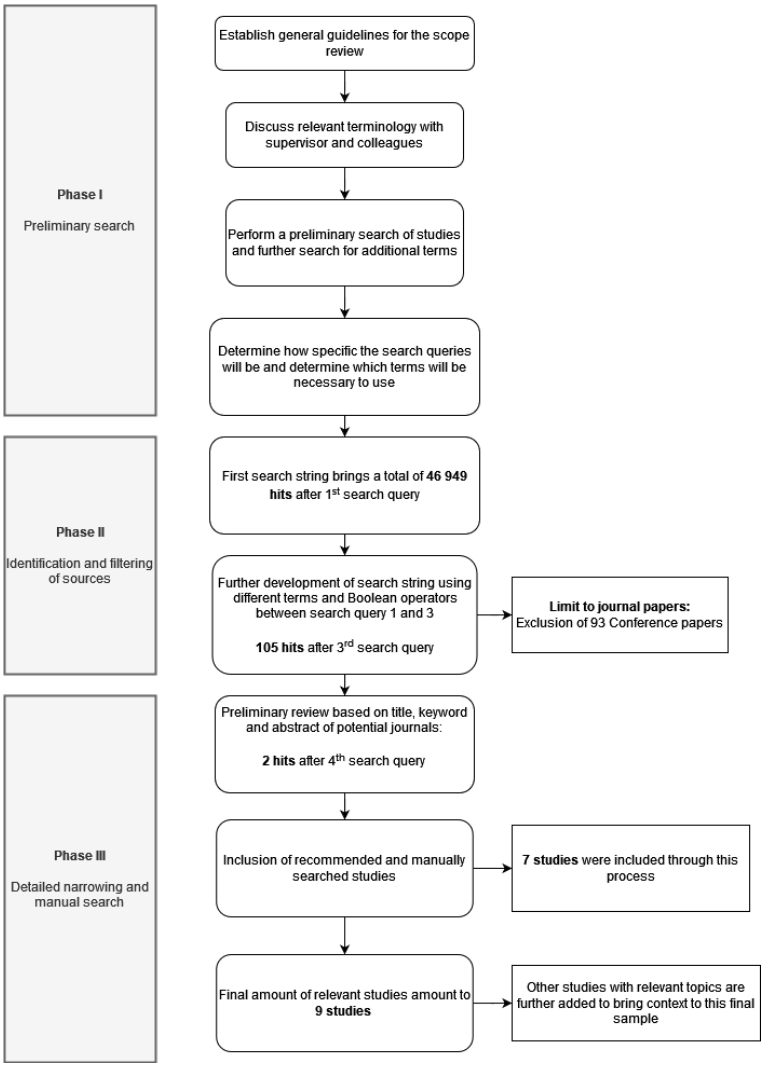

Figure 1.1: Flowchart of process for narrowing down relevant literature for the final sample.

Although the established terms and boolean operators used through the search queries were not too narrow, the final sample still becomes minimal. Considering the limited size of the final sample, and discussions with both colleagues and supervisor, it is evident that a knowledge gap remains regarding the study of the dynamic response of railway bridges supported by elastomeric bearings with varying stiffness.

1.1.2 Relevant Studies

Using a preliminary scope review, a selection of relevant studies has been gathered for the current thesis. Together with this refined sample, an additional selection of studies related to the dynamic behaviour of railway bridges with elastomeric bearings is further reviewed more in detail. Although these studies are not directly related to this topic, they are deemed as necessary to fully understand the concepts used through this refined sample. Each of these studies are reviewed onwards through this sub-chapter.

Table 1.4: Additional topics from relevant studies.

Topics of Additional Studies	
VBI models on Railway Bridges	Deterioration of Elastomeric Bearings

Yang et al. [10] present different VBI models with varying complexity while using FEM as basis. These models are further verified with analytical results as a reference. Compared with the moving load and moving mass model, the proposed sprung mass model (SMM) also considers parameters such as suspension stiffness and damping, mass of car body and wheel, rail irregularity, and ballast stiffness. By further implementing *Hermitian Interpolation*, the coupled nonlinear relationship between the traversing sprung mass and bridge elements is established while performing an iterative numerical calculation. Parametric studies were also conducted using different types of bridges and traversing vehicles in order to compare and determine the relevant results between the VBI models. When comparing the moving load and sprung mass model, the inclusion of the inertial effect through the SMM resulted in a slight reduction of the peak response of the bridge. This phenomenon can be explained by how the sprung mass behaves as a tuned mass.

With the introduction of both a sprung mass and a half-car model, A. Gonzalez [11] studies the suitability of an uncoupled numerical method and further compares this approach to a coupled numerical method. Rather than combining the equation of motion for the bridge and vehicle, the uncoupled method assumes that the dynamic effect of the bridge and the vehicle remains independent of each other. The matrices of both sub-systems remain constant, which in turn makes it possible to implement modal superposition. Using properties such as mass ratio (MR) and the ratio between the frequency of the vehicle over the first frequency of the bridge (FR), the study presents how the errors of the uncoupled method generally increase due to a higher MR and velocity, which represents a greater vehicular dynamic force.

Yong et al. [12] investigate the relationship among the parameters, which influence the dynamic response of a railway bridge. Through the use of a moving mass model, numerical data was gathered while identifying different characteristics between the traversing train and the bridge. In the simple case of only one traversing vehicle, the dynamic effect was mainly influenced by the driving frequency, which emerge from the load pulse due to first contact between the vehicle and the bridge. To achieve resonance, this driving frequency simply needs to be equal to the natural frequency of the bridge. However, when deploying multiple carriages, the results show that the dominant frequencies are mostly influenced by the repeated loads. The ratio between the

length of the bridge and the distance between the relevant carriages determines the spectral peaks, which show the dominant frequencies associated with the resonance condition.

More extensive studies were conducted by Yang and Yau [13] for a series of single-span bridges traversed by trains with high speeds. By using approaches that are both analytical and numerical, the study not only investigates the mechanism of resonance induced by the train onto the bridge, but also the resonance induced by the bridge on the train carts. In doing so, the study shows that resonance imposed on the bridge is mostly achieved through a higher train speed, while resonance on the train is achieved through lower speeds.

With consideration to the relevant aging effect of elastomeric bearings, E. Erduran et al. [14] study the impact of varying support stiffness on the dynamic behaviour for single-span railway bridges. Using the moving load model, the modal frequencies, and the maximum acceleration at the midspan of the bridge is gathered. Only subtle changes are observed for the modal frequency after passing a threshold value of $1x10^8 kN/m$. By further implementing the Fourier Amplitude Spectrum (FAS), the study shows how a vertical support stiffness lower than the given threshold makes the higher modes become more dominant on the acceleration at midspan.

By using viscoelastic supports for a simple beam, A. Zangeneh et al. [15] has developed a discrete model, which considers the soil-structure interaction effects on the modal properties of a beam. By implementing this model, the effect of the dynamic stiffness from the foundation on the natural frequency and damping ratio of the railway bridge was investigated. Together with close-form expressions, a parametric study was further conducted on a short and medium size bridge, which were resting on shallow foundations with different subsoil conditions. By including the foundation damping on a viscoelastically supported beam, the results generally bring a higher natural frequency when compared with a beam, which is only elastically supported. This study indicates that modelling elastic bearings can also be of use when considering the soil-structure interaction effect on the foundation of a railway bridge.

Yang et al. [16] examine the mechanisms of dynamic behaviour regarding resonance and cancellation when using elastic bearings. By implementing a moving load model with equal distance between each axle, an analytical study was conducted with verification from a field test. As a result of using elastic supports, the bridge achieves a lower natural frequency. This means a lower resonant speed is necessary when compared with simple supports. Meanwhile, the cancellation speed for an elastically supported beam remains equal to a simply supported beam. Although the use of elastic bearings for railway bridges have several benefits, the study also brings attention to the prevention of transmitting the vehicle-induced vibrations to the ground, in which the potential accumulation of induced vibrations may occur, and as a result create high-amplitude peaks that promote greater fatigue of the bridge. Yau et al. [17] also investigated many of the same topics regarding the use of elastic supports using a simply supported beam. In this case, an envelope impact formula which can be used for preliminary design of railway bridges was further introduced.

In the case of elastic bearings for multi-span bridges, C. Kim et al. [18] focus on the reduction of traffic-induced vibrations by reinforcing the end-cross beam and removing bumps at expansion joints. By computing the natural frequencies of the bridge through an analytical model while idealizing the elastomeric support as an

elastic spring, the proposed model is further compared with the gathered field-test results and is shown to be in agreement. In comparison with steel pin bearings, an elastically supported bridge vibrates more easily by moving vehicles. For elastomeric bearings, the dominant vibration level is located at the member near the expansion joint. By installing end-cross beam reinforcement, it is possible to reduce this dominant vibration near the expansion joint. Meanwhile, for a steel pin bearing, dominant vibration occurs near the span center.

Following the use of elastic bearings on multi-span bridges, H. Xu and W.L. Li [19] further investigate the effect of coupling conditions between each span while using a moving load model. In this case, discontinuity is allowed between each span, which makes it possible to consider the effect of steps. This in turn, affects the vehicle bridge interaction. While focused on the dynamic effect of the coupling condition between the spans, the study presents through a proposed model how the deflection of each span strongly depends on its local coupling condition between the spans. It is finally concluded that improvements can be done on the bridge performance through modifications of joint parameters.

Through a technical paper written by Yang et al. [20], the use of a tuned mass (TM) is introduced to reduce the accumulating vibrations that is a reoccurring problem when using elastic supports for a bridge. More of a physical interpretation is made through a function of this tuned mass, where the dynamic behaviour is studied using a moving load model of a simply supported beam. With a feasible mass ratio of one percent between the tuned mass and the bridge, a substantial reduction of the accumulating vibrations within the bridge can be achieved. It is also concluded that in order to reduce the vibrations occurring on the bridge potentially leading to resonance, the TM should be tuned with consideration to the beam, rather than the driving frequency from the traversing load.

There are different types of elastomeric bearings with a wide variety of properties. A majority of these bearings consist of rubber, and the deterioration of this type of bearing has been studied using different methodologies. In countries such as Japan, which is prone to the effect of earthquakes, have several studies been conducted regarding the behaviour of rubber bearings for bridges.
Using accelerated thermal oxidation, Itoh Y. et al. [21] performed a systematic study of the deterioration and long-term behaviour of high damping rubber (HDR). This type of rubber bearing is combined with other damping devices such as lead plugs and steel bars. This provides both flexibility and a high damping ratio. After determining that thermal oxidation is one of the predominant degradation factors affecting HDR, the study concludes that the effect of such a chemical process results in a more brittle support with an increased stiffness and reduced elongation at break. It is therefore concluded that the deterioration of rubber bearings needs to be considered in the design phase of a bridge. Other studies have also been conducted by Itoh Y. et al. [22] with other types of rubber bearings and accelerated exposure tests. These studies show much the similar results.

With more of a focus on structural health monitoring of elastomeric supports for bridges, M. Fayyadh and H. A. Razak [23] study the use of rubber bearings with varying vertical stiffness to simulate the deteriorating conditions of a bridge deck. By conducting force vibration testing on a scaled down simply supported RC girder with varying stiffness on the supports, the necessary vibration data was gathered. Using Modal Assurance

Criteria (MAC) and Frequency Response Function (FRF), results were gathered to detect the deterioration of the relevant elastic support. It is observed that the first mode of vibration has a high sensitivity to the deterioration of the elastic bearing. This makes it favourable when determining the condition of the elastic support. Meanwhile, the third mode of vibration can be used as a tool to determine whether the origin of the deterioration is in the elastic support or the structural element. Further, when the elastic bearing deteriorates, the first mode will achieve a higher change in the MAC values, while higher modes will change much less. In comparison, if the structural element deteriorates, the higher modes achieve a higher MAC value, while the first mode remains almost the same.

When reviewing the relevant studies presented through the following sub-chapter, different observations have been made on the current relevant body of knowledge. A majority of these limited studies mostly consider the use of a moving load model when representing the interaction between the traversing train and railway bridge. This means that the dynamic response of the train itself becomes neglected. It is therefore of interest to instead apply a sprung mass model, which will bring more realistic results for the dynamic response from the railway bridge and the traversing train. When implementing this interaction model, the effect from the elastic supports for the bridge will also be taken into consideration.

1.2 Aim and Scope of Study

A present knowledge gap has been detected through the preliminary literature review. The main aim of this thesis is to further gain an understanding of the impact of elastomeric bearings on the dynamic response of railway bridges and corresponding traversing trains. The effect of deteriorating stiffness due to aging of the elastomeric bearings is also of interest, and is further simulated by varying the stiffness on the supports. When conducting this study, the time-independent absolute maximum acceleration (AMA) is gathered and presented through the length of the relevant bridges as an envelope curve. The frequency domain is also studied, as it provides vital insight into the dominant frequencies occurring on both the railway bridge and the train axles. Considering this, the following analyses are conducted through a parametric study in which the support stiffness, number of spans and train velocity are varied.

Using the MATLAB code previously developed by A.M Al-Kanany [1] as a basis, and following conventional assembly procedures in finite element method (FEM), the original restricted supports become substituted with idealized elastic springs, which can vary in stiffness. By implementing principles for a sprung mass model, the interaction between the traversing train and bridge becomes more realistic. As the train and railway bridge is treated as two separate subsystems, the mentioned VBI model also makes it possible to analyse the dynamic response of the train as well. Since new algorithms and principles are proposed for the MATLAB code in the current thesis, it is also essential to methodically verify the accuracy by using relevant reference cases before any parametric study is conducted. The efficiency of this proposed algorithm consisting of both the spring support and sprung mass model will further be evaluated.

1.3 Limitations

Due to the amount of relevant parameters and the required time dedicated both to the development of the proposed algorithms and the computations in the parametric study, it becomes necessary to define limitations for the current thesis.

- The proposed MATLAB code with a basis from FEM is established for 2D planar beam elements. Torsional behaviour is therefore neglected in this case.
- The surface before and after the railway bridge is regarded as infinitely stiff.
- Due to the principles of the sprung mass model, effects such as *pitching* will be neglected for the relevant train.
- Only movement in the vertical direction is considered.
- Both rail irregularity and ballast stiffness are neglected while implementing the sprung mass model.
- The bridge support stiffness, number of bridge spans and train velocity vary. Meanwhile, other parameters for both the train and bridge remains constant.
- While traversing, the velocity of the train is constant.
- The results are not compared and verified with measured physical data.

2 Theoretical Context

2.1 Principles of Structural Dynamics

Often when considering the complex effects of dynamic loading from a traversing train over a railway bridge, the use of a dynamic amplification factor (DAF) or an impact factor (I) is introduced through the European Standard by amplifying the results gathered from the static analysis [10]. Using this approximation as basis, the design of the railway bridge is established while also considering the dynamic loading. The following expression is typically used when defining this approximation, where R_d is the dynamic response of the railway bridge and R_s is the static response.

$$\mathrm{I} = \frac{R_d - R_s}{R_s} \qquad (2.1)$$

Although this is a typical approach when considering the dynamic effect through the design of a railway bridge, it is regarded as both conservative and limited when further studying the dynamic response of the bridge in more detail.

2.1.1 Equation of Motion

By defining the railway bridge using the Finite Element Method (FEM) together with the principles established through the equation of motion, it is possible to accurately express the behaviour of the railway bridge in terms of acceleration, velocity and displacement through time.

$$[\mathrm{M}_b]\{\ddot{u}\} + [C_b]\{\dot{u}\} + [K_b]\{u\} = \{p\} \qquad (2.2)$$

Where M_b, C_b and K_b are the mass matrix, damping matrix and stiffness matrix of the railway bridge subsystem respectively. Vector p, represents applied dynamic loading on the railway bridge. Meanwhile, vectors $\ddot{u}$, $\dot{u}$,u are the time-dependent acceleration, velocity and displacement of the relative structure respectively. When further idealizing the railway bridge by describing the structure as planar beam elements through the FEM, the following symmetric matrices consist of a size equal to 6x6 representing the beam elements individually, where each node located at each end of the beam elements consist of three degrees of freedom (DOF). These DOF consider axial, lateral and rotational movement. With the idealization of planar beam elements, the corresponding mass and stiffness matrices are presented through Appendix B. By discretizing the relevant railway bridge using these individual elements connected through each node, total matrices are further established for the structure.

2.1.2 Natural Frequency and Mode of Vibration

When describing a structure in terms of dynamic response, the natural frequency is a property which provides a basis when studying such interactions. Considering the natural frequency, modes of vibrations are further developed in order to describe the shape in which the relevant structure would prefer to vibrate about. For a multi degree of freedom (MDOF) system, these properties are calculated through an eigenvalue problem. While

currently focusing on natural frequencies and mode shapes, the MDOF system is simplified using equivalent single degree of freedom (SDOF) systems through modal superposition.

$$u(t)=q_n\phi_n \qquad (2.3)$$

Using an undamped free vibration MDOF system, the following expression is derived.

$$[-\omega_n^2 m\phi_n + k\phi_n]q_n(t) = 0 \qquad (2.4)$$

When only considering non-trivial solutions of Equation 2.4, the determinant is further calculated through Equation 2.5 to attain the natural frequency, which is later used in Equation 2.4 to gather the mode shapes of the relevant structure.

$$\det[k-\omega_n^2 m] = 0 \qquad (2.5)$$

2.1.3 Damping

While considering the defined parameters of the structure through the stiffness and mass matrix, classical damping is often applied while idealizing the complex phenomenon of damping for the relevant structure. When developing a damping matrix for a MDOF system, *Rayleigh Damping* is often used while considering classical damping defined through two modes. This idealization consists of both mass-proportional damping and stiffness-proportional damping. Each of these proportions is required to accurately define the damping of the total structure [2].

$$c = a_0 m + a_1 k \qquad (2.6)$$

Through the coefficients a_0 and a_1 related to the mass and stiffness of the structure, the damping ratio is defined for both the relevant modes of the structure. It is reasonable to assume they both have the same damping ratio [2]. In the case of reinforced concrete structures, a damping ratio of 5% is often recommended for earthquake applications [24].

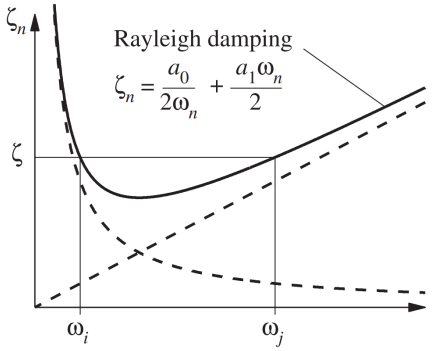

$$\frac{1}{2}\begin{bmatrix} 1/\omega_i & \omega_i \\ 1/\omega_j & \omega_j \end{bmatrix}\begin{Bmatrix} a_0 \\ a_1 \end{Bmatrix} = \begin{Bmatrix} \zeta_i \\ \zeta_j \end{Bmatrix} \qquad (2.7)$$

Figure 2.1: Rayleigh Damping [2].

Although Rayleigh damping is regarded as relatively accurate when defining classical damping for a structure, it is important to be aware of certain aspects regarding this approach. Through Equation 2.7, which is further presented through Figure 2.1, the relationship between the varying modes of vibration and corresponding damping ratios is presented. For the higher modes of vibration beyond ω_j and lower modes below ω_i, a greater damping ratio develops above what was originally defined. Meanwhile, between ω_i and ω_j, the relevant damping ratio becomes smaller than what was originally defined.

2.1.4 Vehicle Bridge Interaction Model

A variety of different models has been developed over the decades when defining the dynamic interaction between the traversing train over the corresponding railway bridge. The *moving load model* is regarded as one of the most simple of these models, in which the axles are defined as constant loads, while the *moving mass model* further considers the contribution of mass from the train on the railway bridge. Within each of these individual VBI models, different studies have proposed varying approaches as of how to define the relevant interactions.

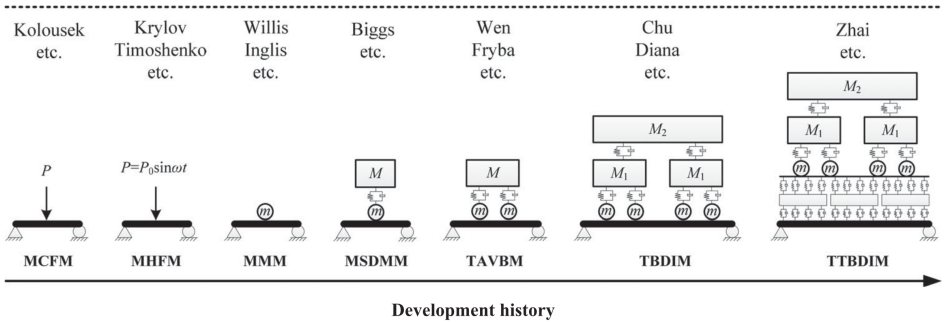

Figure 2.2: Development history of VBI models [3].

Through the following thesis, the more complex sprung mass model introduced by Biggs and Testa [25], considers the effect of suspension stiffness and damping from the train. As with the moving load and moving mass model, general parameters regarding the velocity and position of each train axle are relevant together with the properties of the railway bridge. Along the lumped mass from the train body located on top of each axle, the stiffness and damping from the train sub-system is integrated with the initial parameters of the railway bridge. In comparison with the moving load and moving mass model, the effects induced by the bridge on the train also need to be taken into consideration. With the assumption that train axles should continuously stay in contact with the railway bridge, a criterion is set for the contact force in which the bottom displacement of the sprung mass and the relevant position of the railway bridge remains coupled to each other.

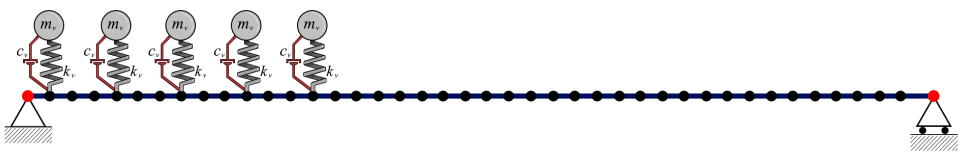

Figure 2.3: Sprung Mass VBI Model.

2.1.5 Direct Time Integration through Newmark's Method

While considering the principles of the sprung mass model with varying stiffness and damping, the method consisting of modal superposition becomes nonviable for solving the second-order differential equation defined through the equation of motion. Different direct time integral methods are commonly implemented instead to numerically solve the corresponding dynamic response. Most studies regarding the sprung mass model apply direct time integral methods such as Newmark-β method or Wilson-θ method [5, 10, 26]. In such cases, a nonlinear relationship is defined between the sprung masses coupled with the relevant beam elements composing the railway bridge. This interaction also considers properties such as ballast stiffness and rail irregularities. Although this is the case, a simplified approach is proposed in this thesis where Newmark's method for a *linear system* becomes sufficient when solving for such a VBI model. Through the following time-step equations developed by N.M. Newmark [27], the basis of the Newmark's method are provided together with the equilibrium established through the incremental form for the equation of motion.

$$\dot{u}_{i+1} = \dot{u}_i[(1-\gamma)\Delta t]\ddot{u}_i + (\gamma\Delta t)\ddot{u}_{i+1} \tag{2.8}$$

$$u_{i+1} = u_i + (\Delta t)\dot{u}_i + [(0.5-\beta)(\Delta t)^2]\ddot{u}_i + [\beta\Delta t)^2]\ddot{u}_{i+1} \tag{2.9}$$

While determining the stability and accuracy of the following system, the parameters β and γ define the variation of acceleration and artificial damping between each time increment respectively. With the values $\beta = 1/4$ and $\gamma = 1/2$ representing both constant acceleration and no artificial damping, it has been established that the following method becomes unconditionally stable and is therefore often implemented [10]. While this unconditional stability is relevant, the size of the time step Δt is still limited and is usually defined between 0,01 sec and 0,02 sec [2].

$$\frac{\Delta t}{T_n} \leq \frac{1}{\pi} \tag{2.10}$$

Since the system is defined as linear, an additional modification is made where no iterations are necessary when solving each incremental time step. The following coefficients are used when further presenting the initial conditions for the modified method.

$$a_1 = \frac{1}{\beta(\Delta t)^2}m + \frac{\gamma}{\beta\Delta t}c \tag{2.11}$$

$$\ddot{u}_0 = \frac{p_0 - c\dot{u}_0 - ku_0}{m} \tag{2.12}$$

$$a_2 = \frac{1}{\beta\Delta t}m + (\frac{\gamma}{\beta} - 1)c \tag{2.13}$$

$$\hat{k} = k + a_1 \tag{2.14}$$

$$a_3 = (\frac{1}{2\beta} - 1)m + \Delta t(\frac{\gamma}{2\beta} - 1)c \tag{2.15}$$

After establishing the initial conditions, each of the time increments (*i=1,2,3,..*) is calculated in chronological order, using the following equations [2]. In the case of a linear system, the resisting force $\hat{p}$ can be solved directly. instead.

$$\hat{p}_{i+1} = p_{i+1} + a_1 u_i + a_2 \dot{u}_i + a_3 \ddot{u}_i \tag{2.16}$$

$$u_{i+1} = \frac{\hat{p}_{i+1}}{\hat{k}} \tag{2.17}$$

$$\dot{u}_{i+1} = \frac{\gamma}{\beta \Delta t}(u_{i+1} - u_i) + (1 - \frac{\gamma}{\beta})\dot{u}_i + \Delta t(1 - \frac{\gamma}{2\beta})\ddot{u}_i \tag{2.18}$$

$$\ddot{u}_{i+1} = \frac{\gamma}{\beta(\Delta t)^2}(u_{i+1} - u_i) - (\frac{1}{2\beta} - 1)\dot{u}_i - (1 - \frac{\gamma}{2\beta})\ddot{u}_i \tag{2.19}$$

2.2 Properties of Elastomeric Bearings

As the following thesis considers the use of elastomeric bearings for railway bridges, it is essential to understand what parameters are commonly defined when implementing such a support. Through product descriptions and catalogues, it is evident that such bearings consist of a variety of different types and properties, which are generally designed in accordance with **EN1337-3** [28]. Elastomeric bearings typically consist of natural rubber, which is further reinforced with layered internal steel plates that provide vertical stiffness. Such a bearing allows for slight movement in relation to the support, which in turn minimizes the accumulation of internal stresses from thermal expansion, concrete shrinkage, foundation settlements, wind loads, and more. Elastomeric bearings can also be designed as *roller* supports where more horizontal movement is allowed through a sliding surface.

Although several properties and material specifications are presented through relevant product catalogues, the parameters related to vertical stiffness are of main importance in this thesis, where *"compressive stiffness at zero shear"* defines this property. When considering the different types of elastomeric bearings, the initial vertical stiffness prior to any deterioration is defined between $1x10^4$ kN/m and $1x10^6$ kN/m [28]. While further considering the effect of aging and deterioration, this stiffness may vary even more.

(a) Physical Example of an Elastomeric Bearing [29].

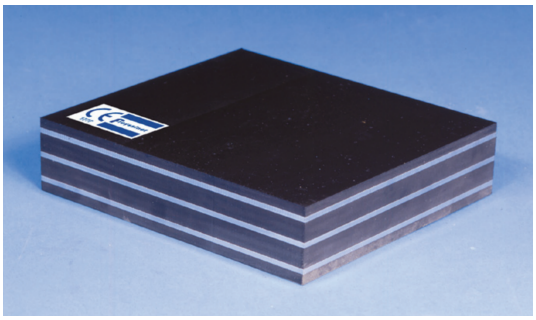

(b) *Freyssinet* Elastomeric Bearing [29].

Figure 2.4: Examples of Elastomeric Bearings.

3 Development of Numerical Model

With the introduction of new principles through the MATLAB software previously developed by A.M. Al-Kanany [1], it is deemed necessary to follow an appropriate software development life cycle (SDLC) to maintain both quality and functionality of the proposed software. While the linear *Waterfall Model* is typically used in civil engineering, an updated version called the *Incremental Model* is used instead when processing the proposed MATLAB software. The following SDLC model is developed in which the relevant build is based on a previous build, the software is therefore developed in increments, which provide flexibility [4, 30]. Following this SDLC model, the spring support algorithm is first fully processed and used as a basis when further applying the sprung mass algorithm. The general procedure for each build within an *Incremental Model* is presented through Figure 3.1.

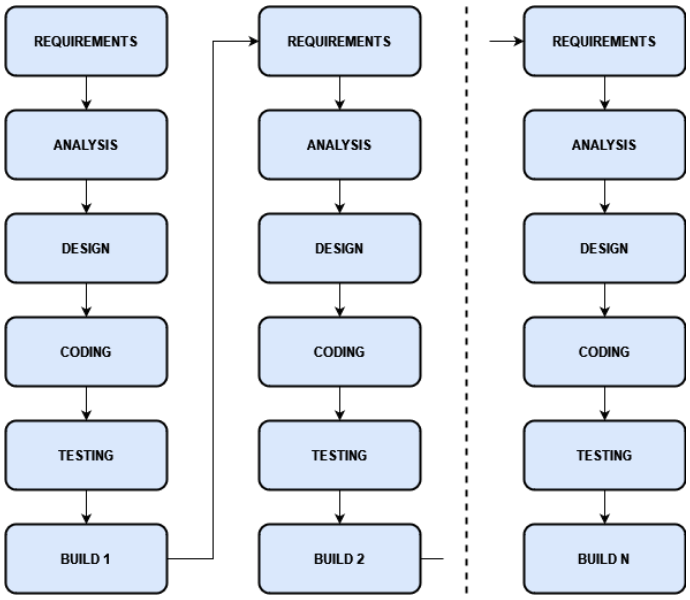

Figure 3.1: Incremental Model [4].

3.1 Content of MATLAB Program

Through the following sub-chapter, the general principles that are implemented when using both elastic spring supports and the sprung mass model are presented using the previously verified MATLAB software developed by A.M. Al-Kanany [1] (hereby termed as the *initial MATLAB software*) as a basis. With this, certain modifications are described to fully understand and further develop the software in the future.

3.1.1 Spring Support Algorithm

The initial MATLAB software has certain limitations. It has been observed that the software only considers specific pre-defined types of supports. When using the previous software, the first support will always be defined as pinned, while the remaining relevant supports become rollers. This naturally provides a limitation when analysing the railway bridge. It is therefore of interest to also analyse the dynamic response of the railway bridge, given different types of supports other than those that are already pre-defined. Hence, it has been decided to adapt a new code where it is possible to customise the stiffness applied on the relevant degrees of

freedom (DOF) for each support. This new adapted code will also be compared with the initial MATLAB software in order to verify whether the results are satisfactory.

There are different methods that can be applied when imposing the user-defined supports. One method of interest consists of restricting the relevant DOF using ''springs", in which a spring with a defined stiffness represents a restriction of the relevant DOF. In contrast with the original software, this method requires the calculation of the total matrices for the railway bridge. The general principle of the following spring algorithm is implemented by simply adding the relevant additional stiffness from the spring support on the diagonal of the total stiffness matrix for the railway bridge. The relevant DOF for the corresponding supports determines at which position this additional stiffness is added within the diagonal of the stiffness matrix.

Additional definitions of different boundary conditions are made available when defining the characteristics of the relevant railway bridge. In this case, it is possible to define the spring stiffness on the relevant DOFs for the supports at the start and end of the bridge. If the bridge consists of multiple spans, it is further possible to define the spring stiffness DOFs for all the supports.

```
%Spring stiffness in [kN/m]

BC1=1e10;               % Horizontal spring stiffness at start of bridge
BC2=1e10;               % Vertical spring stiffness at start of bridge
BC3=0;                  % Rotational spring stiffness at start of bridge
BCx=0;                  % Horizontal spring stiffness at end of bridge
BCy=1e10;               % Vertical spring stiffness at end of bridge
BCz=0;                  % Rotational spring stiffness at end of bridge


% For a potential multi-span bridge, the following boundary conditions can
% be set for the supports in the middle of the bridge.

%Spring stiffness in [kN/m]

BChor=0;                % Horizontal spring stiffness at middle supports
BCver=1e10;             % Vertical spring stiffness at middle supports
BCrot=0;                % Rotational spring stiffness at middle supports
```

Figure 3.2: Definition of relevant supports.

For the supports located at the beginning and end of the bridge, each of the user-defined DOFs is taken into consideration through a *"for-loop"*.

```
%Support at beginning and end of bridge

Boundary=[BC1;BC2;BC3;BCx;BCy;BCz];

for i = 1:3
        BC(i,i) = Boundary(i,:);
        BC(i+GDof-3,i+GDof-3) = Boundary(i+3,:);
end
```

Figure 3.3: Definition of relevant supports.

The application of supports through the length of a multi-span bridge is more complex in comparison as it requires identification of the position for the supports in-between multiple spans. Hence, a code has been developed in which the coordinates of these supports are located with respect to the individual spans. The

implementation of spring stiffness on the support between start and end of the bridge is implemented through an *"if"*-statement in which the number of spans exceeds 1.

```
243     % Identification of which nodes are supported
244
245 -       for i=1:AmountOfNodes
246 -           XA(i,:)=nodeCoord(i,:)-L_span(UY,:)-AZ;
247
248 -       if  abs(XA(i,:))<1e-6
249
250 -           XA(i,:)=0;
251
252 -           BC(3*i-2,3*i-2)=BoundaryMiddle(1,:);
253 -           BC(3*i-1,3*i-1)=BoundaryMiddle(2,:);
254 -           BC(3*i,3*i)=BoundaryMiddle(3,:);
255
256 -           AZ=AZ+L_span(UY,:);
257 -           UY=UY+1;
258 -       end
259 -       end
260 -   end
```

Figure 3.4: Definition of relevant supports.

The original algorithm consisted of using effective matrices throughout its calculations. With the use of total matrices when adding the spring stiffness for the relevant supports, the rest of the algorithm is promptly adapted to the use of total matrices, instead of effective matrices.

3.1.2 Sprung Mass Algorithm

Together with the implementation of elastic spring supports, a sprung mass model (SMM) is further substituted for the following MATLAB code instead of a moving load or a moving mass model. As previously presented through the literature review, different approaches can be implemented with varying complexity and accuracy for this third VBI model. A simple, yet efficient approach is proposed through this sub-chapter.

The MATLAB code for the proposed SMM contains numerous similarities with the initial MATLAB software consisting of either a moving load or a moving mass model. The first significant difference is located where the train properties are defined. In comparison with the previous moving load and mass model, the proposed SMM further makes it possible to define both the spring stiffness and damping for the traversing sprung masses representing the axles of a train.

```
% Train properties
V = 130;                % Speed [km/h]
delta_t = 0.005;        % Desired time step [s]
t_extra = 3;            % Desired extra calculation time [s]
nAxles=56;              % Number of axels
kAxle=4800;             % Stiffness at each axel [kN/m]
cAxle=109;              % Damping at each axel [kN.s/m]
AxleLoad=-196.15095;    % in kN
```

Figure 3.5: Train properties of proposed SMM.

While calculating through the use of total matrices, the first significant difference is identified by the additional dimension of each of the relevant matrices. These additional dimensions to the original bridge dimension attribute to the amount of axles traversing the railway bridge, as shown through Figure 3.6.

```
for cnt=1:nAxles
    ESM(nRows+cnt,nRows+cnt)=kAxle;
    MM(nRows+cnt,nRows+cnt)=F(cnt,1)/-9.81;
    C(nRows+cnt,nRows+cnt)=cAxle;
    F_Load(nRows+cnt,1)=F(cnt,1);
end
```

Figure 3.6: Total matrices with additional axles.

Since the current dynamic analyses mainly consider motion in the vertical direction, the MATLAB code further relates to the node coordinate in the horizontal direction with a corresponding vertical DOF. Following this principle, a mapping array is also established in order to relate the horizontal coordinate of the sprung mass with the corresponding vertical DOF on following nodes within the railway bridge on which it is located upon. This is later used when calculating the time variant stiffness and damping matrices for each time increment.

```
Ydofs=zeros(numNode,2);
A=1;

for cnt2=2:3:GDof
   Ydofs(A,2)=cnt2;
   Ydofs(A,1)=nodeCoord(A,1);
   A=A+1;
end
```

(a) Node coordinate with vertical DOF.

```
for i = 1:x
    for N = 1:f
        for n = 1:nRowsDOF

            if LoadCoord(N,i)>0
            diff =abs(LoadCoord(N,i)-Ydofs(n,1));

            if diff<=(distNode/2.0)*1.00000001
                Mapping(N,i)=Ydofs(n,2);
            end
            end
        end
    end
end
```

(b) Mapping loop.

Figure 3.7: Algorithms which define the position of the relevant sprung mass for each time increment.

In contrast with previous literature regarding different proposals of a sprung mass model, the current MATLAB code does not use shape functions such as *Hermitian Interpolation*. Instead, the proposed SMM only considers the position of each individual sprung mass directly to the closest relative node by relocation through the mapping array. This simplification achieves a less complicated formulation of the coupled relation between the sprung mass and the relevant bridge element. In case the relative sprung mass is located directly in the middle between the nodes of interest, the sprung mass will be relocated on the left-most node if such an event occurs.

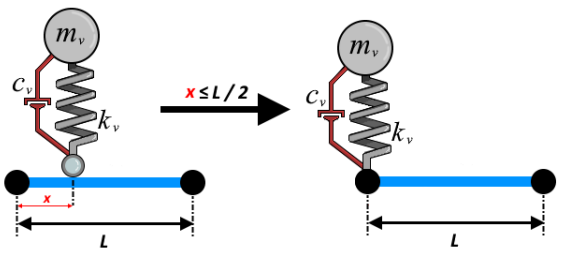

Figure 3.8: Principle of relative position for the proposed sprung mass model.

With a basis from the mapping matrix, the time variant stiffness and damping matrices are calculated and temporarily stored through each time increment. These matrices vary depending on the position of each of the traversing sprung masses.

```
for cnt4 = 1:f

    if Mapping(cnt4,i)~=0

        dofSpring1=cnt4+nRows;
        dofSpring2=Mapping(cnt4,i);
        %Update the stiffness matrix
        K_temp(dofSpring2,dofSpring2)=K_temp(dofSpring2,dofSpring2)+kAxle;
        K_temp(dofSpring1,dofSpring2)=-kAxle;
        K_temp(dofSpring2,dofSpring1)=-kAxle;
        %Update the damping matrix
        C_temp(dofSpring2,dofSpring2)=C_temp(dofSpring2,dofSpring2)+cAxle;
        C_temp(dofSpring1,dofSpring2)=-cAxle;
        C_temp(dofSpring2,dofSpring1)=-cAxle;

    end

end
```

Figure 3.9: Loop for time variant stiffness and damping matrices.

Through Equation (3.1), the following principles from Figure 3.5 to Figure 3.9 are presented in which the respective subsystems are combined into a total time variant stiffness matrix. This theory also applies to the calculation of the time variant damping matrix.

$$\begin{bmatrix} K_{bb} & K_{vb} \\ K_{bv} & K_v \end{bmatrix} = \begin{bmatrix} k_{1,1} & k_{1,2} & \cdots & k_{1,i-1} & k_{1,i} & k_{1,i+1} & \cdots & k_{1,n-1} & k_{1,n} & 0 \\ k_{2,1} & k_{2,2} & \cdots & k_{2,i-1} & k_{2,i} & k_{2,i+1} & \cdots & k_{2,n-1} & k_{2,n} & 0 \\ \vdots & \vdots & \ddots & \vdots & \vdots & \vdots & \ddots & \vdots & \vdots & \vdots \\ k_{i-1,1} & k_{i-1,2} & \cdots & k_{i-1,i-1} & k_{i-1,i} & k_{i-1,i+1} & \cdots & k_{i-1,n-1} & k_{i-1,n} & 0 \\ k_{i,1} & k_{i,2} & \cdots & k_{i,i-1} & k_{i,i}+k_v & k_{i,i+1} & \cdots & k_{i,n-1} & k_{i,n} & -k_v \\ k_{i+1,1} & k_{i+1,2} & \cdots & k_{i+1,i-1} & k_{i+1,i} & k_{i+1,i+1} & \cdots & k_{i+1,n-1} & k_{i+1,n} & 0 \\ \vdots & \vdots & \ddots & \vdots & \vdots & \vdots & \ddots & \vdots & \vdots & \vdots \\ k_{n-1,1} & k_{n-1,2} & \cdots & k_{n-1,i-1} & k_{n-1,i} & k_{n-1,i+1} & \cdots & k_{n-1,n-1} & k_{n-1,n} & 0 \\ k_{n,1} & k_{n,2} & \cdots & k_{n,i-1} & k_{n,i} & k_{n,i+1} & \cdots & k_{n,n-1} & k_{n,n} & 0 \\ 0 & 0 & \cdots & 0 & -k_v & 0 & \cdots & 0 & 0 & k_v \end{bmatrix} \tag{3.1}$$

Following the principle shown through Equation (3.1), the corresponding load vector from Equation (3.2) and the total mass matrix from Equation (3.3) are further established, both considering the bridge structure and the additional traversing sprung masses. While the stiffness and damping matrix are time dependent, the mass matrix and load vector remain constant throughout each time increment following this approach. The load vector is dedicated to the constant force related to each relevant sprung mass. The position of these loads is dependent on the previously referred mapping array. The additional effects due to inertia and speed on the sprung mass are considered through the previously referred time-dependent stiffness and damping matrix.

$$\mathrm{F}_{Load}^{\top} = \left\langle 0 \quad 0 \quad \cdots \quad 0 \quad 0 \quad 0 \quad \cdots \quad 0 \quad 0 \quad Axel_{Load,v} \right\rangle \tag{3.2}$$

$$\begin{bmatrix} M_b & 0 \\ 0 & M_v \end{bmatrix} = \begin{bmatrix} m_{1,1} & m_{1,2} & \cdots & m_{1,i-1} & m_{1,i} & m_{1,i+1} & \cdots & m_{1,n-1} & m_{1,n} & 0 \\ m_{2,1} & m_{2,2} & \cdots & m_{2,i-1} & m_{2,i} & m_{2,i+1} & \cdots & m_{2,n-1} & m_{2,n} & 0 \\ \vdots & \vdots & \ddots & \vdots & \vdots & \vdots & \ddots & \vdots & \vdots & \vdots \\ m_{i-1,1} & m_{i-1,2} & \cdots & m_{i-1,i-1} & m_{i-1,i} & m_{i-1,i+1} & \cdots & m_{i-1,n-1} & m_{i-1,n} & 0 \\ m_{i,1} & m_{i,2} & \cdots & m_{i,i-1} & m_{i,i} & m_{i,i+1} & \cdots & m_{i,n-1} & k_{i,n} & 0 \\ m_{i+1,1} & m_{i+1,2} & \cdots & m_{i+1,i-1} & m_{i+1,i} & k_{i+1,i+1} & \cdots & m_{i+1,n-1} & m_{i+1,n} & 0 \\ \vdots & \vdots & \ddots & \vdots & \vdots & \vdots & \ddots & \vdots & \vdots & \vdots \\ m_{n-1,1} & m_{n-1,2} & \cdots & m_{n-1,i-1} & m_{n-1,i} & m_{n-1,i+1} & \cdots & m_{n-1,n-1} & m_{n-1,n} & 0 \\ m_{n,1} & m_{n,2} & \cdots & m_{n,i-1} & m_{n,i} & m_{n,i+1} & \cdots & m_{n,n-1} & m_{n,n} & 0 \\ 0 & 0 & \cdots & 0 & 0 & 0 & \cdots & 0 & 0 & m_v \end{bmatrix} \tag{3.3}$$

As in previous cases consisting of either a moving load or a moving mass model, the Newmark's method is modified and implemented considering the current approach of a SMM. Due to the simplified principles, the proposed SMM can be solved as a linear system. In order to avoid the "Out of Memory" error, each of the time variant stiffness and damping matrices are calculated and used temporarily within each relevant loop of the Newmark's method.

3.2 Verification of Proposed Program

Prior to performing an analysis, it is crucial to verify the legitimacy of both the new spring support algorithm and the proposed sprung mass model. Both of these algorithms are verified using different relevant reference cases. The moving load and moving mass model are implemented when verifying the proposed spring support algorithm. The reference cases ''Norddalsbrua 1" and ''Norddalsbrua 2" are used as a basis from A.M. Al-Kanany [1]. For the introduction of a sprung mass model, which also implements the spring support algorithm, a different case is introduced to verify the proposed VBI model separately.

3.2.1 Verification of Spring Support Algorithm

As a reference, "Norddalsbrua 1", which is a single span 50 m long railway bridge previously presented by A.M. Al-Kanany [1], is first used when verifying the proposed spring support algorithm. This reference case consisting of a traversing heavy freight train with multiple defined axles is used to further verify the following algorithm. From Table 3.1, relevant properties for the MATLAB software of both the bridge and the train are presented for the reference case consisting of one span. When comparing the results, the spring stiffness is set to $1x10^{10}$ kN/m to replicate the behaviour of a restricted DOF. The reference algorithm consisting of rigid supports have previously been verified by A.M. Al-Kanany [1] using SAP2000 as a basis. Both the moving load and moving mass model are compared with the reference case individually. Several comparisons are made with regards to natural frequencies, displacements and accelerations. These are shown through the following figures, in which the remaining of these are presented in Appendix C.

Table 3.1: Properties of Norddalsbrua 1 [1].

Bridge Properties		Train Properties	
Young's Modulus	32 GPa	Speed	50 km/h
Area of Intertia	16, 89 m^4	Train type	Iron-ore train
Density	2.55 $tonn/m^3$	Axles	272
Length	50 m	Time step	0, 005 s
Damping Ratio		Meshing Properties	
Damping Ratio	2 %	Total elements	50
Desired modes	1 & 4	Element length	1 m

Table 3.2: Properties of Norddalsbrua 2 [1].

Bridge Properties		Train Properties	
Young's Modulus	32 GPa	Speed	50 km/h
Area of Intertia	16, 89 m^4	Train type	Iron-ore train
Density	2.55 $tonn/m^3$	Axles	272
Length	44 $m + 41$ m	Time step	0, 005 s
Damping Ratio		Meshing Properties	
Damping Ratio	2 %	Total elements	85
Desired modes	1 & 4	Element length	1 m

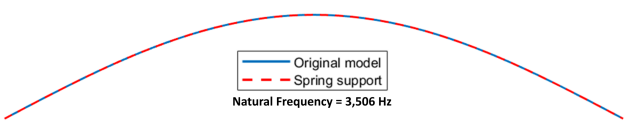

(a) First mode of vibration.

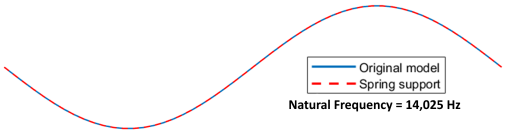

(b) Second mode of vibration.

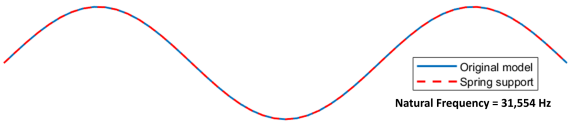

(c) Third mode of vibration.

Figure 3.10: Comparisons of mode shapes between proposed algorithm and reference case with single span.

The modal analysis calculated through the proposed algorithm brings identical results to the reference case. Given this similarity, it can further be deduced that the proposed algorithm has the same pattern of deviation from SAP2000 as the reference algorithm developed by A.M. Al-Kanany [1].

The displacement and acceleration at the midpoint of the reference bridge are further compared with the reference. Both the spring support algorithm and reference algorithm bring identical plots when using the moving load model.

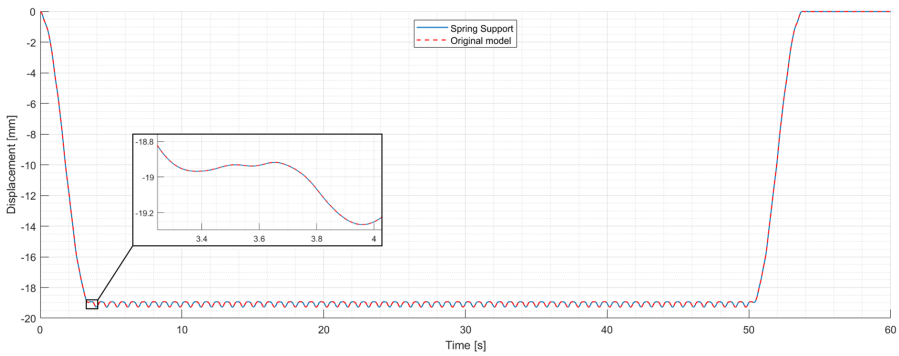

Figure 3.11: Comparison of displacement at midspan for "Norddalsbrua 1" reference case for moving load model.

When further including the mass from the traversing train, the mass matrix of the structure changes by each time increment when using the moving mass model. Both the mode shape and the natural frequency of the bridge change with each time increment as a result. Modal analysis is therefore excluded when verifying the proposed spring support algorithm for the moving mass model. Instead, comparisons are directly made for both the displacement and acceleration at the midpoint of the reference bridge. When comparing the spring support algorithm with the reference plot, it is evident that both the displacement and acceleration at the midpoint become almost identical. Though negligible, small differences can still be observed when implementing elastic spring supports. This can mainly be explained by how the spring supports consist of a finite stiffness, which means a small movement is still allowed at the supports. For the rigid supports, these motions are defined as zero instead.

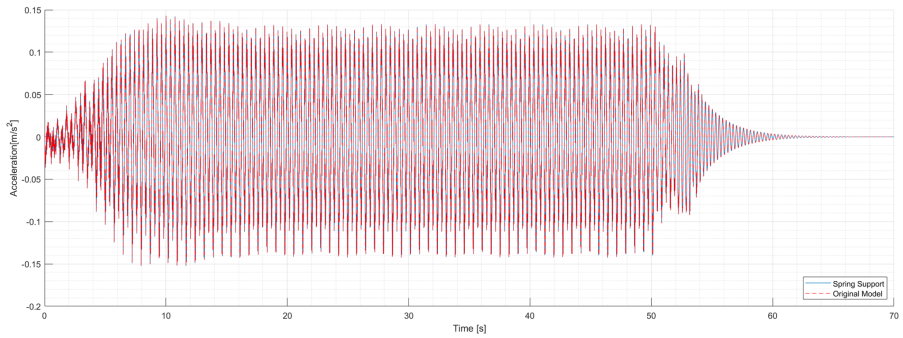

Figure 3.12: Comparison of accelerations at midspan of "Norddalsbrua 1" reference with moving mass model.

When verifying the algorithm for continuous multiple spans, the verification case is adjusted accordingly. For the following comparison, ''Norddalsbrua 2" is used as a reference case with the same properties previously used by A.M. Al-Kanany [1], which is further presented through Table 3.2. This reference bridge consists of two spans, where the first span is 44 m long, while the second span is 41 m. As in the previous reference, the modal frequencies, displacements, and accelerations are compared at midpoint of the first span for the moving load and moving mass models. The remaining plots of these comparisons are also presented through Appendix C. For both the moving load and moving mass model, the results from the modal analysis, displacements, and accelerations at the midpoint of the first span calculated through the spring support algorithm are almost identical to the reference algorithm with rigid supports. Again, a negligible difference is observed due to the finite stiffness of the supports, which allows for small motions on the supports, these motions are not considered when using rigid supports.

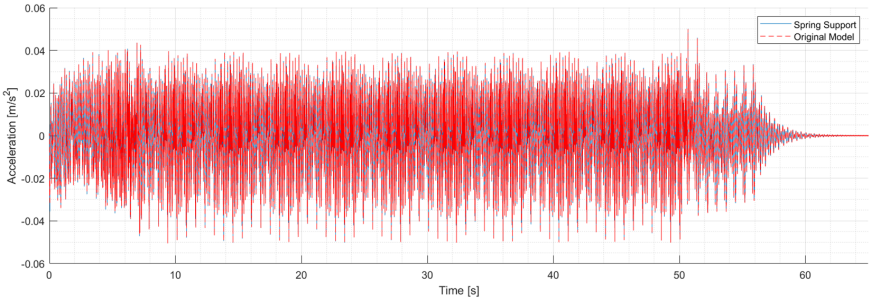

Figure 3.13: Comparison of accelerations at first midspan of "Norddalsbrua 2" with moving load model.

When using the references that either consists of a simply supported bridge or a continuous multi-span bridge, all the comparisons with the reference algorithm can be regarded as identical. Although further comparisons can be made due to the complexity of the reference case, the following results are deemed as sufficient proof. Nonetheless, there is still a possibility that an error may emerge, and it is therefore recommended to stay aware of the legitimacy of the results when they may seem unrealistic.

3.2.2 Verification of Sprung Mass Algorithm

With the introduction of a sprung mass model (SMM), it is further necessary to verify the results, which are calculated through the proposed algorithm also consisting of spring supports. Various studies use different references when comparing these relevant results. Studies such as Yang et al. [10] and Majka et al. [5] use a verification case initially presented by Biggs et al. [31], which consists of a simply-supported beam traversed by a single sprung mass. A majority of studies regarding the use of a sprung mass model often use this simple yet efficient reference when verifying the proposed SMM. Comparisons are made by using the deflection and acceleration at the midpoint of the beam and of the single sprung mass as a basis. In this case, all damping, both for the sprung mass and the beam is neglected while only vertical movement is considered as well. The elastic spring supports have a stiffness of $1x10^{10}\ kN/m$ to replicate the behaviour of rigid supports.

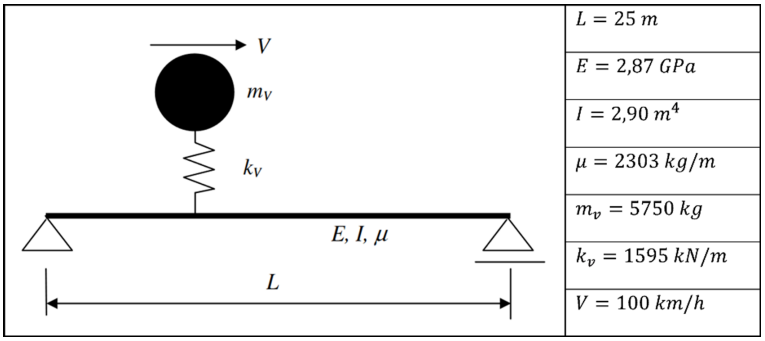

Figure 3.14: Verification case [5].

After implementing the defined data related to the verification case, it is possible to compare the dynamic response that has been calculated. The results plotted for the proposed SMM is compared with graphs by Yang et al. [10]. These graphs present both an analytical and a proposed numerical solution. The current analytical solution only considers the first mode of vibration for both the bridge and the sprung mass.

Initially, it was observed that the graph presented by the proposed SMM was shifted one time step ahead of the reference. This was promptly tended to by moving the gathered results one time step backwards. After passing this trivial issue, the results gathered from the proposed model proved almost identical to the analytical solution. It can further be observed that the current model achieves closer results to the analytical solution than the proposed SMM made by Yang et al. [10], which also achieves accurate results and is quite similar.

Meanwhile, the acceleration at the midspan from the proposed model becomes significantly different from the analytical solution presented. The following analytical expression is idealized by only considering the first mode of vibration, meanwhile, both the proposed sprung mass models further consider all modes of vibration. When

regarding acceleration, the higher modes of vibration become more significant when compared to the first mode, hence the following difference occurs. Certain similarities for the acceleration can still be observed with the moving load and moving mass model, which is presented by Yang et al. [10]. This further provides as evidence for the previous statement.

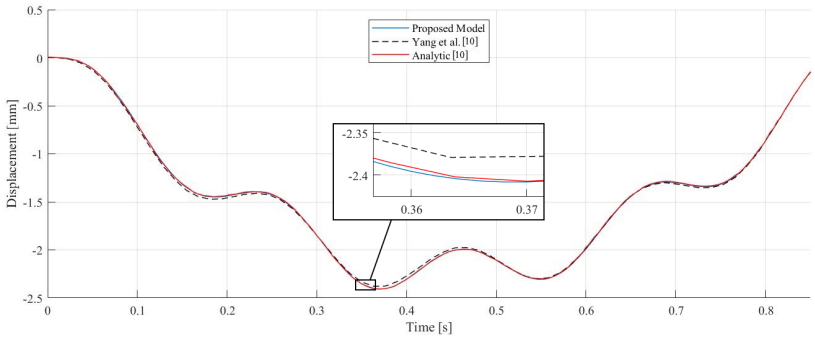

Figure 3.15: Comparison of midpoint vertical deflection of reference beam.

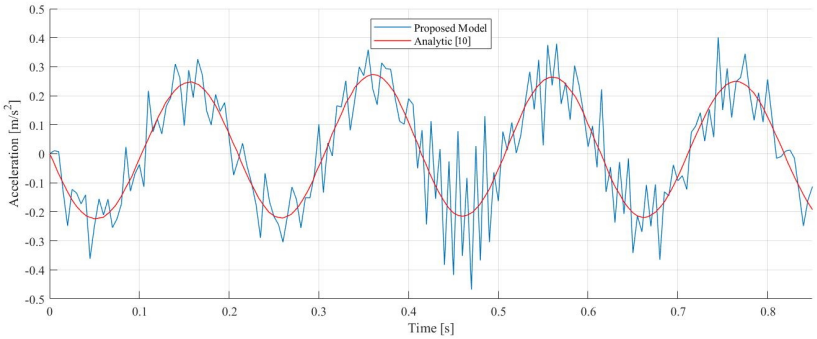

Figure 3.16: Comparison of midpoint vertical acceleration of reference beam.

Using the same reference case, plots are further gathered on the vertical deflection and acceleration of the single traversing sprung mass. From what can be observed, the plots from the proposed SMM become almost identical to the SMM presented by Yang et al. [10]. Both of these models are different from the analytical plot. This difference occurs due to the analytical solution only considering the first mode vibration. When comparing this effect between the plots from the midpoint of the beam and the sprung mass, it is further shown that the deflections of the sprung mass is more sensitive to the higher modes of vibration than the beam. For the acceleration, both cases become significantly affected by the higher modes of vibration.

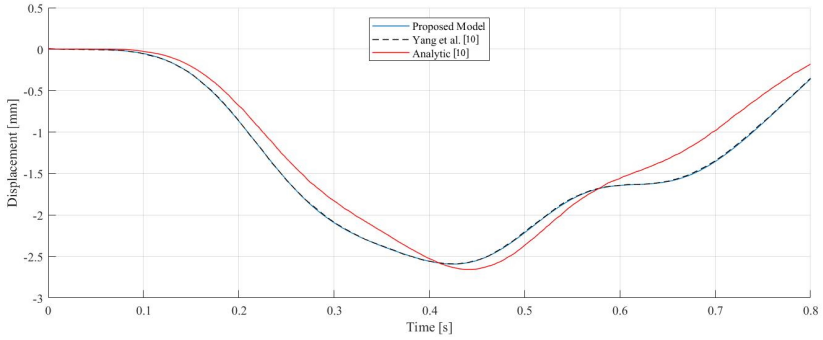

Figure 3.17: Comparison of deflection on reference sprung mass.

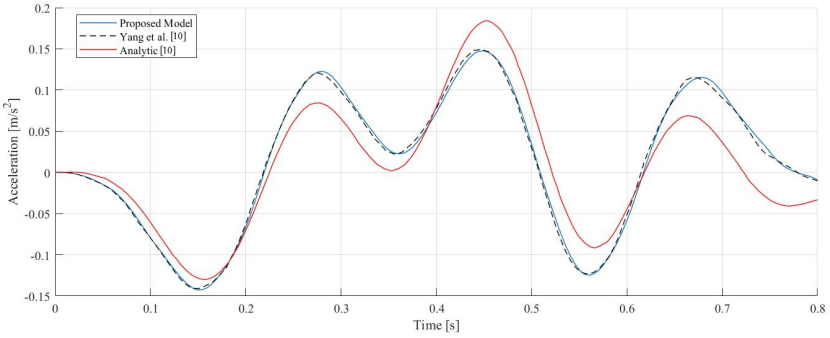

Figure 3.18: Comparisons of acceleration on reference sprung mass.

The proposed sprung mass model can further replicate either a moving load or a moving mass model. By making the spring stiffness and damping equal to zero for the traversing sprung mass, the effect of inertia becomes neglected. This makes it possible to replicate the special case of a moving load model. When implementing a relatively high value for these same parameters, the proposed sprung mass model replicates a moving mass model instead.

Using the previous reference case for the sprung mass model, different plots are compared between the proposed SMM replicating the relevant VBI models and the code developed by A.M Al-Kanany [1] with rigid supports. The support stiffness for the SMM is $1x10^{10}\ kN/m$ to replicate rigid supports. When observing the displacement and acceleration for both these comparisons, it is evident that the plots from the proposed SMM becomes almost identical to the equivalent moving load and moving mass model made by A.M Al-Kanany [1]. Some minuscule difference occurs, this can be explained by the small movements on the supports, which are allowed through the relatively stiff SMM. The remaining comparisons are presented within Appendix D.

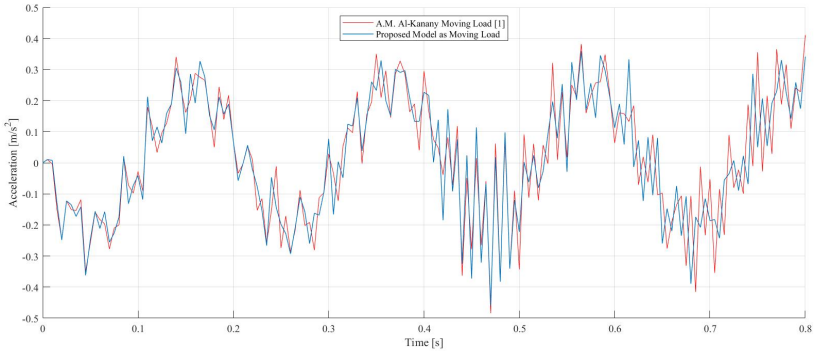

Figure 3.19: Comparison of acceleration at midspan with moving load model and proposed sprung mass model.

Through methodical comparisons made with different reference cases, both the proposed spring support algorithm and sprung mass model have been verified to provide accurate calculations. Using this as a basis, a parametric study is conducted onwards.

4 Parametric Study

With the development and verification of the proposed planar sprung mass model with elastic spring supports, it is further of interest to perform a parametric study which considers the implementation of such a proposed numerical model given varying parameters. Although a significant number of different studies has previously been conducted using the sprung mass model and is relevant for the current study [13], almost none of these have directly considered the effect of such a VBI model in terms of elastic bearings. Previous studies regarding the effect of elastic bearings on the dynamic response of railway bridges have generally been conducted by implementing the moving load model [14]. Using the simplicity of the moving load model, studies further tend to investigate different phenomena when using an analytical approach, which is often approximated to finalize simple closed-form solutions [15, 16].

In contrast with a moving load model, the sprung mass model brings a different mode of vibration for the relevant railway bridge due to the time dependent stiffness and damping matrix, which changes with the additional contributions in terms of stiffness and damping from the traversing train on the structure. This makes the concept of modal superposition unreliable. These are some of many factors which make it unsustainable to generalize and analytically express the following parametric study. Hence, more of a physical interpretation will be made when using realistic parameters of both the train and bridge to gain a better understanding of the complex relationship between both these subsystems. By varying parameters such as the vertical stiffness on the supports, velocity of the traversing train and number of bridge spans, it is possible to determine the significance of each parameter with the following proposed numerical model.

4.1 General Parameters through the Parametric Study

The following parametric study is based upon ''Norddalsbrua 1", which is a 50 m long single-span prestressed concrete bridge. The relevant properties of this bridge have been defined in the previous thesis conducted by A.M. Al-Kanany [1] and a related paper written by E. Erduran et al. [14]. With reinforced concrete, the modulus of elasticity is assumed as 32 GPa, while the moment of inertia about the main bending axis is $16,89\ m^4$ with an area of $6,81\ m^2$. Considering this defined area, the mass of the bridge is distributed with a value of 0,4865 tonnes/m. This value considers both the self-weight of the reinforced concrete and the additional non-structural elements such as the ballast and railway track. As with most concrete bridges, the damping ratio of the bridge is assumed to be 2 %. Given the need to frequently discretize the bridge due to the principle of the proposed sprung mass model, the rate of discretization varies with each train speed.

While each end of the railway bridge is free to rotate, the same ends are relatively restricted in terms of vertical movement throughout the current dynamic analyses. Horizontal movement on the first support of the bridge is also restricted. The elastic springs supporting each end of the single-span railway bridge are defined with a vertical stiffness $k_{support}$ and are assumed to be massless in this case. Meanwhile, the traversing separate sprung masses are defined through m_v , k_v and c_v, which represent the relevant train mass, suspension stiffness and dashpot respectively.

When studying the accelerations on the relevant railway bridges, the criteria established through NS-EN 1990 becomes important when evaluating the accumulation of the dynamic response on the bridge. Through this standard, the suggested limit of acceleration on the bridge becomes $3,5\ m/s^2$ [7].

When conducting the following parametric study, the configuration, and data from an ICE-2 train is used as a reference onwards when imposing the traversing load, this standard passenger train being frequently used throughout Germany. The original train, which will be used in the following study, consists of 12 carts and a locomotive at each end, with the relevant axle configuration presented through Figure 4.1. The total number of axles is 56.

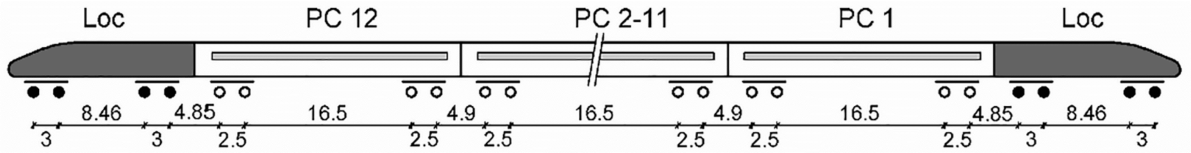

Figure 4.1: Axle distance and configuration for a typical ICE-2 train [6].

In terms of using a planar two degree of freedom sprung mass model, certain adaptations are made when further expressing the relevant parameters for the current ICE-2 train through Table 4.1. Given the limitations of the proposed SMM, the relatively small mass contribution from the cartwheels is neglected.

Table 4.1: Parameters of planar sprung mass for an ICE 2 train [6].

Component	**Value**	**Unit**
Body mass	19,995	t
Suspension stiffness	4800	kN/m
Suspension damping	109	kNs/m

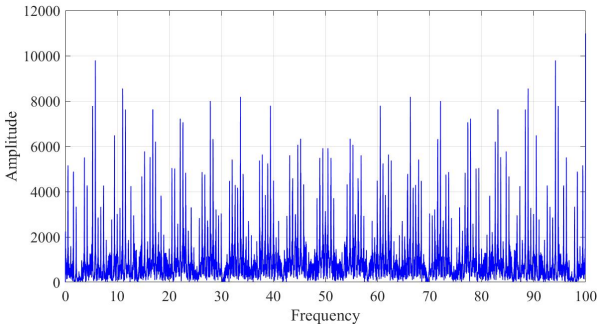

(a) Train velocity of 50 km/h.

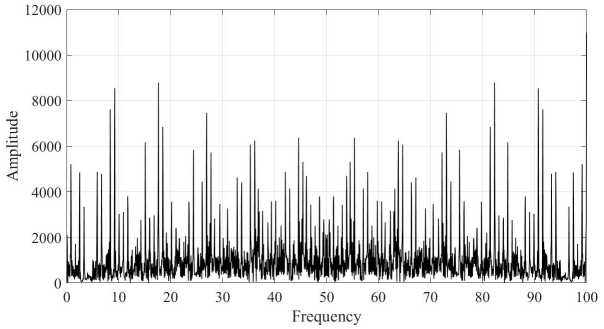

(b) Train velocity of 80 km/h.

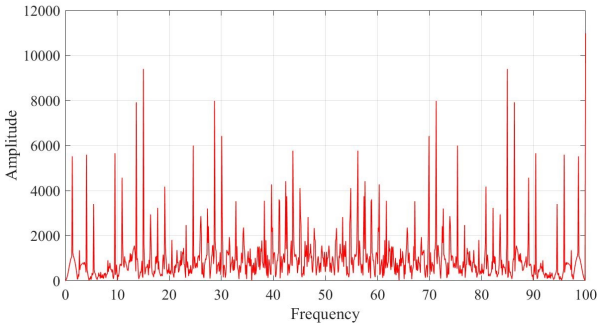

(c) Train velocity of 130 km/h.

Figure 4.2: FAS of loading frequency for each train velocity from traversing ICE-2 train.

4.2 Single-Span Bridge

Using the general parameters previously introduced, a single-span railway bridge is first analysed. Together with the previously defined ICE-2 train, the support stiffness and the train velocity is varied through this chapter while implementing the proposed sprung mass model. As these parameters are varied, the maximum acceleration and acceleration response of the railway bridge is studied in this chapter.

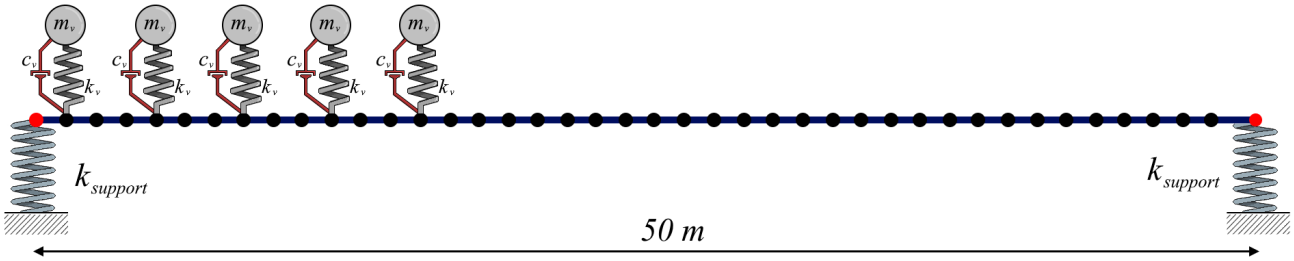

Figure 4.3: Overview of proposed sprung mass model with elastic vertical spring supports on each end.

First, with the defined single-span bridge, it is of interest to study how varying the support stiffness affects the natural vertical bridge frequency. This is necessary to understand, as the following factor defines the planar dynamic response of the railway bridge. As the ICE-2 train traverses the bridge, each modal frequency changes at most by 1%. This means that the initial modal frequencies mostly define the dynamic response of the structure in this case.

Through Figure 4.4, the corresponding modes of vibration to the relevant support stiffness (hereby termed as k_s) is presented. When implementing $k_s \geq 1x10^8\ kN/m$, the modal frequencies remain almost constant to each other. As $k_s < 1x10^8\ kN/m$, the modal frequencies significantly lower for each of the relevant modes of vibration, the modes of vibration above *Mode 2* changing more drastically. For $k_s < 1x10^6\ kN/m$, the modal frequencies become constant to each other again. This behaviour is an indication of a *threshold value* at $k_s = 1x10^7\ kN/m$, which will be taken into consideration along this analysis. Values of the corresponding natural bridge frequencies for the single-span railway bridge are also presented within Appendix E.

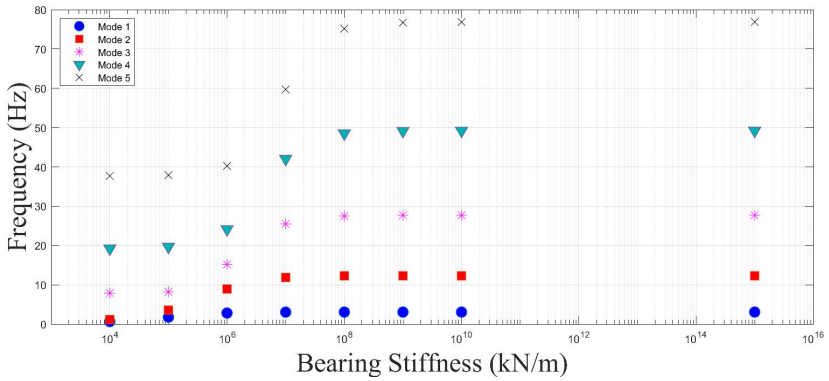

Figure 4.4: Natural vertical frequencies of single-span bridge with varying support stiffness.

4.2.1 Absolute Maximum Acceleration Envelope Curve for Single-Span Bridge

Through envelope curves consisting of the absolute maximum acceleration (AMA) on every meter of the bridge, it is possible to determine where the highest value of acceleration develops as the ICE-2 train traverses each relevant case. Due to the principles of the current sprung mass model, it is necessary to avoid the "*jumping*" phenomenon, which occurs when having a low ratio between the discretization and relative velocity of the traversing train. The number of elements per meter (epm) varies with every speed that is presented through Figure 4.5. With a velocity of 50 km/h, 80 km/h and 130 km/h, it is necessary with 20 epm, 40 epm and 80 epm respectively when capturing the sensitive acceleration.

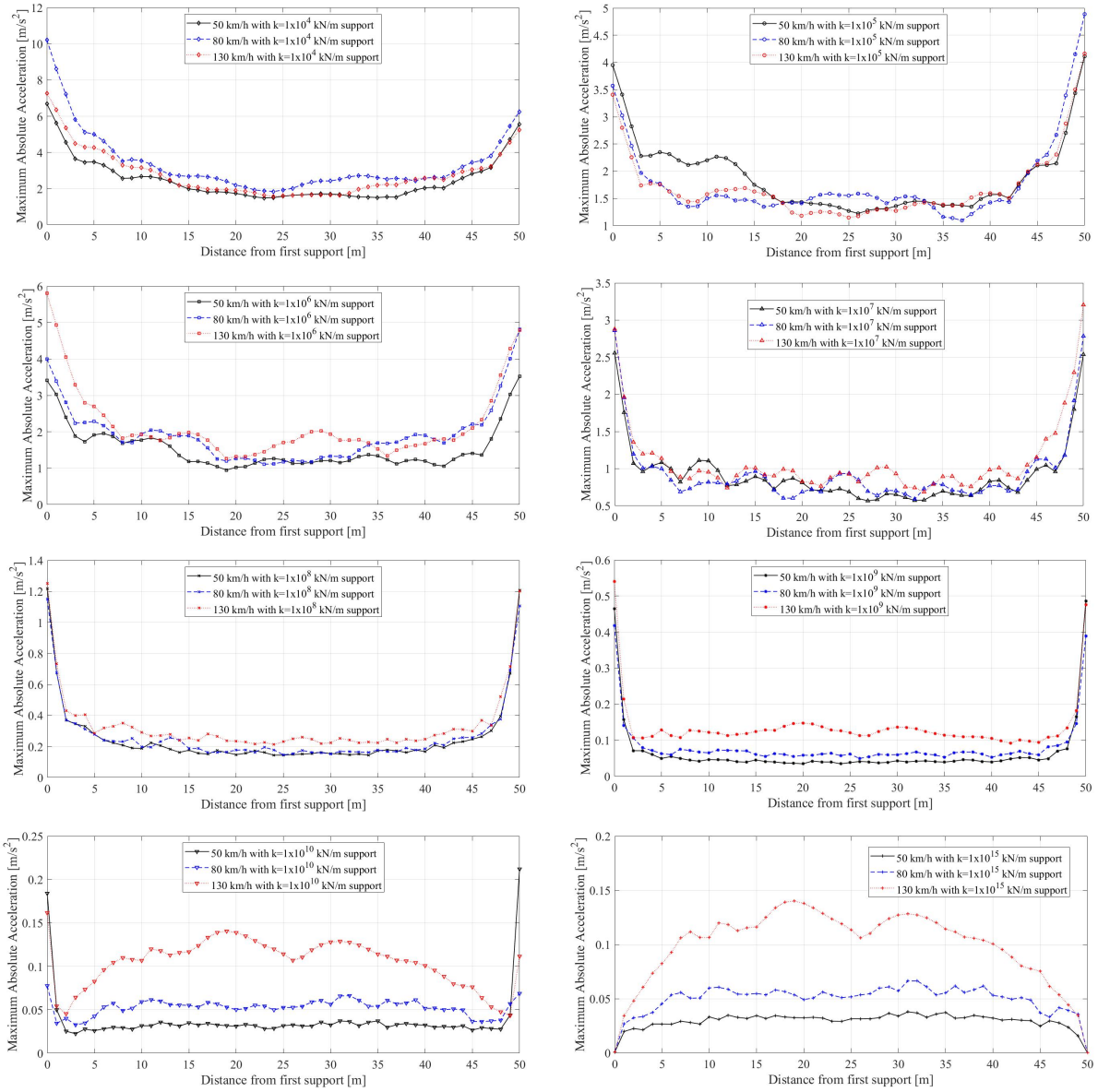

Figure 4.5: AMA envelope curves for single-span bridge.

Through the AMA envelope curves presented in Figure 4.5, the maximum generally develops at the midspan of the railway bridge for every train velocity where $k_s > 1x10^9\ kN/m$. While this is the case, for $k_s = 1x10^{10}\ kN/m$, a drastic increase in maximum acceleration is observed at each end of the railway bridge. This is an indication of a potential numerical inaccuracy, which will be discussed later.

It is observed for all the train velocities where $k_s \leq 1x10^9\ kN/m$, the largest values of acceleration develop on the supports at each end of the railway bridge instead. As the results may become unstable near the supports, through Figure 4.6, relevant examples of the time-history for the acceleration occurring on the supports are presented in order to ensure some stability of the gathered AMA. Although a higher train velocity is related to a higher value of acceleration, certain cases with $k_s < 1x10^8\ kN/m$ create a local variation in which lower train velocities become dominant. This phenomenon can be related to a potential resonance that is achieved with a lower train velocity.

While considering the threshold value previously presented through Figure 4.4 for the modal frequencies of the corresponding support stiffness, it is shown that the development of the maximum acceleration at the midspan mainly follows the development of the modal frequencies with varying support stiffness. For the relatively rigid supports where $k_s \geq 1x10^8\ kN/m$, the maximum acceleration remains quite constant. For $k_s \leq 1x10^7\ kN/m$ beyond the threshold value, the maximum acceleration increases significantly with more local variations as the stiffness lowers.

A special case regarding the following development is observed for $k_s = 1x10^6\ kN/m$ in which the maximum acceleration generally becomes greater than $k_s = 1x10^5\ kN/m$. This contradicts the previous statement regarding the development of maximum acceleration along the single-span railway bridge. A significant increase in acceleration for 50 km/h with a value near $2,5\ m/s^2$ at $k_s = 1x10^5\ kN/m$ is also of interest for further study. To fully understand this behaviour, it is necessary to implement the Fourier Amplitude Spectrum (FAS).

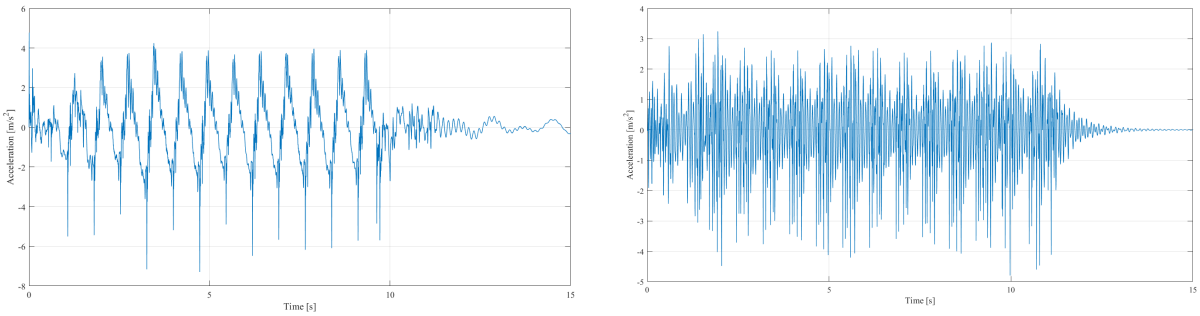

(a) First support with support stiffness 1e4 kN/m.

(b) Last support with support stiffness 1e6 kN/m.

Figure 4.6: Example of time-history for acceleration on supports with 130 km/h.

4.2.2 Frequency Domain for Single-Span Bridge

By further gathering the time-history of the accelerations occurring at the midpoint of the railway bridge, *Fast Fourier Transformation* (FFT) is implemented in the MATLAB software, which is presented through a Fourier Analysis Spectrum (FAS). Through this spectrum, relevant frequencies of the bridge are sorted and scaled to each other through an amplitude. In the following analysis, the FAS is used as a tool to observe which frequencies become dominant when defining the dynamic response of the bridge. This means that only the relation between the amplitudes is of significance. The FAS for each support stiffness is therefore further normalized separately about the maximum amplitude value for the relevant support stiffness. This provides a better overview between each case in the development of the dominant frequencies and relevant modes of vibration. In this analysis, both the loading frequencies presented in Figure 4.2 and the modal frequencies in Figure 4.4 are considered while analysing the relevant FAS.

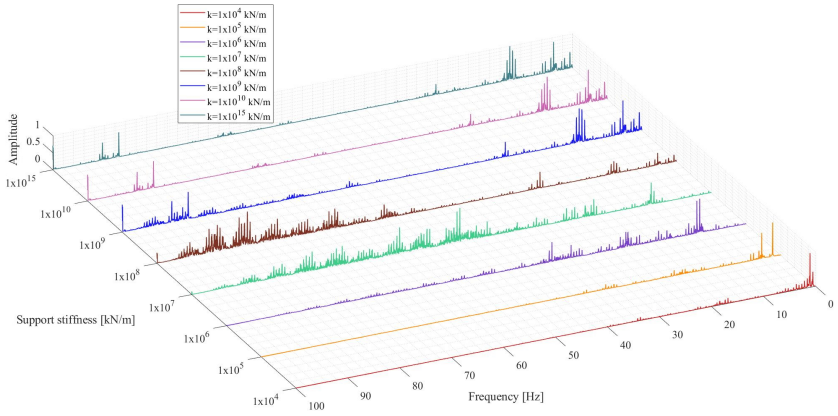

Figure 4.7: Fourier Amplitude Spectrum at midspan with 50 km/h train velocity.

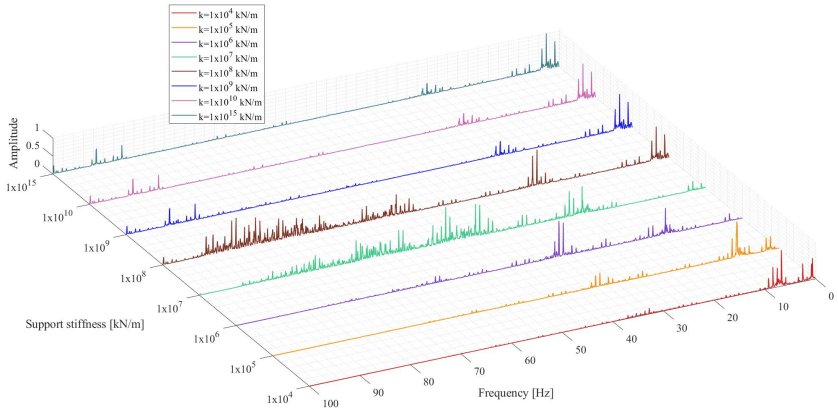

Figure 4.8: Fourier Amplitude Spectrum at midspan with 80 km/h train velocity.

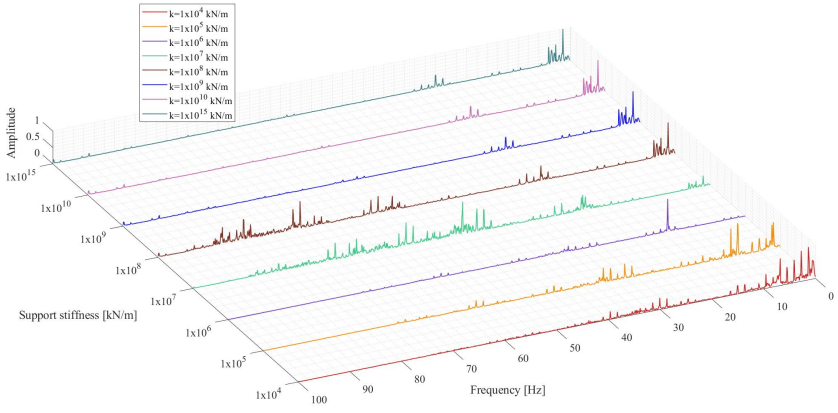

Figure 4.9: Fourier Amplitude Spectrum at midspan with 130 km/h train velocity.

When studying the train velocities separately through the FAS, it is evident that the ratio of dominant frequencies show little change within each respective velocity when the support stiffness is (hereby termed as k_s) greater than or equal to $1x10^9$ kN/m. In this case, most of the maximum amplitudes are achieved at lower frequencies near 3 Hz, which indicates that the first mode of vibration (see Figure 4.4) becomes dominant as it achieves resonance with the loading frequency for all train velocities (see Figure 4.2). Additional peaks with varying significance are also observed between 10-15 Hz, 20-30 Hz and 80-90 Hz, which indicate a prevalence of the second, third and fourth mode of vibration respectively.
Although the ratio of frequencies remains relatively constant while implementing $k_s > 1x10^8$ kN/m, when further comparing the FAS between each train velocity, a significant increase in amplitude is observed near 12,5 Hz with a train velocity of 50 km/h. Through Figure 4.2a and 4.4, the following response is an indication that the loading frequency at 50 km/h coincides more with the second mode vibration of the bridge. The frequencies gathered with $k_s = 1x10^8$ kN/m is quite similar below 50 Hz to these stiffer supports.

Several differences are observed when comparing the FAS between $k_s = 1x10^8$ kN/m and the stiffer supports. In general, for each train velocity, a less distinct response emerges over 50 Hz for the respective support stiffness in which several concentrations of peaks are observed. Each of these represent potential resonance occurring between the higher modes of vibration and the relevant loading frequency.
Below 50 Hz, with a train velocity of 50 km/h and $k_s = 1x10^8$ kN/m , lower amplitudes between 0-15 Hz are shown, while for the loading frequency at 80 km/h, a significant increase in amplitude is observed between 20-30 Hz. Although the modal frequency remains almost identical to the stiffer supports, the minuscule change may explain how the first and second mode of vibration coincides less, while the third mode of vibration coincides better at 80 km/h. At 130 km/h, the amplitudes remains identical to the stiffer supports.
When lowering the stiffness to $k_s = 1x10^7$ kN/m, similar results to $k_s = 1x10^8$ kN/m are also generally observed. In this case, the less distinct concentration of peaks over 50 Hz through the FAS is shifted towards a lower frequency for $k_s = 1x10^7$ kN/m. The first mode of vibration also becomes less prevalent for all train velocities.

Through the FAS at $k_s = 1x10^6$ kN/m, the frequencies become more distinct again. Between each train velocity, the dominant frequencies vary. For all train velocities, the loading frequency coincides at 15 Hz with the third mode of vibration. This is especially true for the train velocity at 130 km/h with almost no energy anywhere else. While the third mode of vibration is less prevalent at 80 km/h, the fourth mode of vibration becomes more dominant near 40 Hz instead. To better show the condition of resonance, the following phenomena between the dominant loading frequency at 130 km/h, the FAS from $k_s = 1x10^6$ kN/m at the midspan together with the corresponding initial natural bridge frequency is presented through Figure 4.10. Through this figure, it is shown how all these factors coincide with each other.

For the less stiff supports where $k_s < 1x10^6$ kN/m, it is evident that lower frequencies define the response of the railway bridge in the FAS. At $k_s = 1x10^5$ kN/m, the dominant frequency at 8,3 Hz for both the train velocities 130 km/h and 80 km/h indicate that the third mode vibration of the bridge contributes. The second mode vibration of the bridge also becomes dominant for 50 km/h and 130 km/h at 1,6 Hz, which coincides with the first mode vibration of the bridge.

The lowest stiffness at $k_s = 1x10^4\ kN/m$, creates a different response for each train velocity. At 130 km/h, the dominant frequency becomes less distinct, though it is apparent that most of the contribution is between 0 to 10 Hz. For 80 km/h, more distinct frequencies from the first and second mode vibrations near 0,66 Hz and 7,9 Hz coincides with the relevant loading frequency. At 50 km/h, most of the contribution comes from 0,5 Hz and 1,1 Hz, which derives from the first and second mode respectively.

Although the mentioned frequencies coincide with the relevant loading and natural bridge frequencies, some margin is implemented. The difference in alignment between the gathered response of the bridge through the FAS, initial natural bridge frequencies and corresponding loading frequencies will therefore be discussed later on.

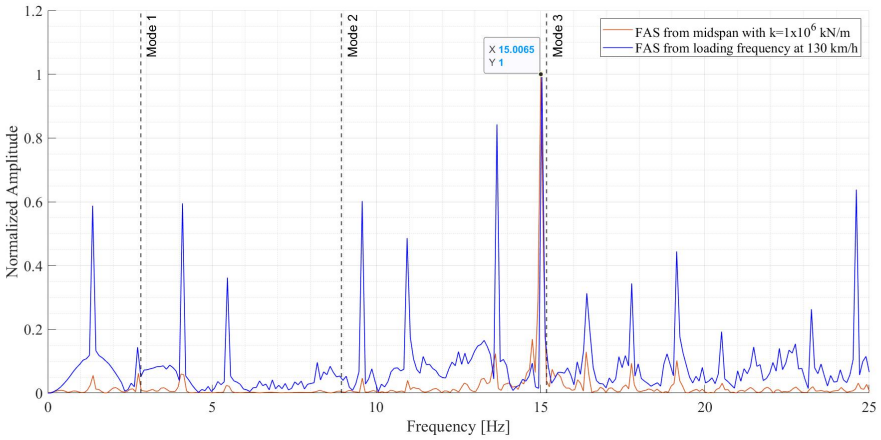

Figure 4.10: Example of necessary condition between each factor to achieve resonance.

In summary, when considering all the previous results presented for the single-span bridge, it is evident that the response of the railway bridge is sensitive to changes in the support stiffness. The threshold value first presented through Figure 4.4 for the different modal frequencies becomes prevalent both for the AMA envelope curves and the FAS at the midspan of the corresponding railway bridge. It is also shown that while the maximum generally occurs at each end of the bridge when $k_s \leq 1x10^{10}\ kN/m$, certain peaks in value for maximum acceleration are observed through the length of the bridge. When also considering the following FAS at the midspan, it is evident that the location of these peak values correlates with the dominant mode vibration of the bridge. With this, it is also important to understand that the reduction in support stiffness also influences the relevant mode shapes themselves. As $k_s \leq 1x10^7\ kN/m$, the third mode vibration of the bridge generally dominates the behaviour of the single-span bridge, which is also shown by the local maximums of acceleration moving towards each end of the bridge instead of the middle.

4.3 Symmetrical Two-Span Railway Bridge

Following the parameters established through the previous single span bridge, it is further of interest to study what effect such supports have for a continuous two-span bridge as well. In this case, an additional elastomeric support is placed in the middle of the 50 m long span of the bridge. As a result, each span of the symmetrical two-span continuous bridge is at 25 m. Since the previously defined ICE-2 train is still implemented, the loading frequencies from Figure 4.2 continues to become relevant for the multi-span bridges.

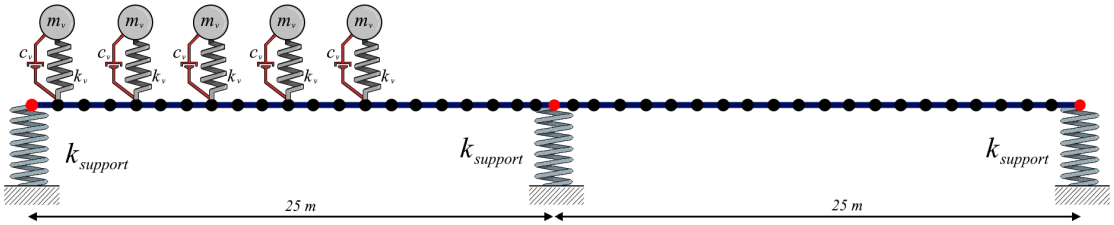

Figure 4.11: Overview of proposed sprung mass model with two-span bridge supported by elastic vertical springs.

As in the previous case for the single-span bridge, the corresponding vertical modes of vibrations for each support stiffness is presented for the two-span bridge. For the modal frequencies where $k_s > 1x10^8\ kN/m$, each modes of vibration remains almost constant. At $k_s = 1x10^8\ kN/m$, the modes of vibration higher than *Mode 3* start to reduce. When approaching the *threshold value* of $k_s = 1x10^7\ kN/m$, all the modes of vibration drastically reduce. Again, when $k_s < 1x10^7\ kN/m$, each mode of vibration becomes relatively constant with some changes for the modes higher than *Mode 2*. The following initial natural bridge frequencies for multi-span bridges are further presented through tables within Appendix E.

In comparison with the single-span bridge, the modal frequencies remain similar when $k_s < 1x10^5\ kN/m$. When the stiffness increases to $k_s > 1x10^7\ kN/m$ beyond the threshold value, the modal frequencies become much higher compared to the single-span bridge. This implies that the additional support does not significantly affect the modal frequencies until a higher value of stiffness is implemented.

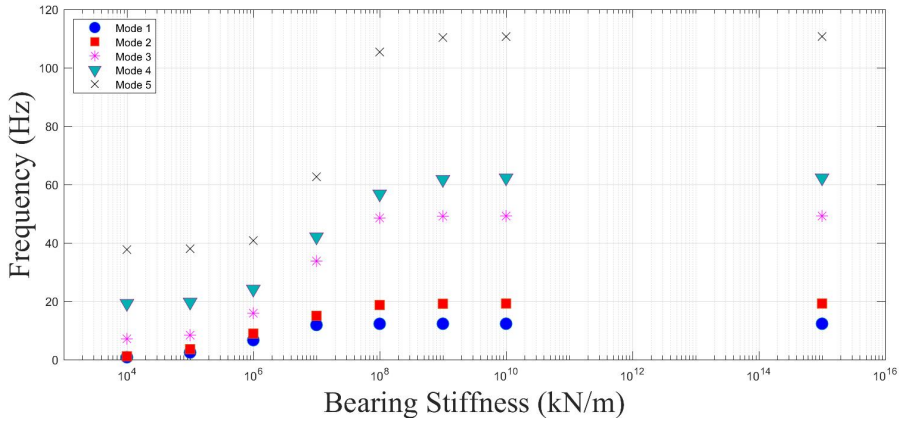

Figure 4.12: Natural vertical frequency of two-span bridge with varying support stiffness.

4.3.1 Absolute Maximum Acceleration Envelope Curve for Symmetrical Two-Span Bridge

By implementing an additional support, it is of interest to study how this affects the AMA envelope curves for each train velocity and support stiffness. Following the same principle for 50 km/h, 80 km/h and 130 km/h, the bridge is discretized for each case with 20 epm, 40 epm and 80 epm respectively to accurately gather the acceleration of the railway bridge.

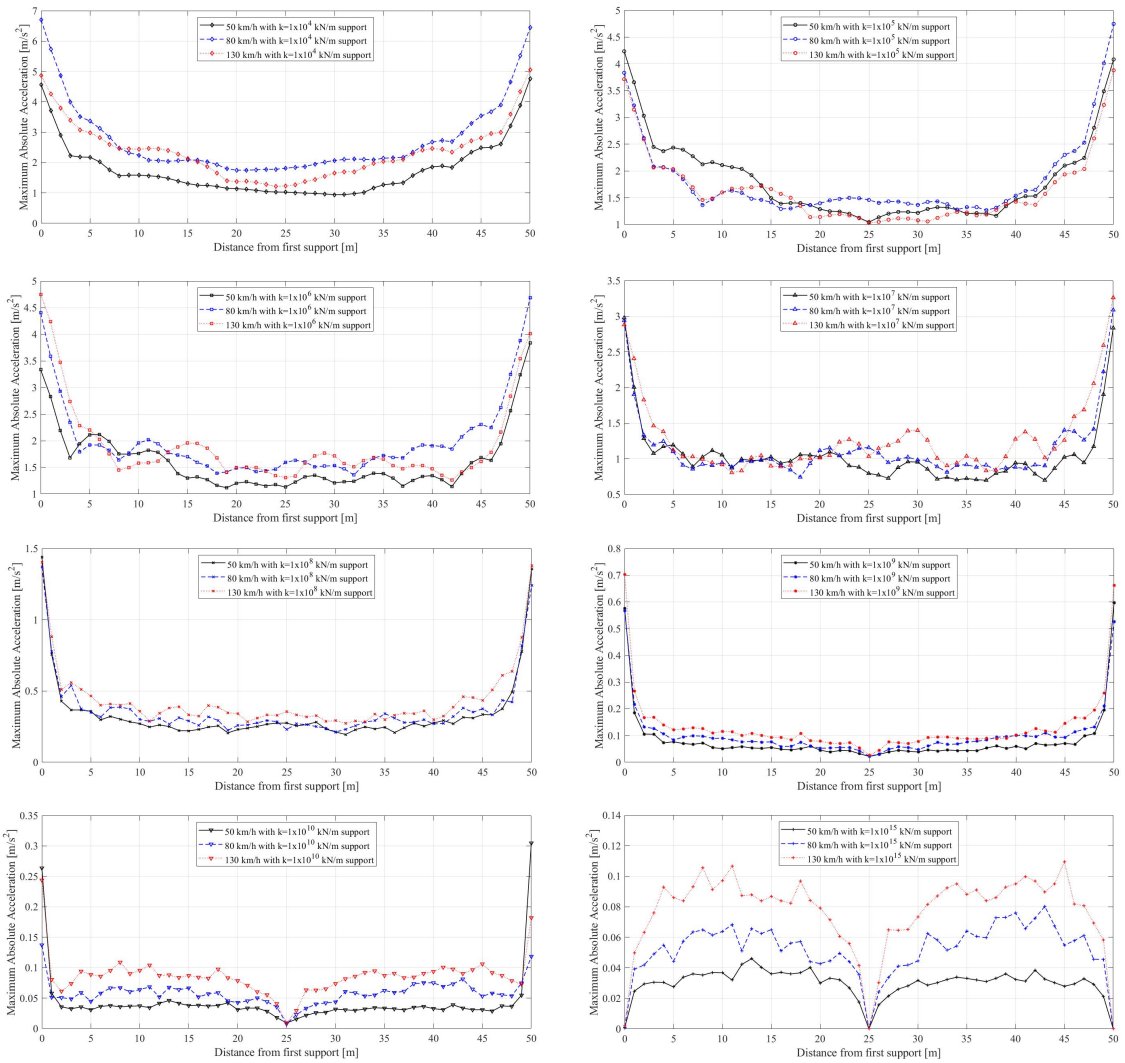

Figure 4.13: AMA envelope curves for a continuous two-span bridge.

With the inclusion of an elastomeric support at the midpoint of the railway bridge, additional observations are made. In comparison with the single span bridge, the AMA generally becomes lower as the stiffness of the system increases with the additional support at the midpoint of the bridge. The values become symmetrical about the midpoint of the bridge.

When $k_s = 1x10^{15}\ kN/m$, the maximum acceleration develops at each of the mid-spans of the continuous bridge, while the minimum is on each of the almost rigid supports. A similar result also occurs for $k_s = 1x10^{10}\ kN/m$, but in this case, a drastic increase in acceleration is yet again detected near each end of the bridge. This discrepancy will be discussed later through the thesis.

While the highest values of acceleration are located at each end of the bridge with a lower support stiffness than $1x10^{15}\ kN/m$, the support stiffness of $1x10^{9}\ kN/m$ provides an interesting result where the lowest value is located at the midpoint on the support. This minimum at the midpoint develops ahead of the values at each end of the bridge while the support stiffness further increases. In this case as well, does $k_s = 1x10^{5}\ kN/m$ bring similar maximum accelerations to $k_s = 1x10^{6}\ kN/m$, which contradicts the general development when varying the support stiffness.

When $k_s > 1x10^{8}\ kN/m$, the AMA becomes higher with an increasing train velocity for each separate case. For $k_s < 1x10^{8}\ kN/m$, the higher velocities no longer result in the greatest values of maximum acceleration in certain areas of the bridge. The train velocity at 80 km/h becomes dominant near the right-end of the bridge with a value of $2,5/m/s^2$ when $k_s = 1x10^{6}\ kN/m$. For $k_s = 1x10^{5}\ kN/m$, 50 km/h prevails with $2,5m/s^2$ near the left-most end.
With the condition of $k_s \leq 1x10^{7}\ kN/m$ is it evident that distinct peaks of the maximum acceleration start to develop for each of the train velocities. For $k_s = 1x10^{7}\ kN/m$, does two distinct peaks at 130 km/h with a value close to $1,5/m/s^2$ emerge. The location and value of these peaks could be an indication of which mode of vibration becomes dominant for each relevant case.

4.3.2 Frequency Domain for Continuous Symmetrical Two-Span Bridge

The relevant time-dependent acceleration occurring at the midpoint located between the first support and middle support is gathered and afterwards calculated using FFT in MATLAB. With the normalized FAS, the relevant frequencies are presented. After presenting the normalized FAS for each case, the natural bridge frequencies for the two-span bridge presented through Figure 4.12 and the corresponding load frequencies from Figure 4.2 are used continuously when analysing the following results.

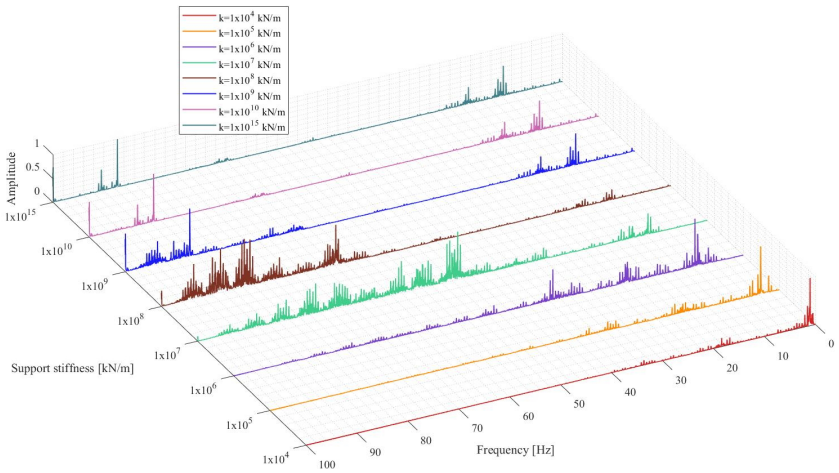

Figure 4.14: FAS at first midspan with 50 km/h train velocity.

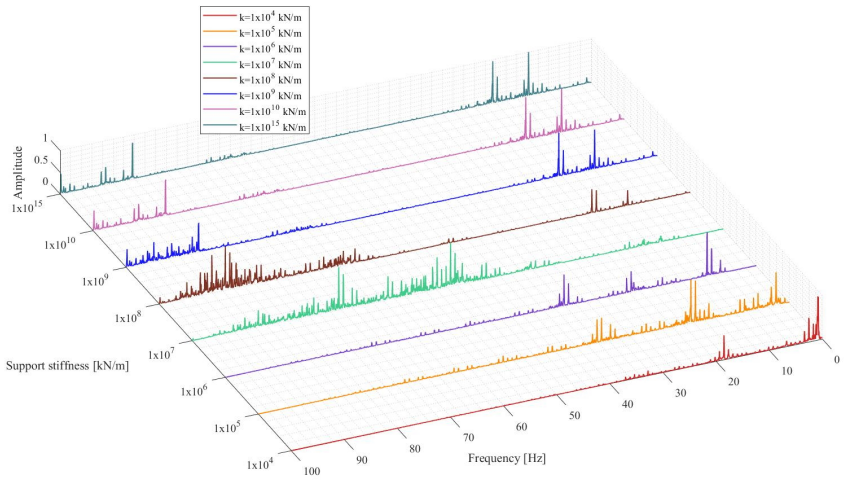

Figure 4.15: FAS at first midspan with 80 km/h train velocity.

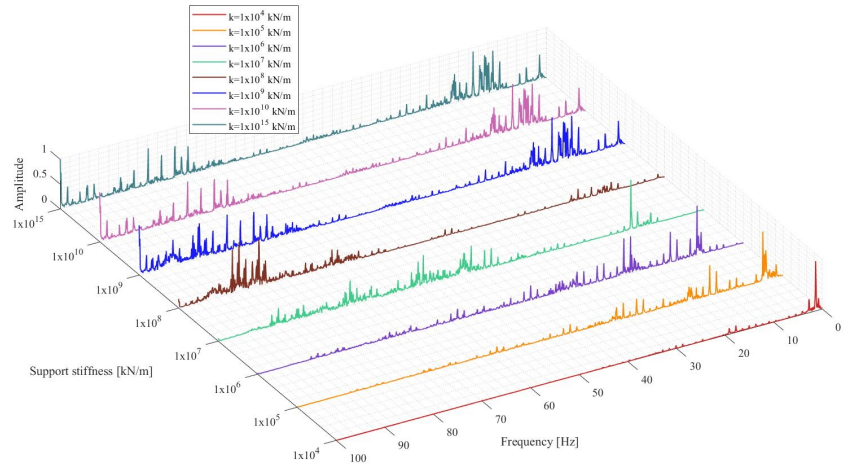

Figure 4.16: FAS at first midspan with 130 km/h train velocity.

As the modal frequencies have increased with the additional elastic support, the corresponding peaks which indicate resonance have shifted to a higher frequency for the cases where $k_s \geq 1x10^9\ kN/m$ at all train velocities. For both the train velocities at 50 km/h and 80 km/h, distinct peaks emerge near 12 Hz and 19 Hz, each of these loading frequencies (see Figure 4.2) coincide with the first and second mode presented through Figure 4.12 respectively. Another distinct case of potential resonance is detected near 86 Hz for each of the previously mentioned train velocities. Although this frequency coincides well with each of the dominant loading frequencies, no corresponding modes of vibration are detected within this area of frequency. This will later be discussed in more detail. While similar behaviour is observed for the train velocity at 130 km/h, the response frequencies become less distinct in comparison with the previous train velocities.

At $k_s = 1x10^8\ kN/m$, the response on the first and second mode of vibration becomes significantly reduced for all train velocities compared to the stiffer supports. Most of the dominant frequencies of the responses are located between 80 Hz to 90 Hz, where the following only coincide with the loading frequencies with no corresponding natural bridge frequency. In the case of 50 km/h, a dominant frequency is further established

near 65 Hz, this agreeing relatively well with the fourth mode of vibration. Some response from the other train velocities is also detected near the fourth mode of vibration, though not as significant.

Through the previously known threshold value where $k_s = 1x10^7\ kN/m$, the less distinct peaks of the FAS for each train velocity shift towards a lower frequency. Again, the dominant loading frequencies coincide well with the presented response. Meanwhile, the corresponding natural bridge frequencies remain relatively irrelevant in this case as well. For the train velocity at 130 km/h, the condition of resonance at 15 Hz is achieved as the dominant loading frequency coincides with the second mode vibration of the bridge. In Figure 4.17, a relevant section of the FAS for $k_s = 1x10^7\ kN/m$ is compared with the corresponding dominant loading frequency at 80 km/h and modal frequencies. In this case, it is evident that the maximum through the FAS of the response is only dependent on the loading frequency without considering the mode of vibrations.

Beyond the threshold value, when $k_s = 1x10^6\ kN/m$, more distinct dominant frequencies emerge through the FAS for each train velocity. For all train velocities, a dominant frequency near 9 Hz is detected, this response coincides both with the corresponding loading frequency and the second mode vibration of the bridge. Additional contributions of frequencies near 24 Hz and 37 Hz, which align with the fourth and fifth mode vibration of the bridge respectively are also observed.

As $k_s = 1x10^5\ kN/m$, the first mode vibration of the bridge at 2,5 Hz contributes the most as it coincides with the dominant loading frequency from all the different train velocities. While this is the case, for 80 km/h, dominant frequencies are further located at 18,5 Hz and 35 Hz, which relates to the second and third mode of vibration for the bridge respectively.
With the lowest support stiffness where $k_s = 1x10^4\ kN/m$, a dominant frequency at 0,85 Hz is observed for all train velocities, with this, the resonance condition is achieved through the first mode vibration of the bridge together with each of the train velocities. An additional response at 18,5 Hz is further detected in the case of 80 km/h. This is related to the fourth mode vibration, which coincides with the relevant dominant loading frequency.

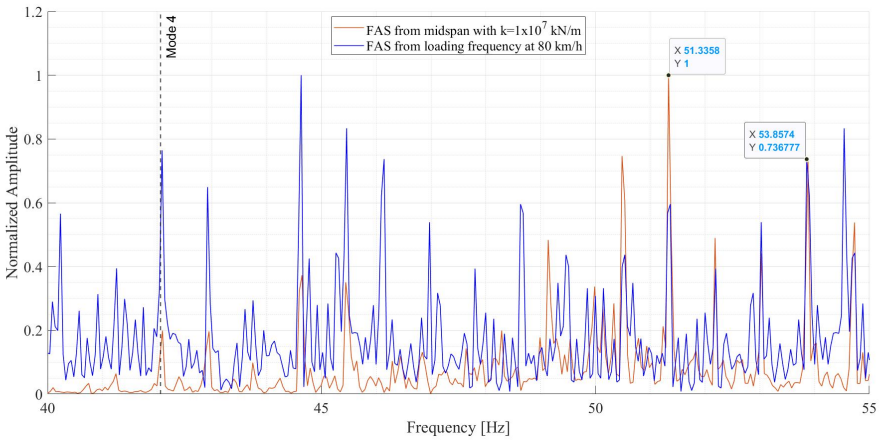

Figure 4.17: Comparison between all relevant factors for response at midspan of two-span bridge.

With the introduction of continuous multi-spans, it is possible to select different midspans when gathering the relevant FAS of the railway bridge. As an example, a comparison is made of the relevant FAS on each midspan through Figure 4.18. In general, the FAS from each of these midspans become equal to each other. Only at 15 Hz, does a significant difference develop between each of these spectrums. This is an indication that the contribution from the third mode vibration of the bridge is greater on the second midspan. The other dominant frequencies remain equal. While the difference becomes negligible in this case, it is important to consider how this affects the FAS when determining which midspan to use for the study.

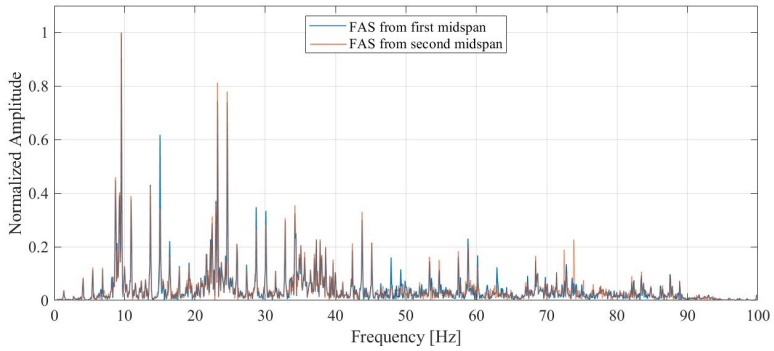

Figure 4.18: Comparison of point for FAS when $k_s = 1x10^6\ kN/m$ at 130 km/h.

When introducing an additional elastomeric support on the midspan, the results significantly change as the stiffness of the bridge increases. At a higher support stiffness when $k_s \geq 1x10^9\ kN/m$, most of the response of the bridge is dominated by less distinct high frequencies near 86 Hz with a contribution from the fifth mode vibration of the bridge. As the support stiffness is lowered, lower modes of vibration start to contribute. At a lower support stiffness where $k_s \leq 1x10^7\ kN/m$, the first, second and third mode vibration of the bridge become prevalent. While the different modes of vibrations are related to the results from the FAS, it is also important to understand that a significant portion of these responses present a misalignment between the natural bridge frequency and the relevant loading frequencies. This discrepancy will be discussed later on.

Nonetheless, the results from the AMA envelope curves correlate with the dominant mode vibrations of the bridge presented through the FAS. Especially for $k_s = 1x10^7\ kN/m$, visible peaks are present for the max acceleration, which are related to the resonance condition between the second mode vibration of the bridge and the loading frequency at 130 km/h. In comparison with the single-span bridge, a less distinct increase in acceleration is observed when $k_s = 1x10^6\ kN/m$. In this case, the second and third mode vibration of the bridge is shown to contribute through the relevant FAS.

4.4 Three-Span Railway Bridge

With the introduction of yet another elastomeric support, the following continuous railway bridge consists of three spans. In this case, the outer spans become 15 m long, while the middle span becomes longer at 20 m. In terms of consistency of the results, the previously defined ICE-2 train is implemented in this case as well.

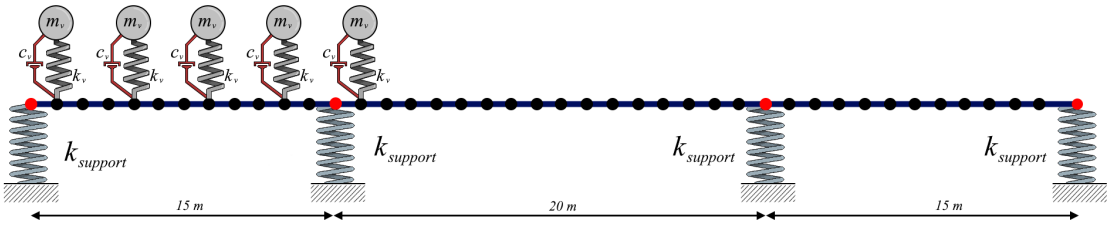

Figure 4.19: Overview of sprung mass model with three-span bridge supported by elastic vertical springs.

Using the vertical modes of vibration presented in Figure 4.19, the following modal frequencies from the defined three-span bridge are studied and applied through the following chapter. The modal frequencies for each relevant mode of vibration generally increases by implementing yet another support. The previous *threshold value* was mainly dedicated to $k_s = 1x10^7\ kN/m$ considering the other bridges with fewer supports. For the three-span bridge, the *threshold value* is established in a wider range of stiffness of $1x10^7\ kN/m \leq k_s \leq 1x10^8\ kN/m$, where mode 3,4 and 5 change the most. When $k_s > 1x10^8\ kN/m$, the modal frequencies remain relatively constant, and the same behaviour also occurs while $k_s < 1x10^7\ kN/m$. The following modal frequencies presented in Figure 4.20 are further established through tables within Appendix E.

As with the two-span bridge, the modal frequencies remain similar to the single-span bridge when $k_s < 1x10^5\ kN/m$. Beyond the *threshold value* of $k_s > 1x10^7\ kN/m$, the modal frequencies become even higher when compared with the two-span bridge.

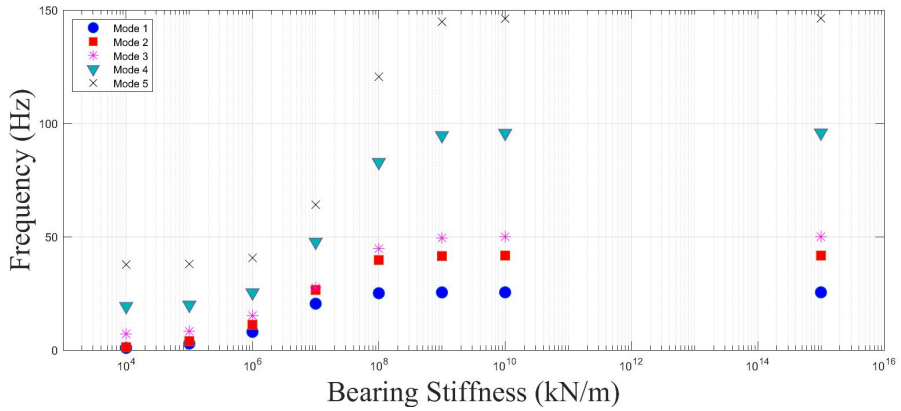

Figure 4.20: Natural frequency of three-span bridge with varying support stiffness.

4.4.1 Absolute Maximum Acceleration Envelope Curve for Three-Span Bridge

Following the previous railway bridges, the AMA envelope curves are presented for the continuous three-span bridge considering each support stiffness and train velocity of interest. To avoid the "*jumping*" phenomenon, each case is frequently discretized by several elements per meter (epm). For the velocities 50 km/h, 80 km/h and 130 km/h, the bridge is discretized by 20 epm, 40 epm and 80 epm respectively.

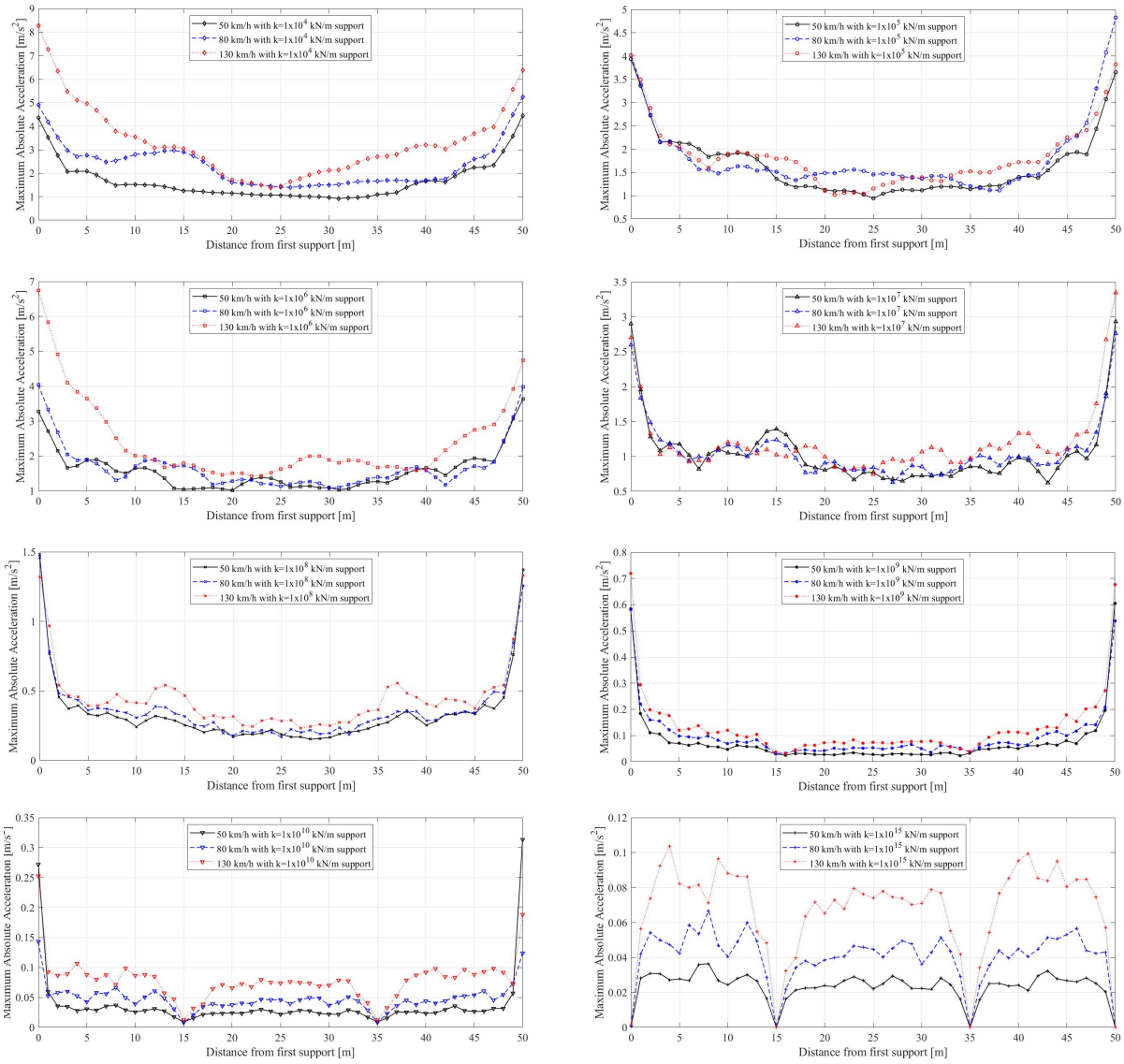

Figure 4.21: AMA envelope curves for a continuous three-span bridge.

Following a similar behaviour to what has been previously observed from the two-span bridge, as $k_s = 1x10^{15}\ kN/m$, the bridge becomes rigidly supported. This results in the lowest acceleration on every support, while the maximum develops on each of the midspans. In this case, a relatively greater value of acceleration is observed on each of the shorter spans at each end of the bridge.

While still implementing a relatively high support stiffness at $k_s = 1x10^{10}\ kN/m$, significant changes occur. The supports located along the span of the bridge develop a minimum of acceleration. Meanwhile, the acceleration at each end of the bridge drastically increases in value and becomes a maximum instead. While a high value

in acceleration is fully possible at each end of the bridge, this drastic increase in acceleration will need to be discussed, as this is an indication of numerical inaccuracy close to each end of the railway bridge.

As the support stiffness becomes $k_s < 1x10^{10}\ kN/m$, both the value and the difference in maximum acceleration between each train velocity generally becomes lower. For $k_s = 1x10^{9}\ kN/m$, the minimum in acceleration on the supports along the bridge can further be observed, though not as significant as from $k_s = 1x10^{10}\ kN/m$. For $k_s = 1x10^{8}\ kN/m$, local maximum beyond $0,5\ m/s^2$ is recognized on each of the shorter midspans. This is especially shown with a train velocity at 130 km/h. These distinct peaks frequently occur for each of the cases when $k_s < 1x10^{9}\ kN/m$ and can be associated with a potential modeshape. At $k_s = 1x10^{6}\ kN/m$, the same discrepancy observed from the previous bridges is also detected. In this case, the three-span bridge achieves higher values of AMA similar with the single-span bridge.
In general, the highest train velocity at 130 km/h results in the greatest value of maximum acceleration along the railway bridge. Although this is the case, for $k_s = 1x10^{7}\ kN/m$, both the velocities at 50 km/h and 80 km/h bring a higher value close to $1,5\ m/s^2$ on the first midspan. At $k_s = 1x10^{5}\ kN/m$, the maximum acceleration from 80 km/h surpasses 130 km/h in the middle of the bridge as well.

While the additional support on the two-span bridge resulted in a significantly lower maximum acceleration when compared with the single-span bridge at $k_s > 1x10^{7}\ kN/m$, the same reduction is not as significant between the current three-span and two-span bridge. In certain cases, such as when $k_s = 1x10^{8}\ kN/m$, the maximum acceleration on the three-span bridge exceeds the values in certain locations established from the previous two-span bridge, though not by a large margin. This disrepancy mainly occurs through the peaks, which indicates an alignment with the relevant mode vibration of the bridge.

4.4.2 Frequency Domain for Three-Span Bridge

Using the second midspan as a basis, the FAS of the acceleration is established on the following three-span bridge. The dominant frequencies determined through the following spectrums indicate which mode of vibration contributes the most to the acceleration response of the relevant bridge. As in previous cases, the FAS is normalized, in which the maximum value is used as basis. While studying the following spectrums, the initial natural bridge frequencies presented from Figure 4.20 and loading frequencies in Figure 4.2 are also applied.

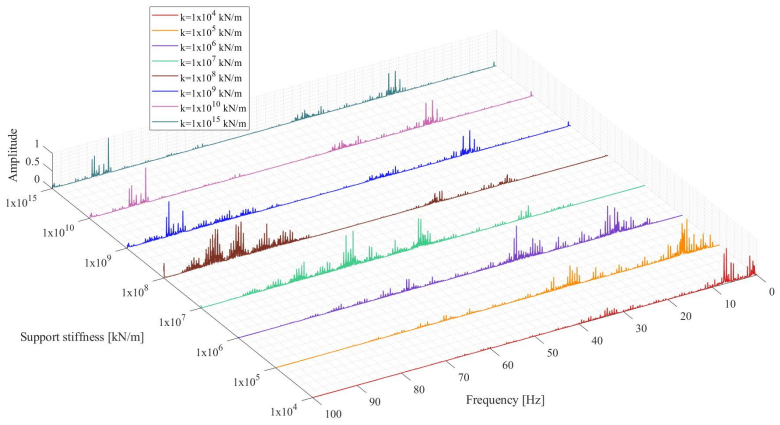

Figure 4.22: FAS at second midspan with 50 km/h train velocity.

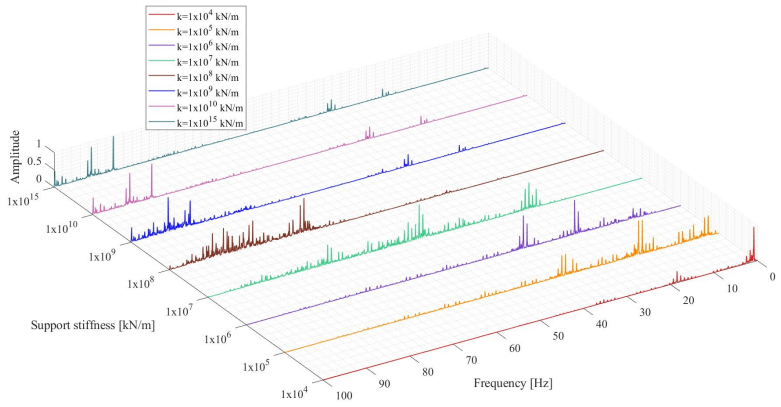

Figure 4.23: FAS at second midspan with 80 km/h train velocity.

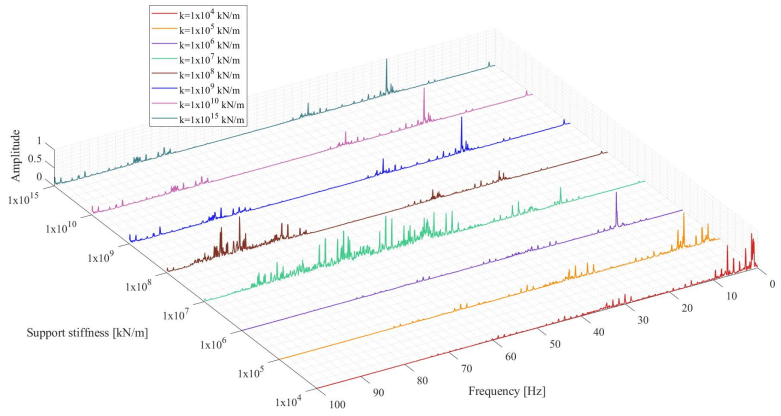

Figure 4.24: FAS at second midspan with 130 km/h train velocity.

In general, for all train velocities, the allocation of the dominant frequencies remains relatively constant when $k_s > 1x10^8\ kN/m$. At 130 km/h, the first mode vibration for the stiffer supports of the bridge coincides with the loading frequency, this establishes a distinct dominant frequency near 25 Hz. This alignment is further shown through Figure 4.25. An additional response at 42,4 Hz is also observed, this relatively coincides with the second mode vibration of the bridge and the following dominant loading frequency.
For the other train velocities at 50 km/h and 80 km/h, though less distinct, most of the dominant frequencies occur at 87 Hz and 91 Hz. While these coincide well with the corresponding loading frequencies, no appropriate mode of vibration is within the vicinity of the mentioned frequencies.

While the support stiffness $k_s = 1x10^8\ kN/m$ is defined as a *threshold value* when considering the change in modal frequencies, the response through the FAS becomes less distinct while also shifting to a lower value from the stiffer supports. For all train velocities, the previously dominant frequencies deriving from the first and second mode vibration of the bridge is significantly reduced. This is an indication that the following change in modal frequency is sufficient in making it differ to the corresponding loading frequencies. Meanwhile, different less distinct dominant frequencies are observed between 70 Hz and 95 Hz, which vary between each train velocity. In general, the following frequencies only coincide with the corresponding dominant loading frequencies and not with the mode vibrations of the bridge.

Through the other *threshold value* at $k_s = 1x10^7\ kN/m$, the development of less distinct dominant frequencies is also observed, in which they further shift to lower values of frequencies. In this case, the less distinct dominant frequencies that are mainly dependent on the loading frequencies, vary to an even greater extent between 50 Hz and 90 Hz. While this is the case, a dominant frequency at 26 Hz is observed through the FAS, this corresponds well with both the second mode vibration of the bridge and the loading frequency at 80 km/h.

Below the *threshold values* with $k_s = 1x10^6\ kN/m$, the response from each case of the FAS becomes relatively distinct again. At 130 km/h, the third mode vibration of the bridge at 15 Hz contributes the most to the acceleration response of the bridge, all the energy within this spectrum is dedicated to this resonance condition. When lowering the train velocity to 80 km/h , most of the energy is devoted to the frequencies 24,4 Hz and 36,2 Hz. Although these mentioned frequencies are related to the fourth and fifth mode vibration of the bridge, a marginal difference in alignment is detected. For 50 km/h, the dominant frequencies become less distinct with maximum values near 16,8 Hz and 37,3 Hz. As with 80 km/h, the mentioned response does not coincide as well with the relevant modes of vibration.

For $k_s = 1x10^5\ kN/m$, each train velocity creates a different acceleration response. At 130 km/h, most of the contribution is made through a dominant frequency of 8,25 Hz, which coincides with the third mode vibration of the bridge. When lowering the velocity to 80 km/h, the response of the bridge becomes less distinct, but peaks in the area of 2,5 Hz, 18,5 Hz and 36 Hz are observed. These frequencies align to a certain degree with the first, fourth and fifth mode vibration of the bridge respectively. At 50 km/h, less distinct dominant frequencies at 7,3 Hz and 33,7 Hz are detected, these are related to the contribution of the third and fifth mode vibration of the bridge. These do not align as well.

Similar to $k_s = 1x10^5\ kN/m$, the lowest support stiffness $k_s = 1x10^4\ kN/m$ varies in acceleration response for each train velocity. With the loading frequency from 130 km/h, the second and third mode vibration of the bridge coincide near 1,4 Hz and 6,9 Hz respectively. At 80 km/h, a distinct response occurs at 0,85 Hz, which derives from the first mode vibration of the bridge coinciding with the mentioned train velocity. At the lowest velocity of 50 km/h, most of the energy is dedicated to frequencies near 1.6 and 7 Hz, the second and third mode vibration contributes respectively in this case.

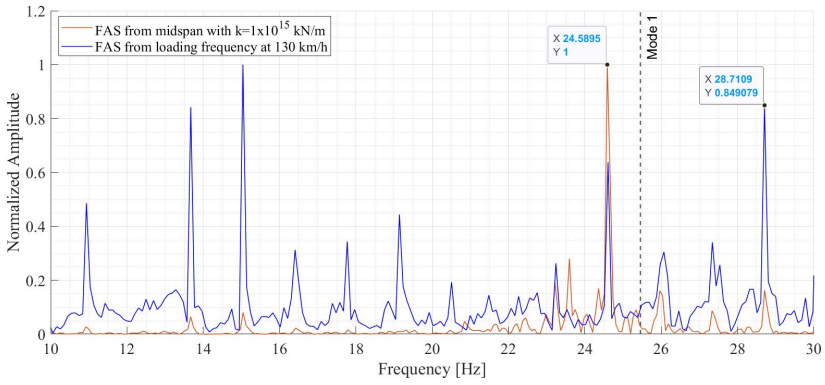

Figure 4.25: Comparison between each relevant factor for response at midspan of three-span bridge.

With three spans, different midspans can be used when gathering the relevant FAS. As with the two-span bridge, it is also of interest to observe the effect of the different locations for the FAS on the three-span bridge. By comparing the FAS on the middle of the shorter 15 m span with the longer 20 m span, an example is presented through Figure 4.26. In this specific case, the maximum in the FAS generally align with each other. Although this is the case, it is evident that the frequencies on the shorter 15 m span shift towards a higher frequency. This indicates that the shorter first midspan responds with a relatively higher frequency, when compared with the longer second midspan. While negligible, it is important to consider this effect, which may vary for other cases.

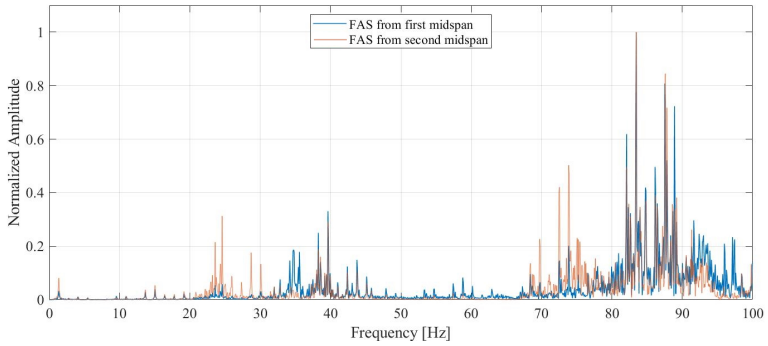

Figure 4.26: Comparison of different points for FAS when $k_s = 1x10^8\ kN/m$ at 130 km/h.

With two supports located along the length of the railway bridge, the stiffness of the system increases yet again. As with the two-span bridge, the three-span bridge also presents several cases for the FAS, in which the acceleration response of the railway bridge only aligns with the loading frequencies and not the natural bridge frequencies. The *threshold value* is defined for a wider spectrum between $k_s = 1x10^7\ kN/m$ and $k_s = 1x10^8\ kN/m$, as opposed to only $k_s = 1x10^7\ kN/m$ for the two-span bridge.

The third mode vibration of the three-span bridge coincides with the loading frequency at 130 km/h when $k_s = 1x10^6\ kN/m$. Similar to the single-span bridge, a significant increase in acceleration is further observed on the corresponding AMA envelope curve. Although the dominant frequencies become less distinct through the FAS, the following can still be related to a mode vibration of the bridge within a certain margin. As the support stiffness becomes $k_s \leq 1x10^6\ kN/m$ below the threshold value, the third mode of vibration becomes more prevalent as well.

4.4.3 Impact of Different Stiffness on Supports

Previously, while studying the effect of varying support stiffness for different number of spans, each of the supports varied equally in stiffness. This may not necessarily be the case, in which a specific support may experience a greater effect of aging. The following chapter is therefore dedicated to studying what impact such a difference in support stiffness may imply. Using a single-span bridge, the right-most support is defined with a relatively high difference of 20% less stiffness on the right-most support. Of the three relevant train velocities, the effect is most visible at 130 km/h. Through Appendix F, the relevant AMA envelope curves for the train velocities 50 km/h, and 80 km/h are also presented in the same manner as in Figure 4.27.

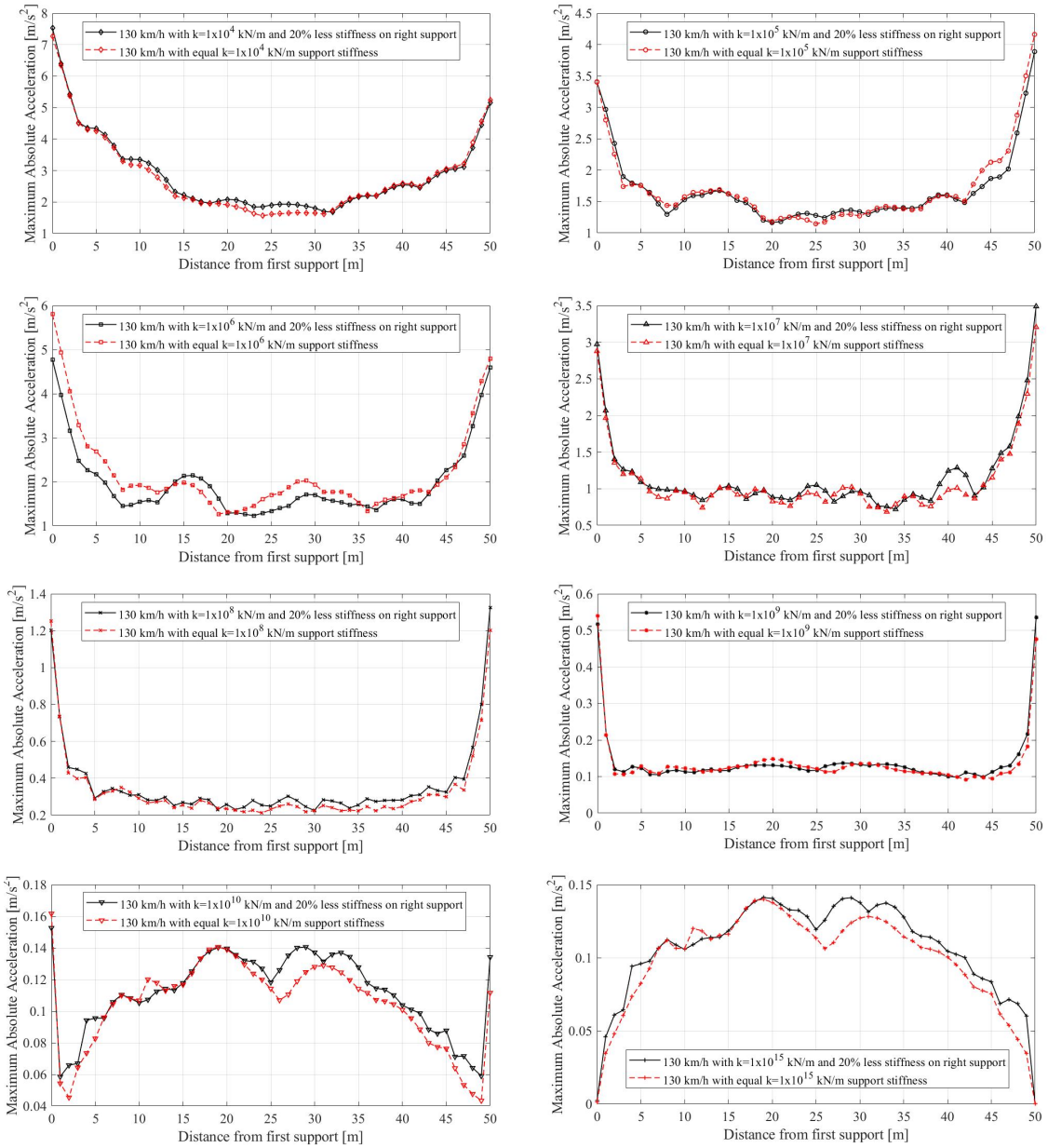

Figure 4.27: Comparison between original and 20% reduced stiffness on right-support at 130 km/h.

When comparing the effect while implementing 20% less vertical stiffness on the right-most support for each train velocity, it is evident that such a difference in support stiffness generally brings similar results to the condition of equal support stiffness at each end of the single-span bridge.
Although this is the case, at a velocity of 130 km/h, a significant difference develops as $k_s > 1x10^9\ kN/m$. For these stiffer supports, the right side of the bridge bring a higher value through the AMA envelope curves. For the slower train velocities 50 km/h and 80 km/h, the values remain almost identical to those with equal stiffness on each support.

When compared with the case of 20% reduction, the bridge with equal stiffness on each support provides a greater value through certain AMA envelope curves in different parts of the bridge. With the reduction in stiffness, the corresponding vertical mode vibrations of the bridge change as well. This in turn, affects the potential resonance condition, which was achieved in previous cases with equivalent stiffness on each support. For $k_s = 1x10^6\ kN/m$ at 130 km/h presented through Figure 4.27, it is evident that the 20% reduction in vertical stiffness on the right-most support makes the loading frequency coincide less when compared with the previous equivalent support stiffness case. Although the system is relatively stiffer, a greater value of acceleration can still be achieved depending on the potential resonance condition, which is prevalent when applying elastomeric bearings.

4.5 Train Response

While mainly focusing on the dynamic behaviour of the bridge, it is also of interest to study the response of the traversing train. Through the SMM, relevant results from each train axle are individually gathered. With the previously defined 50 m long single-span railway bridge, three sprung masses representing the axles along the trains length are selected when gathering the time dependent accelerations. Each node on top of the relevant sprung masses is located at 1/4, 1/2 and 3/4 along the length of the defined ICE-2 train and is used as a basis for the current analysis.

4.5.1 Maximum Acceleration on Train Axles

Following the same procedure as with the railway bridge, it is of interest to analyse the absolute maximum acceleration developing on the relevant sprung masses on the ICE-2 train. This is done while varying the train velocity and support stiffness of the bridge. Through the Eurocode, an acceleration limit for the passenger train is established and presented in Table 4.2 [7]. Only the *acceptable limit* is implemented when studying the following results.

Table 4.2: Eurocode limit for vertical acceleration on railway bridges [7].

Level of Comfort	Vertical Acceleration (m/s^2)
Acceptable	2
Good	1,3
Very Good	1

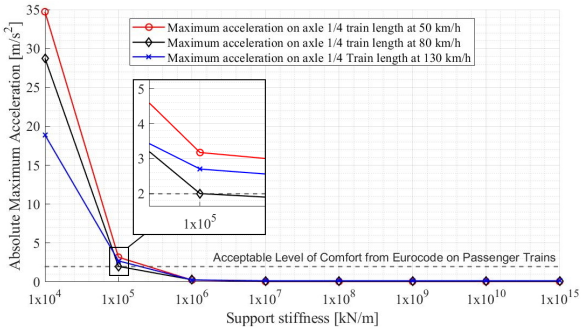

(a) Mass sprung located at 1/4 of train length.

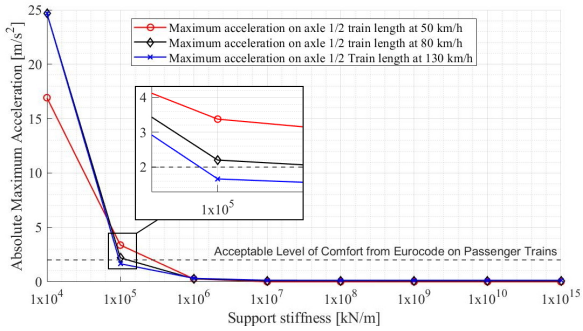

(b) Mass sprung located at 1/2 of train length.

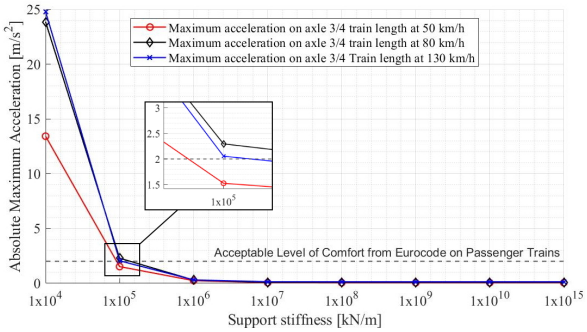

(c) Mass sprung located at 3/4 of train length.

Figure 4.28: AMA on different locations of traversing passenger train.

In general, a higher train velocity and a lower support stiffness of the bridge are associated with a greater value of acceleration on the train. Although this is the case, the slower velocities at 50 km/h and 80 km/h achieve a greater value when given the right circumstances. These conditions only occur when the stiffness on the supports of the bridge becomes $k_s \leq 1x10^6\ kN/m$. As $k_s \geq 1x10^7\ kN/m$, the acceleration on each case stabilizes and remains constant, in which the relative order from highest to lowest maximum acceleration follows 130 km/h, 80 km/h and 50 km/h respectively.

In the case of $k_s = 1x10^4\ kN/m$, significantly higher results of maximum acceleration up to $35/m/s^2$ are achieved. While this value may occur through the current parametric study, the corresponding accelerations are deemed unrealistic for axles of a train. The following results from the case of $k_s = 1x10^4\ kN/m$ are therefore neglected when studying the absolute maximum accelerations on the relevant sprung masses. This discrepancy is due to the transition for the traversing sprung masses between the spring supports with lower vertical stiffness and the infinitely rigid surfaces at each end of the bridge. Some evidence of this phenomenon can already be observed through Figure 4.29a at $k_s = 1x10^5\ kN/m$.

While neglecting the unrealistic accelerations on the train from $k_s = 1x10^4\ kN/m$, the accelerations developing along the train length at $k_s = 1x10^5\ kN/m$ become especially interesting while considering the acceptable limit for passenger comfort established through the Eurocode. In this case, the slower train velocities at 50 km/h achieve the highest value of maximum acceleration compared with the faster train velocities. Only close to the rear of the train does the velocity at 50 km/h contribute to the lowest maximum acceleration. In this case, 80 km/h achieves the greatest maximum acceleration.

When considering the limit at 2 m/s^2, a threshold value is provided through $k_s = 1x10^5\ kN/m$. The location of the sprung mass and the corresponding velocity determines whether the relevant axle is within the criteria.

For 1/4 along the train length, the maximum acceleration is within the limit only at 80 km/h. Further at 1/2 its length, only the fastest velocity at 130 km/h is within the limit. Finally, close to the rear end at 3/4 of the train length, the slowest train velocity at 50 km/h achieves a maximum acceleration value within the criteria. The condition of resonance on the railway bridge may determine whether the relevant sprung mass is within this limit at this threshold value.

The maximum accelerations of the traversing train generally occur when the sprung mass either first comes in contact with or exits the bridge, this being especially true when the support stiffness becomes $k_s \leq 1x10^6\ kN/m$. As $k_s > 1x10^5\ kN/m$, all the relevant cases are within the acceptable level of comfort.

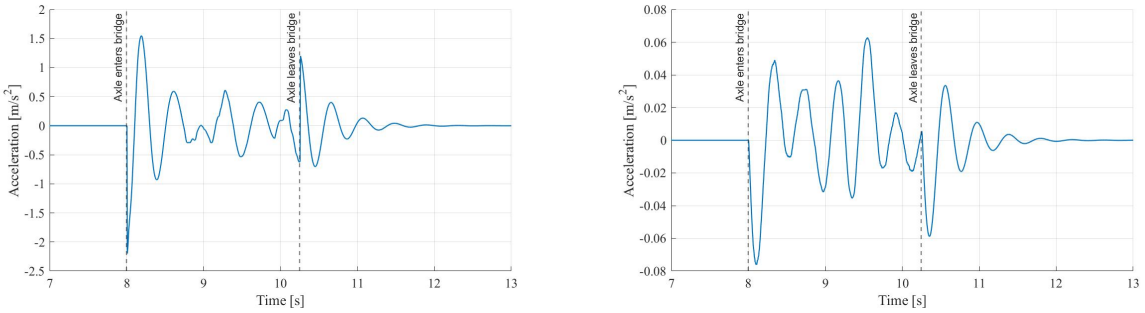

(a) Acceleration on sprung mass at $k_s = 1x10^5\ kN/m$. (b) Acceleration on sprung mass at $k_s = 1x10^{10}\ kN/m$.

Figure 4.29: Time-history of accelerations on relevant sprung mass at 1/2 train length at 80 km/h.

4.5.2 FAS of Relevant Sprung Masses

The previous time-history of the accelerations occurring on each sprung mass is further calculated through FFT in MATLAB. Using this, a normalized FAS about the maximum value is implemented while studying the acceleration response of the relevant train axles when varying both the support stiffness and train velocity. This produces a total of 9 results, which are presented within Appendix G.

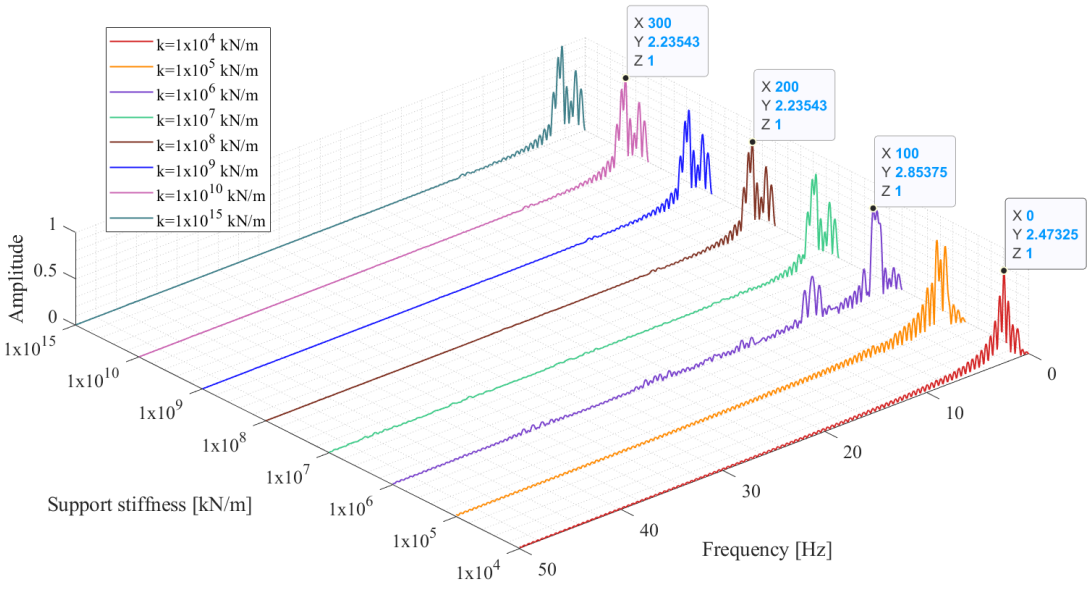

Figure 4.30: FAS on sprung mass 1/2 along the train length at 80 km/h for single-span bridge.

Through simple expressions of a single degree of freedom system, it is possible to calculate the natural frequency of the individual sprung masses without the bridge induced vibrations. By implementing the defined parameters for an ICE-2 train presented in Table 4.1, the following natural frequency of each sprung mass is calculated at 2,47 Hz through Equation 4.1.

$$f_n = \frac{\omega_n}{2\pi} \;\Rightarrow\; f_n = 2,47\ Hz \tag{4.1}$$

Through the FAS presented for each case within Appendix G, all the dominant frequencies develop near the previously calculated natural frequency of 2,47 Hz on the sprung mass. While the variation in support stiffness of the single-span railway bridge has little influence on the relevant train axles in most cases, an interesting observation is further made.

Using the FAS presented in Figure 4.30 as an example, an additional dominant frequency for the relevant sprung mass is observed when implementing a bridge support stiffness of $k_s = 1x10^6\ kN/m$. This observation remains relatively true within Appendix G for all cases related to a train velocity of 80 km/h and 130 km/h. While the amplitude of this frequency is not as high as those located at 2,47 Hz, it is regarded as significant. The location of the additional dominant frequency varies between 10 Hz and 15 Hz for each of the relevant cases, with some responses becoming less distinct. This is a strong indication that the previous resonance conditions achieved with the third mode vibration of the single-span bridge also influences the behaviour of the traversing sprung masses.

5 Discussion of Results

Using a railway bridge with different number of spans, which total 50 m in length together with a defined ICE-2 train, several analyses were conducted while varying parameters such as support stiffness and train velocity. With the defined vertical stiffness on elastomeric bearings presented through different product catalogues together with the effect of aging, the vertical stiffness on the supports of a railway bridge may vary greatly in reality. Through the parametric study, it is evident that the dynamic response of the bridge is sensitive to this variation in support stiffness. A correlation between the relevant FAS and corresponding AMA envelope curves also occurs through the study, in which the dominant mode of vibration dictates the location of maximum accelerations. Many of the dominant frequencies developing through the FAS on the relevant bridges are dependent on the alignment between the natural bridge frequencies and the loading frequencies. Although this is the case, a significant number of these responses only coincide with the loading frequency instead.

For each of the bridges and corresponding train velocities presented through the parametric study, whether it be a single-span or a multi-span bridge, the AMA envelope curves (previously presented through Figure 4.5, 4.13 and 4.21) develop a maximum in acceleration at each end of the bridges as $k_s \leq 1x10^{10}\ kN/m$. A drastic increase in accelerations is further observed on these areas of the bridges. This numerical discrepancy, which has often been referred to, can be explained by the interaction between the boundary conditions and the stiffness of the relevant bridge. Even at a lower support stiffness, the bearings become stiffer compared to the bridge itself. As the train transitions on the supports by an infinitely rigid surface, the acceleration close to these supports is dominated by the higher frequencies developing on the bearings. This results in a higher value of acceleration compared to the rest of the bridge. Once the train traverses some meters within the bridge length, the stiffness of the bridge starts to define the dynamic behaviour instead. The minimum developing on the supports within the bridge length for the multi-span bridges is related to this definition as well. In this case, before coming into contact with the relevant supports, the response is dominated instead by the less stiff bridge as the train travels through.
Due to this mentioned effect, the maximum acceleration at each end of the bridge becomes amplified. This creates an uncertainty when evaluating the AMA envelope curves. When $k_s \leq 1x10^{6}\ kN/m$, the mentioned area of the bridge mainly exceed the established limit for vertical acceleration at $3,5\ m/s^2$ for both the single-span and multi-span bridges.

Much of the misalignment previously referred to between the natural bridge frequency and loading frequency with regard to the FAS, also originates from this influence of the high frequency contribution from the supports at each end. While this influences the FAS for the single-span railway bridge, it is evident that the multi-span bridges are affected by this significantly more. Multi-span bridges consist of a generally higher natural bridge frequencies compared to the single-span bridge, hence the effect becomes greater.

An interesting observation that was referred to in the parametric study was made through the AMA envelope curves at $k_s = 1x10^{6}\ kN/m$. Both for the single-span and multi-span bridges, a significant increase in acceleration was detected. When also considering the relevant FAS, it is evident that a resonance condition occurs between the relevant loading frequencies and third mode vibration of the bridges. This resonance condition is also the only case that contributes to significant bridge induced vibrations on the traversing sprung masses. The vertical stiffness at $1x10^{6}\ kN/m$ is often defined for different products of elastomeric bearings for

bridges [28], this makes the mentioned results especially relevant. In the end, the observations made through the parametric study imply that a lower support stiffness and a faster train velocity are not necessarily related to a greater dynamic response of the bridge.

When conducting the parametric study, it was observed that the efficiency of the proposed algorithm varied with the train velocity. When considering the principles introduced for the sprung mass, it is necessary to frequently discretize the bridge to properly attain the relative position of each sprung mass representing the train axles. This necessity is reasoned by how every sprung mass is positioned and coupled directly on the closest node of the bridge. This means that at a slower train velocity, the relevant sprung mass increases in amount of relative positions before fully traversing the railway bridge. The frequency of discretization is therefore dependent on the train velocity, in which a higher train velocity needs significantly fewer planar beam elements. In the parametric study, the bridge was discretized at 20, 40 and 80 elements per meter to accurately register the acceleration for the train velocities at 130 km/h, 80 km/h and 50 km/h respectively. While it is possible to dicretize the bridge at an even higher frequency for each of these train velocities, the additional calculation time while also considering the miniscule change in accuracy makes this less beneficial.

Through the parametric study where the total bridge length was 50 m with a defined ICE-2 train traversing, the computational time significantly varied for each relevant train velocity. With the train velocities at 130 km/h, 80 km/h and 50 km/h, the calculation time varied by 10 minutes, 1 hour and 8 hours respectively when using the relatively modern CPU *AMD Ryzen 7 5800X*. The following calculation time may vary greatly depending on the hardware.
This comes to show that while the proposed model is relatively simple to code and apply, it is regarded as nonviable when calculating for train velocities slower than 80 km/h for the cases presented through this study with the current CPU. With a lower computational capability, this proposed limit for minimum train velocity may even become higher. Although it is more complex to code and implement shape functions for the current VBI model, it is necessary, as this approach enables interpolation of the relative position of the sprung mass within the relevant beam element. This means that the sprung mass no longer needs to be directly coupled with the nodes, but can instead be located between them. As a result, a smaller number of planar beam elements are needed when performing the same calculations in this study.

As the parametric study is limited to a constant total bridge length of 50 m and a single train configuration of a defined ICE-2 train, the current results are not sufficient to further generalize. While this is the case, the study brings an insight into the dynamic behaviour of rail bridges with varying stiffness of elastomeric bearings. As the current body of knowledge regarding this field of study is limited when implementing a sprung mass model, the study also provides a better understanding on the effect of such bridge bearings for the behaviour of the train as well.

6 Conclusion

While a significant body of knowledge has been dedicated to the study of dynamic behaviour of railway bridges using different VBI models, almost none of these directly consider the effect of elastomeric bearings for these cases. The studies that consider elastic bearings, often idealize and further generalize the results by only implementing the simple moving load model. The current thesis therefore looks more in-depth into the effect of elastomeric bearings on the dynamic behaviour of railway bridges and corresponding traversing trains while implementing a more complex sprung mass model. The effect of aging on such bearings is also considered by varying the support stiffness as well.

With a basis from the previous software developed by A.M. Al-Kanany [1], elastic spring supports were implemented through MATLAB, in which the stiffness of the relevant degree of freedom for the supports can be changed when necessary. A VBI model consisting of a moving sprung mass model was further applied together with the elastic spring supports algorithm in a 2D planar beam element setting with a basis from FEM. After verifying the spring support algorithm together with the sprung mass model, a parametric study was later conducted.

By using a defined train configuration of an ICE-2 passenger train together with the defined parameters of "Norddalsbrua 1", which is a 50 m long single-span railway bridge previously used by A.M. Al-Kanany [1], the velocity of the train, number of spans and stiffness of supports were varied through the parametric study. Mainly the acceleration response of the railway bridge was analysed through this study by implementing both the AMA envelope curve and the FAS, both of these procedures being then compared with each other. As the sprung mass model also enables the gathering of results from the separate train subsystem, the response of the sprung masses representing the train axles was included through this study. The effect of differing stiffness on relevant bridge supports was further considered. The conclusion will be presented in more detail together with a suggestion of future work in the following sub chapters.

6.1 Dynamic Behaviour with Elastomeric Bearings

By using the proposed sprung mass model in combination with the spring support algorithm in MATLAB, a variety of conclusions is made using the different cases presented in this thesis. For the following conclusions, it is important to understand that the parametric study is dedicated to specific cases based on an ICE-2 passenger train and a bridge with a total span of 50 m, which varied in number of spans. The conclusion may therefore vary depending on the relevant train configuration and bridge parameters.

- The AMA envelope curves generally correlate with the corresponding dominant mode of vibration presented through the FAS, in which the maximum acceleration partially resembles the relevant mode shape when $k_s \leq 1x10^7\ kN/m$. This further implies that the dynamic response of the bridge becomes sensitive to the change in vertical support stiffness. The condition of resonance between the relevant loading frequency and mode vibration of the bridge significantly affects the dynamic behaviour of the bridge.
- While the accelerations developing on the bridge generally increase with a lower support stiffness and higher train velocity, certain discrepancies occur. When $k_s = 1x10^6\ kN/m$, a higher acceleration response develops both for the single-span and multi-span bridges due to a resonance condition with the third mode of vibration. The parametric study implies that a lower support stiffness and a faster train velocity is not necessarily related to a greater dynamic response of the bridge.
- Only the resonance condition at $k_s = 1x10^6\ kN/m$ with the third mode vibration of the bridge contributes to significant bridge induced vibrations on the traversing sprung masses at 80 km/h and 130 km/h. The acceleration response of the sprung masses representing the train axles is mostly determined by the natural frequency of the single degree of freedom system from the sprung mass itself in this case.
- In the AMA envelope curves, a significant maximum consistently develop at each end of every relevant bridge when $k_s \leq 1x10^9\ kN/m$. Although an uncertainty is associated with the results gathered near these parts, it is evident that this area of the bridge becomes important when implementing elastomeric bearings.
- At a 20 % difference in stiffness on the right-most support of a single-span railway bridge, most of the accelerations from the AMA envelope curves remain almost identical to the cases with equivalent stiffness on both supports. Only at $k_s > 1x10^9\ kN/m$ with a train velocity of 130 km/h is a significant difference observed.
- While the spring support algorithm and the proposed sprung mass model generate satisfactory results in most cases, certain discrepancies occur due to the high frequency contribution from the bridge supports at each end of the bridge. This also affects the maximum acceleration on the traversing train axles.
- Although the principles introduced in the current study for the sprung mass model are relatively simple to code, a certain drawback was detected. As the frequency of discretization increases at a slower train velocity, the proposed model becomes viable only when the train velocity is over 80 km/h with the defined CPU. By implementing the more complex shape functions, it is possible to interpolate the relative position of the sprung masses, hence the discretization of the bridge becomes independent of the train velocity.

6.2 Further Work

While the current thesis has provided an insight into the dynamic behaviour of railway bridges with elastomeric bearings through a sprung mass model, several factors remain to be analysed when considering this wide field of study. Using the current results as a basis, it is of further interest to study the following topics and improve the relevant MATLAB software.

- As the current study considers the moving sprung mass model when defining the interaction between the traversing train and bridge, the effect of surface roughness and ballast stiffness will also become relevant. Future work should therefore also consider these parameters for the effect on the dynamic response of railway bridges with elastomeric bearings.
- Additional studies as to why a drastic increase in maximum acceleration and frequency occurs at each end of the bridge is of further interest. Development of a measure to reduce this relatively unrealistic phenomena will also become necessary. By defining the surfaces before and after the bridge length as relatively elastic, this unfavourable effect may be significantly reduced.
- Even though the number of bridge spans varied together with the bridge support stiffness and train velocity through this thesis, it would also be of interest to study the impact of varying train parameters such as stiffness of the suspension and the damping of the axles as well. Since the mass of a passenger ICE-2 train is relatively low in comparison with most railway bridges, it is further beneficial to analyse the same effect when a heavier freight train traverses with different axle configurations.
- As previously mentioned when discussing the efficiency of the principles of the proposed sprung mass model, it becomes necessary to implement shape functions when further studying with the sprung mass model at relatively slower train velocities. Though this is harder to apply when coding, the resulting calculation time will be significantly lowered.
- While the sprung mass model is a relatively realistic VBI model in comparison with the less complex moving load and moving mass model, more complex models are still possible to implement. By further simulating the train as a multi-rigid-body system, every two axles become connected by bogies and a rigid body (TAVBM). As a result, this model further considers the more realistic pitching effect, which occurs between the relevant axles.

References

[1] Aya Mohammed Al-Kanany. The impact of the train mass on the dynamic behaviour of railway bridges. Master's thesis, Oslo Metropolitan University, 2020.

[2] Farzad Naeim. Dynamics of structures—theory and applications to earthquake engineering. *Earthquake Spectra*, 23(2):491–492, 2007.

[3] W. Zhai, Z. Han, Z. Chen, L. Ling, and S. Zhu. Train–track–bridge dynamic interaction: a state-of-the-art review. *Vehicle System Dynamics*, 57(7):984–1027, 2019. cited By 147.

[4] Vijay Nath and Jyotsna Kumar Mandal. *Proceeding of the Second International Conference on Microelectronics, Computing & Communication Systems (MCCS 2017)*. Springer, 2019.

[5] Michal Majka and Michael Hartnett. Effects of speed, load and damping on the dynamic response of railway bridges and vehicles. *Computers & Structures*, 86(6):556–572, 2008.

[6] Bernhard Glatz and Josef Fink. A redesigned approach to the additional damping method in the dynamic analysis of simply supported railway bridges. *Engineering Structures*, 241:112415, 2021.

[7] Standard Norge. NS-EN 1991:200+A1:2005+NA:2016, Eurocode: Basis of structural design, 2016.

[8] Tor Midtbø and Susanne Stephansen. Ny Infrastruktur skal gi et bedre togtilbud mellom byområdene. `https://www.regjeringen.no/no/tema/transport-og-kommunikasjon/jernbane_og_jernbanetransport/storbyene-skal-ha-et-godt-togtilbus/id2344770/`, 2021. [Online; accessed 02.04.2022].

[9] Hilary Arksey and Lisa O'Malley. Scoping studies: towards a methodological framework. *International journal of social research methodology*, 8(1):19–32, 2005.

[10] Yeong-Bin Yang, JD Yau, Zhongda Yao, and YS Wu. *Vehicle-bridge interaction dynamics: with applications to high-speed railways*. World Scientific, 2004.

[11] A. González, E. Covián, and M. Casero. Verifying the suitability of uncoupled numerical methods for solving vehicle-bridge interaction problems. *Structure and Infrastructure Engineering*, 2022. cited By 0.

[12] Y. Lu, L. Mao, and P. Woodward. Frequency characteristics of railway bridge response to moving trains with consideration of train mass. *Engineering Structures*, 42:9–22, 2012. cited By 31.

[13] Y.B. Yang and J.D. Yau. Resonance of high-speed trains moving over a series of simple or continuous beams with non-ballasted tracks. *Engineering Structures*, 143:295–305, 2017. cited By 45.

[14] E. Erduran, C. Nordli, M. Salehi, and S. Gonen. Effect of aging of bearings on the behavior of single-span railway bridges. Oslo Metropolitan University:1–10, 2022.

[15] Abbas Zangeneh, Jean-Marc Battini, Costin Pacoste, and Raid Karoumi. Fundamental modal properties of simply supported railway bridges considering soil-structure interaction effects. *Soil Dynamics and Earthquake Engineering*, 121:212–218, 2019.

[16] Y.B. Yang, C.L. Lin, J.D. Yau, and D.W. Chang. Mechanism of resonance and cancellation for train-induced vibrations on bridges with elastic bearings. *Journal of Sound and Vibration*, 269(1-2):345–360, 2004. cited By 94.

[17] J-D Yau, Y-S Wu, and Y-B Yang. Impact response of bridges with elastic bearings to moving loads. *Journal of Sound and Vibration*, 248(1):9–30, 2001.

[18] Chul-Woo Kim, Mitsuo Kawatani, and Won-Sup Hwang. Reduction of traffic-induced vibration of two-girder steel bridge seated on elastomeric bearings. *Engineering Structures*, 26(14):2185–2195, 2004.

[19] Hongan Xu and Wen L Li. Dynamic behavior of multi-span bridges under moving loads with focusing on the effect of the coupling conditions between spans. *Journal of Sound and Vibration*, 312(4-5):736–753, 2008.

[20] Y.B. Yang, C.L. Lin, and J.D. Yau. Vibration reduction of elastically supported beams under moving loads by tuned mass devices. *IES Journal Part A: Civil and Structural Engineering*, 1(1):55–67, 2008. cited By 3.

[21] Y. Itoh, H. Gu, K. Satoh, and Y. Yamamoto. Long-term deterioration of high damping rubber bridge bearing. *Doboku Gakkai Ronbunshuu A*, 62(3):595–607, 2006. cited By 17.

[22] Y. Itoh, H. Gu, K. Satoh, and Y. Kutsuna. Experimental investigation on ageing behaviors of rubbers used for bridge bearings. *Doboku Gakkai Ronbunshuu A*, 62(1):176–190, 2006. cited By 11.

[23] Moatasem M Fayyadh and H Abdul Razak. Condition assessment of elastic bearing supports using vibration data. *Construction and Building Materials*, 30:616–628, 2012.

[24] Dan Lu, Jiayao Meng, Songhan Zhang, Yuanfeng Shi, Kaoshan Dai, and Zhenhua Huang. Damping ratios of reinforced concrete structures under actual ground motion excitations. In *Dynamics of Civil Structures, Volume 2*, pages 259–268. Springer, 2020.

[25] Biggs J.M. and Testa B. *Introduction to structural dynamics.* McGraw-Hill, New York, 1964.

[26] Di Mu and Dong-Ho Choi. Dynamic responses of a continuous beam railway bridge under moving high speed train with random track irregularity. *International Journal of Steel Structures*, 14(4):797–810, 2014.

[27] Nathan M Newmark. A method of computation for structural dynamics. *Journal of the engineering mechanics division*, 85(3):67–94, 1959.

[28] Doshin. Structural bearings en 1337-3. Product Catalogue, 2017.

[29] Freyssinet. Elastomeric bearings. Product Catalogue, 2019.

[30] Robert A Meyers. *Encyclopedia of physical science and technology.* Academic, 2002.

[31] John M Biggs and John Biggs. *Introduction to structural dynamics.* McGraw-Hill College, 1964.

A Final Sample of Relevant Studies

Title	Author(s)	Year	Journal	Country (1st author)
Effect of aging of bearings on the behavior of single-span railway bridges.	E. Erduran, C. Nordli, M. Salehi, and S. Gonen.	2022	Online Conference: EWSHM2022	Norway
Fundamental modal properties of simply supported railway bridges considering soil-structure interaction effects.	Abbas Zangeneh, Jean-Marc Battini, Costin Pacoste, and Raid Karoumi.	2019	Soil Dynamics and Earthquake Engineering	Sweden
Effect of soil properties on the dynamic response of simply-supported bridges under railway traffic through coupled boundary element-finite element analyses	M.D. Martinez-Rodrigo, P. Galvin, A. Domenech, A. Romero	2018	Engineering Structures	Spain
Reduction of traffic-induced vibration of two-girder steel bridge seated on elastomeric bearings.	Chul-Woo Kim, Mitsuo Kawatani, and Won-Sup Hwang	2014	Engineering Structures	Japan
Vibration reduction of elastically supported beams under moving loads by tuned mass devices.	Y.B. Yang, C.L. Lin, and J.D. Yau.	2008	The IES Journal Part A: Civil & Structural Engineering	Taiwan
Dynamic behavior of multi-span bridges under moving loads with focusing on the effect of the coupling conditions between spans.	Hongan Xu and Wen L Li.	2008	Journal of Sound and Vibration	USA
Mechanism of resonance and cancellation for train-induced vibrations on bridges with elastic bearings.	Y.B. Yang, C.L. Lin, J.D. Yau, and D.W. Chang.	2004	Journal of Sound and Vibration	Taiwan
Impact response of bridges with elastic bearings to moving loads.	J.D. Yau, Y-S Wu, and Y.B. Yang. I	2001	Journal of Sound and Vibration	Taiwan
Impact Response of Bridges with Elastic Bearings to Moving Loads	Y.S. Wu, Y.B. Yang	2001	Journal of Sound and Vibration	Taiwan

B Stiffness and Mass Matrix of Planar Beam Elements

Stiffness matrix of planar beam element.

$$\left[k_b\right] = \begin{bmatrix} EA/L & 0 & 0 & -EA/L & 0 & 0 \\ 0 & 12EI/L^3 & 6EI/L^2 & 0 & -12EI/L^3 & 6EI/L^2 \\ 0 & 6EI/L^2 & 4EI/L & 0 & -6EI/L^2 & 2EI/L \\ -EA/L & 0 & 0 & EA/L & 0 & 0 \\ 0 & -12EI/L^3 & -6EI/L^2 & 0 & 12EI/L^3 & -6EI/L^2 \\ 0 & 6EI/L^2 & 2EI/L & 0 & -6EI/L^2 & 4EI/L \end{bmatrix}$$

Mass matrix of planar beam element.

$$\left[m_b\right] = \begin{bmatrix} \rho AL/3 & 0 & 0 & \rho AL/6 & 0 & 0 \\ 0 & 13\rho AL/35 & 11\rho AL^2/210 & 0 & 9\rho AL/70 & -13\rho AL^2/420 \\ 0 & 11\rho AL^2/210 & \rho AL^3/105 & 0 & 13\rho AL^2/420 & -\rho AL^2/140 \\ \rho AL/6 & 0 & 0 & \rho AL/3 & 0 & 0 \\ 0 & 9\rho AL/70 & 13\rho AL^2/420 & 0 & 13\rho AL/35 & -11\rho AL^2/210 \\ 0 & -13\rho AL^2/420 & -\rho AL^2/140 & 0 & -11\rho AL^2/210 & \rho AL^3/105 \end{bmatrix}$$

C Verification Reference Cases for Spring Support Algorithm

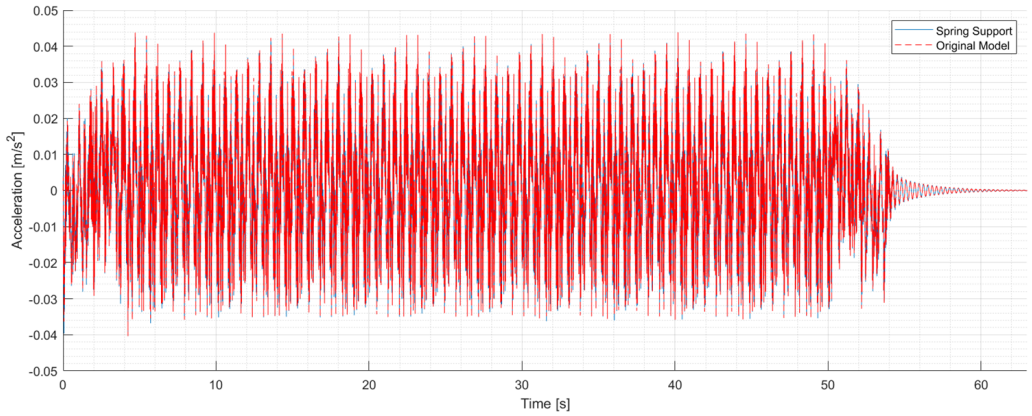

Figure C.1: Comparison of acceleration at midspan of ''Norddalsbrua 1" with moving load model.

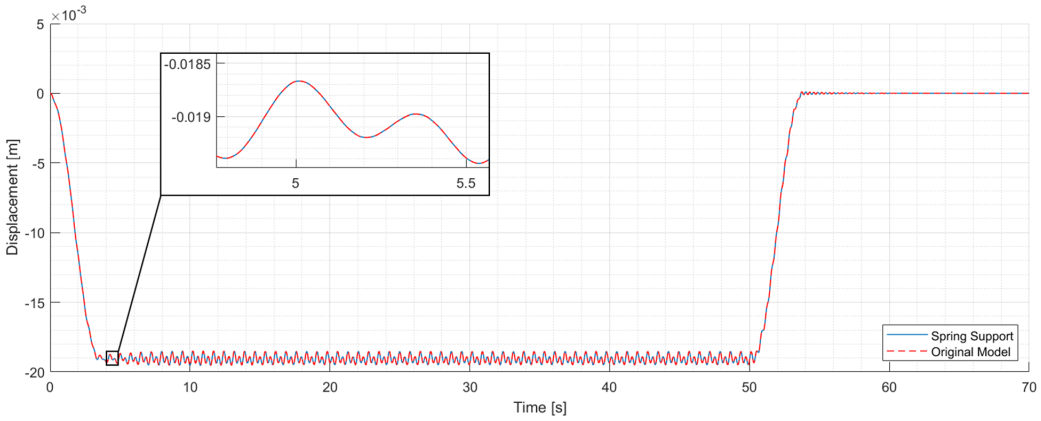

Figure C.2: Comparison of displacement at midspan of "Norddalsbrua 1" reference case for moving mass model.

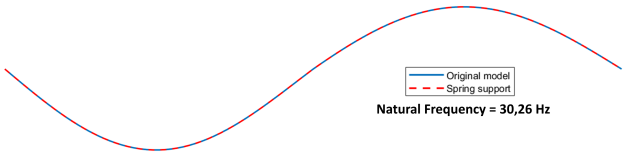

(a) First mode of vibration.

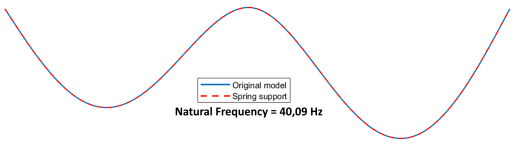

(b) Second mode of vibration.

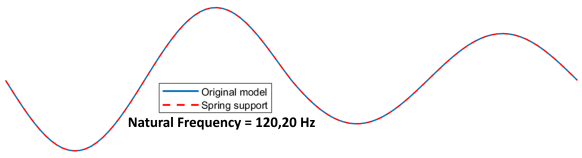

(c) Third mode of vibration.

Figure C.3: Comparisons of modes between proposed algorithm and "Norddalsbrua 2" reference.

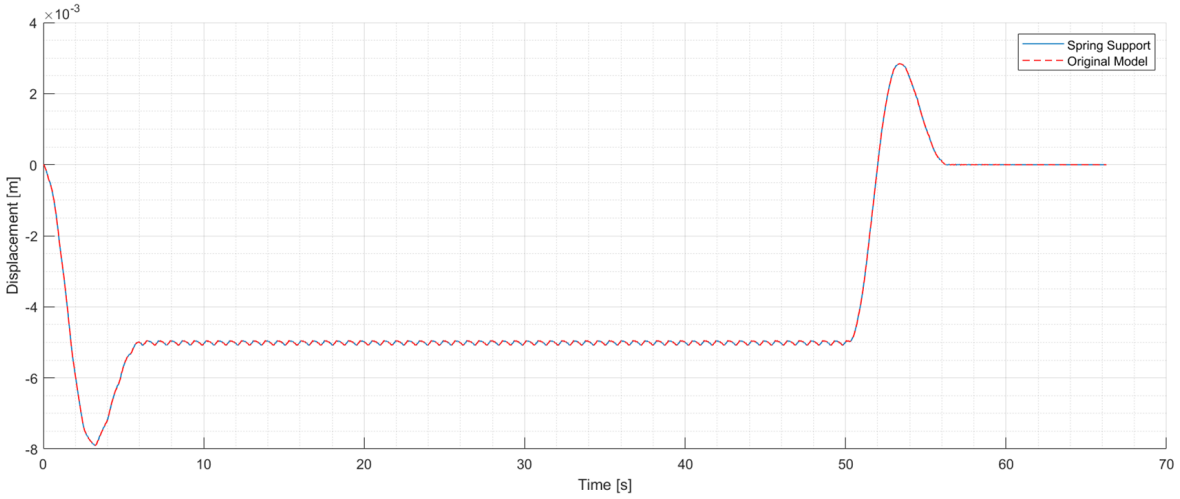

Figure C.4: Comparison of displacement at first midspan with "Norddalsbrua 2" reference moving load model.

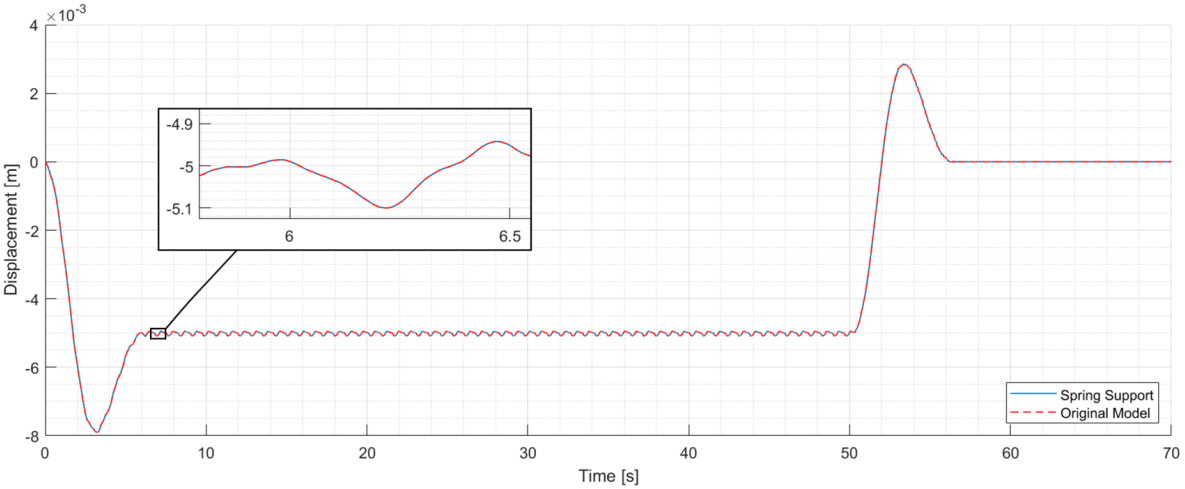

Figure C.5: Comparison of displacement at first midspan with "Norddalsbrua 2" reference moving mass model.

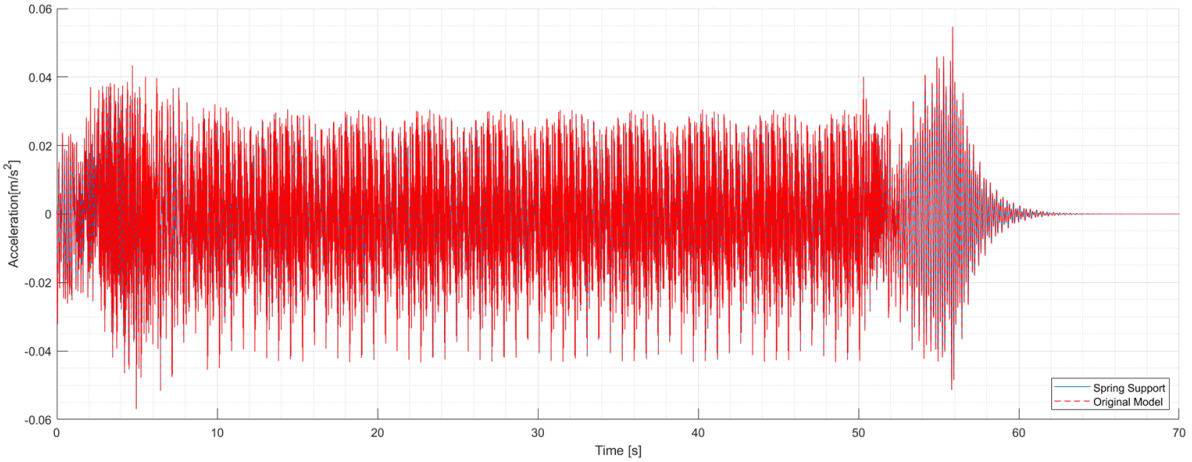

Figure C.6: Comparison of acceleration at first midspan with "Norddalsbrua 2" moving mass model.

D Comparison of VBI Models through Equivalent Conditions

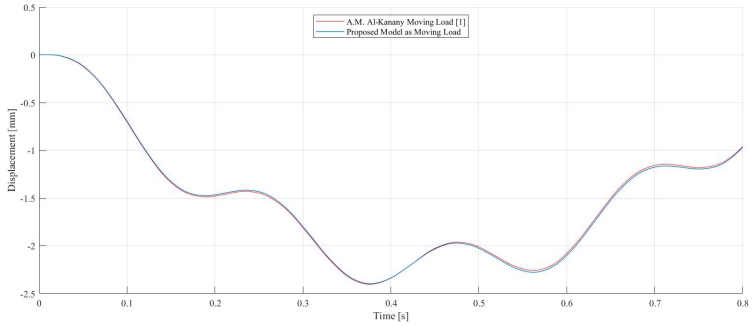

Figure D.1: Comparison of displacement at midspan with moving load model and proposed sprung mass model.

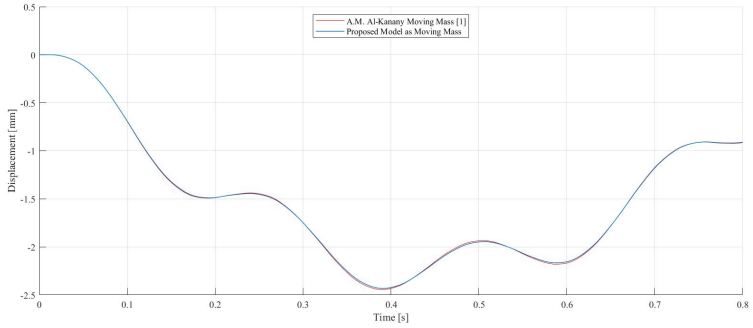

Figure D.2: Comparison of displacement at midspan with moving mass model and proposed sprung mass model.

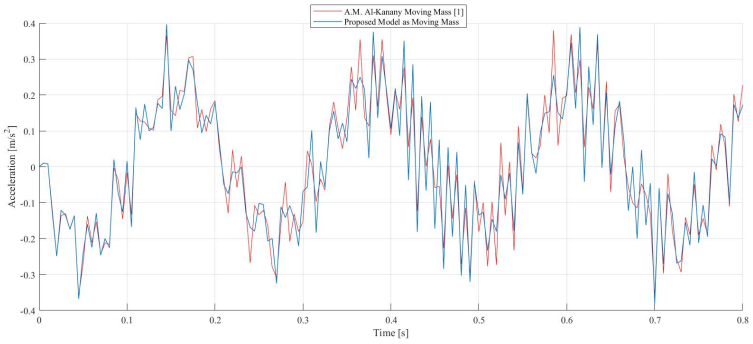

Figure D.3: Comparison of acceleration at midspan with moving mass model and proposed sprung mass model.

E Initial Planar Vertical Natural Frequencies

Table E.1: Initial vertical natural bridge frequencies for single-span bridges.

Support stiffness	1e4 kN/m				
Mode of Vibration	1	2	3	4	5
[Hz]	0,657	1,157	7,91	19,26	37,7
Support stiffness	1e5 kN/m				
Mode of Vibration	1	2	3	4	5
[Hz]	1,78	3,57	8,22	19,7	37,91
Support stiffness	1e6 kN/m				
Mode of Vibration	1	2	3	4	5
[Hz]	2,83	8,94	15,18	24,14	40,25
Support stiffness	1e7 kN/m				
Mode of Vibration	1	2	3	4	5
[Hz]	3,05	11,88	25,5	42,06	59,72
Support stiffness	1e8 kN/m				
Mode of Vibration	1	2	3	4	5
[Hz]	3,07	12,3	27,5	48,52	75,17
Support stiffness	1e9 kN/m				
Mode of Vibration	1	2	3	4	5
[Hz]	3,07	12,3	27,7	49,1359	76,72
Support stiffness	1e10 kN/m				
Mode of Vibration	1	2	3	4	5
[Hz]	3.07	12,3	27,7	49,1965	76,86
Support stiffness	1e15 kN/m				
Mode of Vibration	1	2	3	4	5
[Hz]	3,07	12,3	27,7	49,1965	76,88

Table E.2: Initial vertical natural bridge frequencies for two-span bridges

Support stiffness	1e4 kN/m				
Mode of Vibration	1	2	3	4	5
[Hz]	0,82	1,16	7,12	19,26	37,7
Support stiffness	1e5 kN/m				
Mode of Vibration	1	2	3	4	5
[Hz]	2,46	3,57	8,38	19,69	38
Support stiffness	1e6 kN/m				
Mode of Vibration	1	2	3	4	5
[Hz]	6,69	8,94	15,9	24,14	40.77
Support stiffness	1e7 kN/m				
Mode of Vibration	1	2	3	4	5
[Hz]	11,88	15	33,77	42,06	62.65
Support stiffness	1e8 kN/m				
Mode of Vibration	1	2	3	4	5
[Hz]	12,26	18,72	48,52	56,76	105,4
Support stiffness	1e9 kN/m				
Mode of Vibration	1	2	3	4	5
[Hz]	12,3	19,17	49,14	61,73	110,36
Support stiffness	1e10 kN/m				
Mode of Vibration	1	2	3	4	5
[Hz]	12,3	19,2	49,2	62,27	110,67
Support stiffness	1e15 kN/m				
Mode of Vibration	1	2	3	4	5
[Hz]	12,3	19,2	49,2	62,27	110,7

Table E.3: Initial vertical natural bridge frequencies for three-span bridges.

Support stiffness	1e4 kN/m				
Mode of Vibration	1	2	3	4	5
[Hz]	0,94	1,25	7,11	19,28	37,7
Support stiffness	1e5 kN/m				
Mode of Vibration	1	2	3	4	5
[Hz]	2,87	3,9	8,26	19,88	38
Support stiffness	1e6 kN/m				
Mode of Vibration	1	2	3	4	5
[Hz]	8,02	11,13	15,18	25,31	40,64
Support stiffness	1e7 kN/m				
Mode of Vibration	1	2	3	4	5
[Hz]	20,45	26,47	27,49	47,68	64,1
Support stiffness	1e8 kN/m				
Mode of Vibration	1	2	3	4	5
[Hz]	25,08	39,72	44,7	82,84	120,57
Support stiffness	1e9 kN/m				
Mode of Vibration	1	2	3	4	5
[Hz]	25,42	41,48	49,42	94,66	144,8
Support stiffness	1e10 kN/m				
Mode of Vibration	1	2	3	4	5
[Hz]	25,46	41,67	50	95,7	146,18
Support stiffness	1e15 kN/m				
Mode of Vibration	1	2	3	4	5
[Hz]	25,46	41,67	50	95,8	146,32

F AMA Envelope Curves for Single-Span Bridge with 20% Reduced Stiffness on Right Support

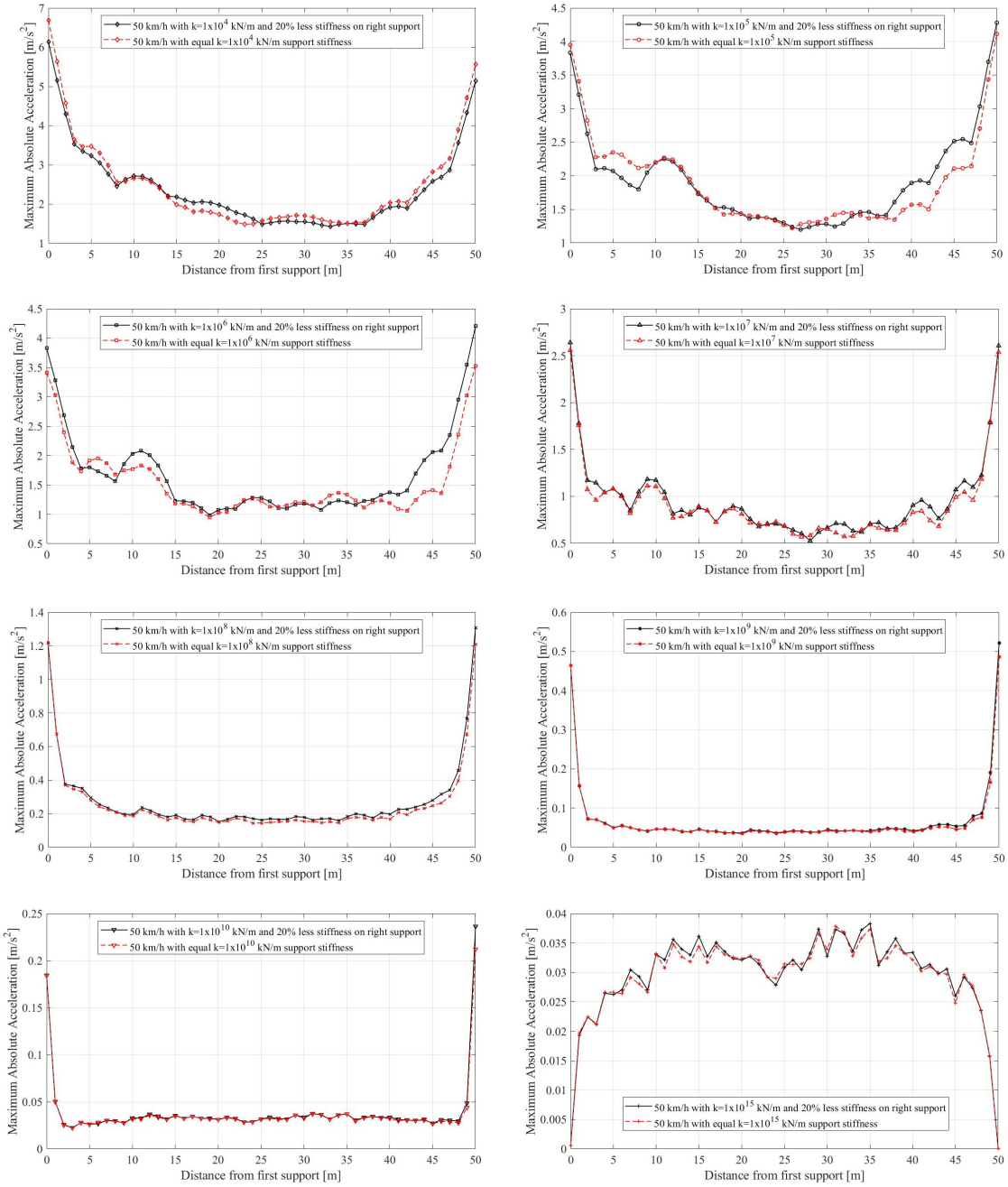

Figure F.1: Comparison between original and 20% reduced stiffness on right-support at 50 km/h.

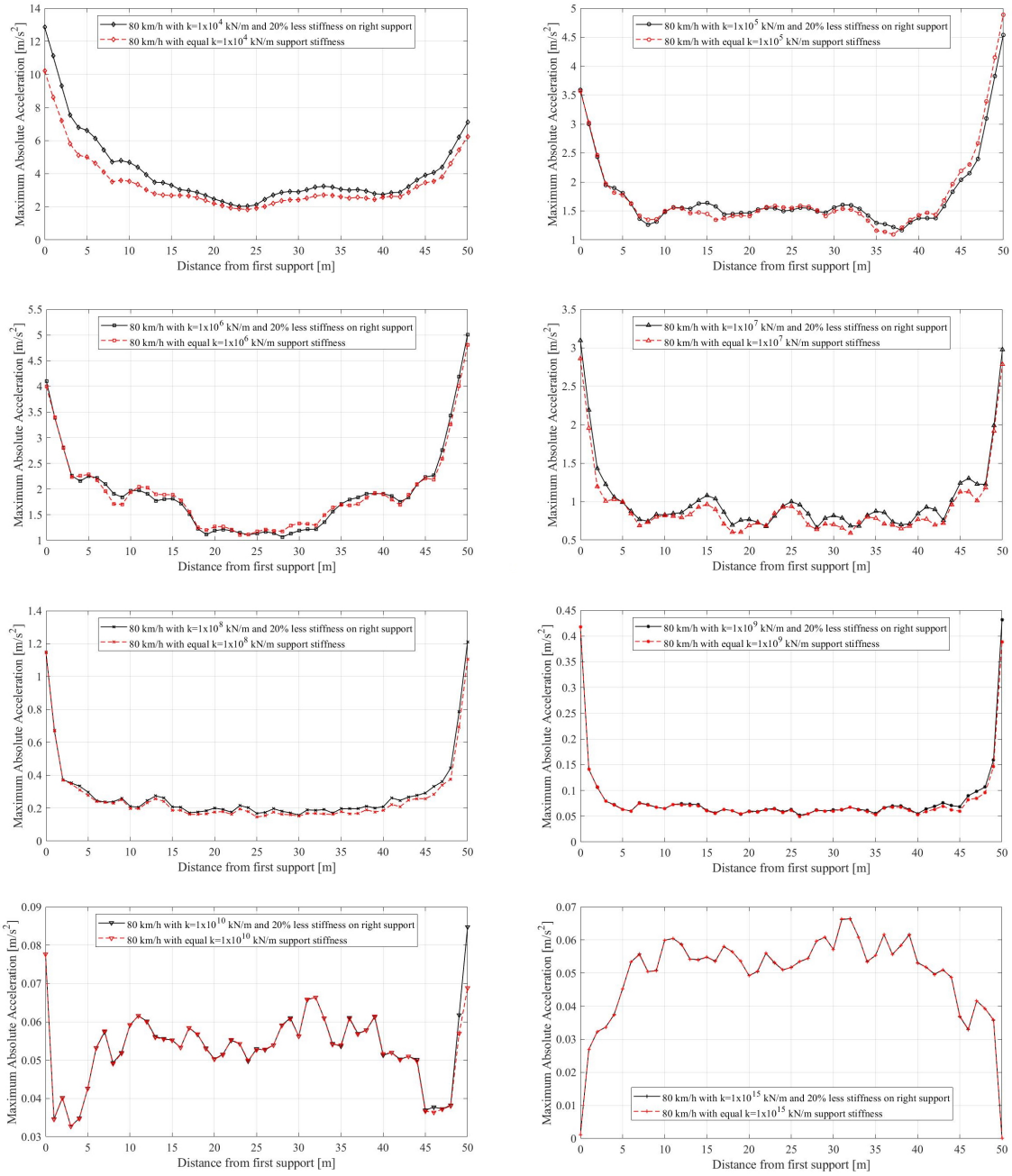

Figure F.2: Comparison between original and 20% reduced stiffness on right-support at 80 km/h.

G FAS of Train Accelerations on Single-Span Bridge

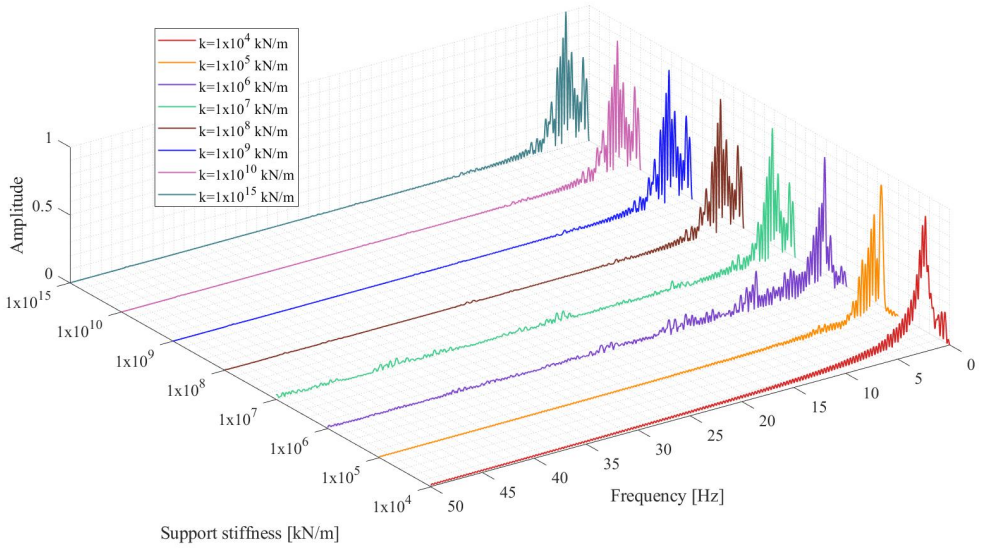

Figure G.1: FAS on train axle 1/4 in train length with varying bridge support stiffness for single span bridge at 50 km/h.

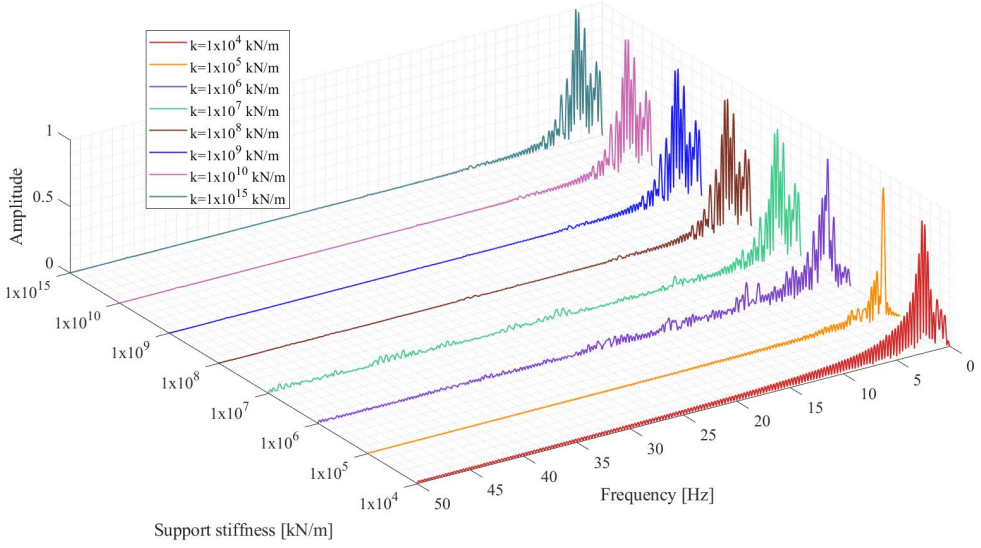

Figure G.2: FAS on train axle 1/2 in train length with varying bridge support stiffness for single span bridge at 50 km/h.

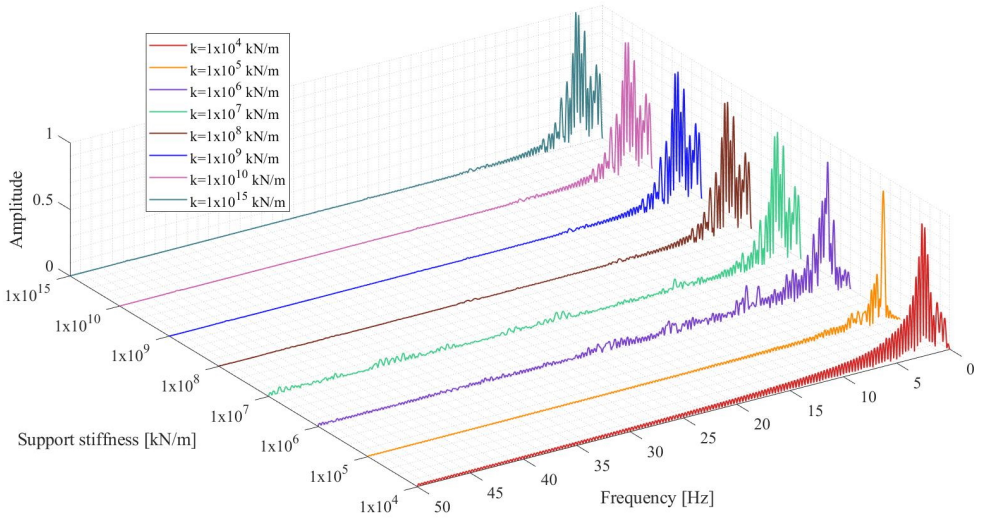

Figure G.3: FAS on train axle 3/4 in train length with varying bridge support stiffness for single span bridge at 50 km/h.

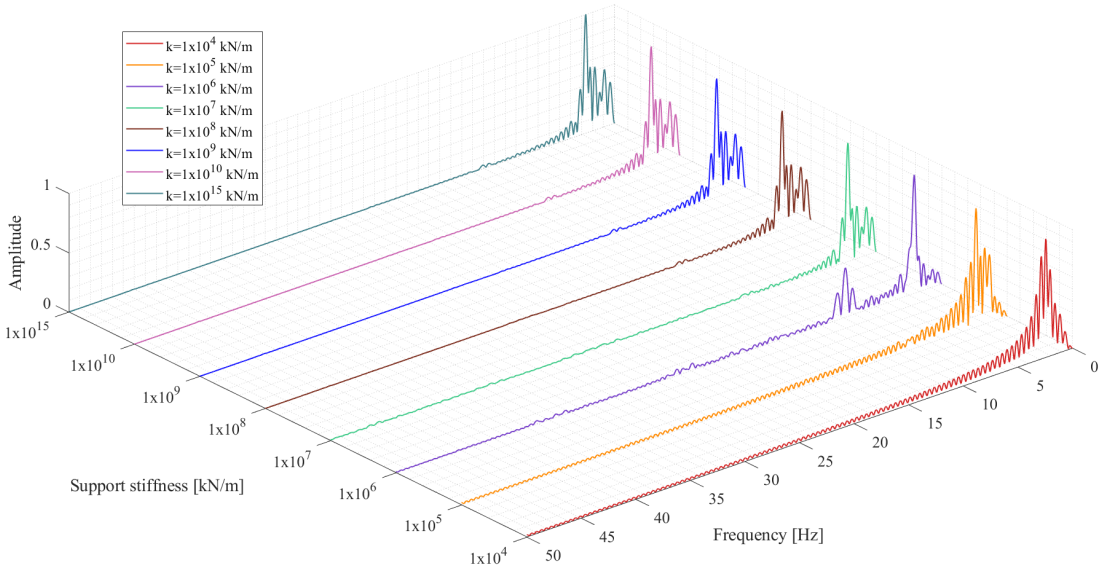

Figure G.4: FAS on train axle 1/4 in train length with varying bridge support stiffness for single span bridge at 80 km/h.

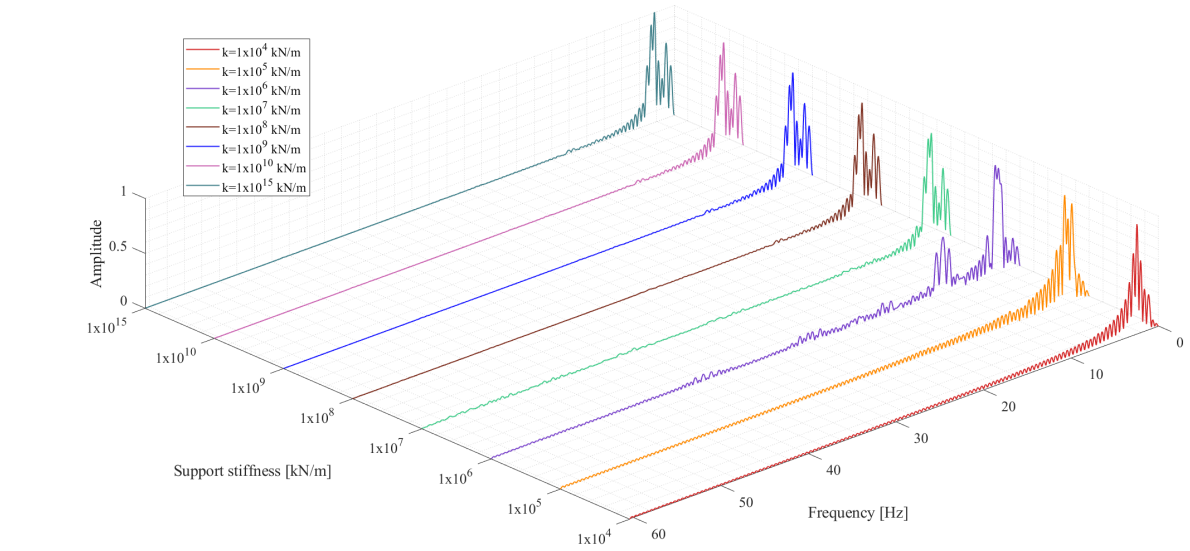

Figure G.5: FAS on train axle 1/2 in train length with varying bridge support stiffness for single span bridge at 80 km/h.

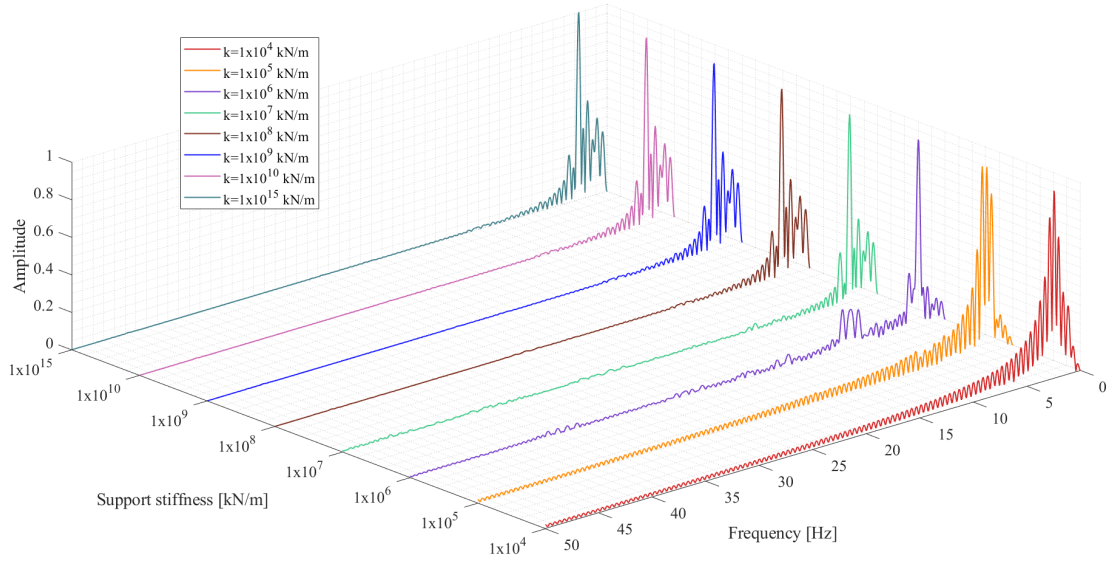

Figure G.6: FAS on train axle 3/4 in train length with varying bridge support stiffness for single span bridge at 80 km/h.

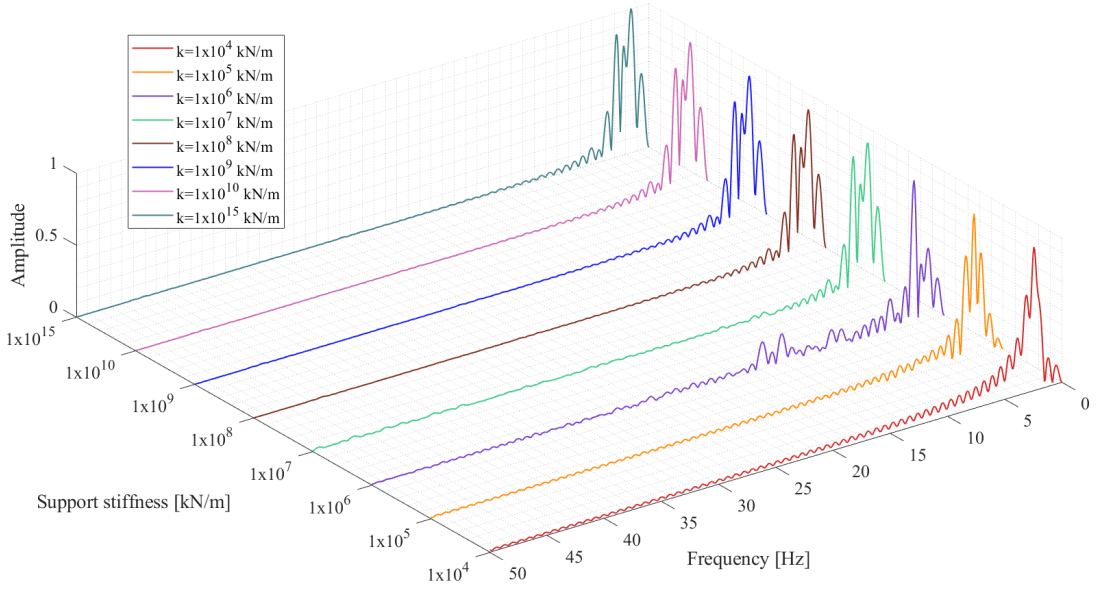

Figure G.7: FAS on train axle 1/4 in train length with varying bridge support stiffness for single span bridge at 130 km/h.

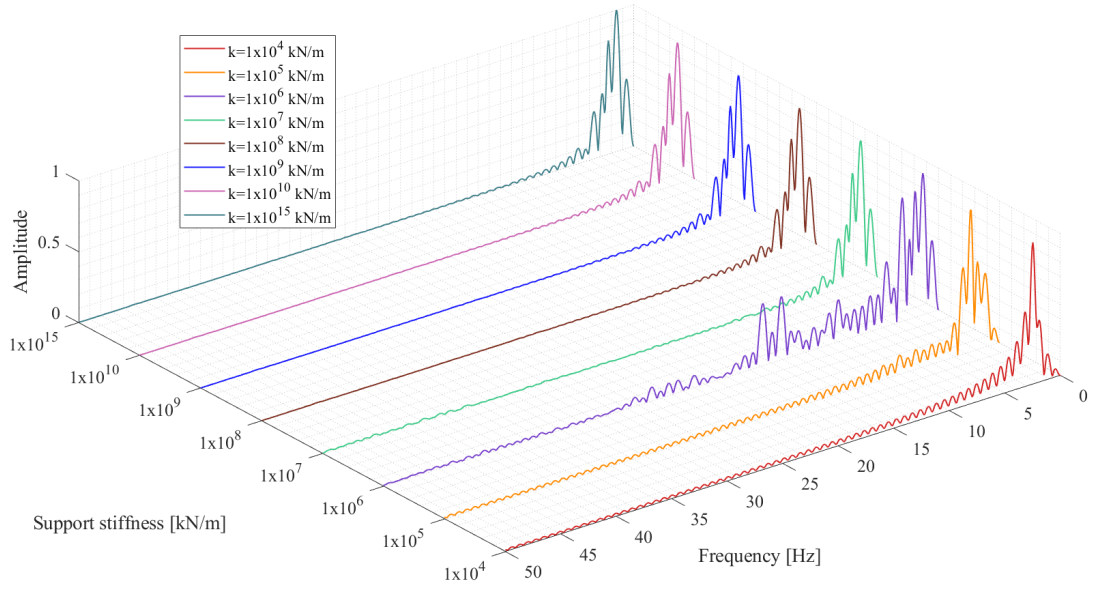

Figure G.8: FAS on train axle 1/2 in train length with varying bridge support stiffness for single span bridge at 130 km/h.

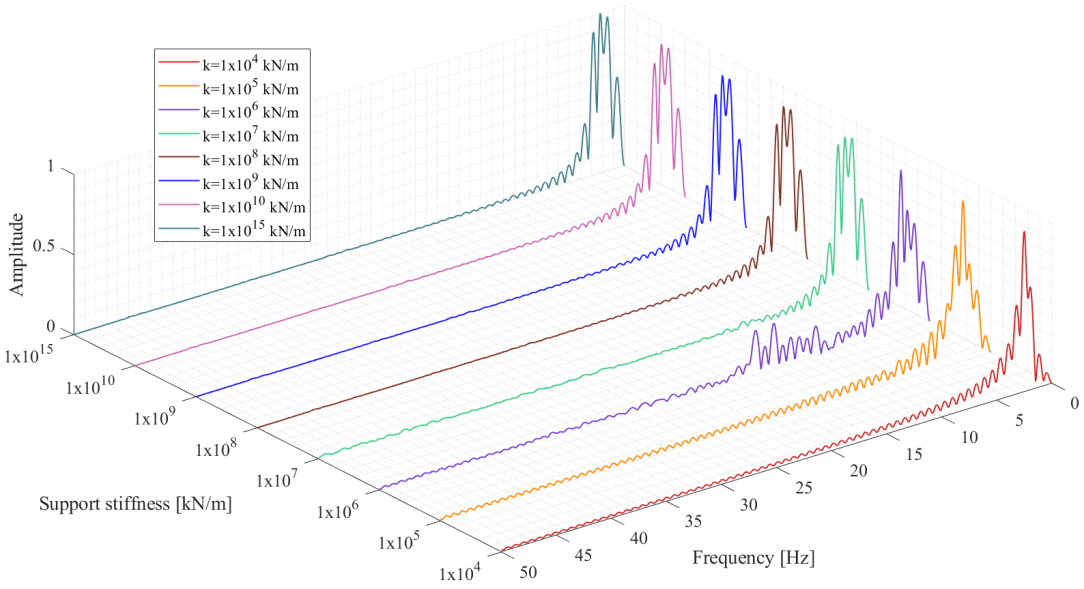

Figure G.9: FAS on train axle 3/4 in train length with varying bridge support stiffness for single span bridge at 130 km/h.